Novel antitubulin agents uncover new players in microtubule regulation and cell division in cancer

Allison E. Cherry

A dissertation

submitted in partial fulfillment of the

requirements for the degree of

Doctor of Philosophy

University of Washington

2016

Reading Committee:

Nephi Stella, Chair

John Scott

Sandra Bajjalieh

Program authorized to offer degree:

Pharmacology

University of Washington

Abstract

Novel antitubulin agents uncover new players in microtubule regulation and cell division in cancer

Allison E. Cherry

Chair of the Supervisory Committee:

Professor Nephi Stella

Department of Pharmacology

Glioblastoma multiforme (GBM) is a devastating and intractable type of cancer. Current antineoplastic drugs do not improve the median survival of patients diagnosed with GBM beyond 14-15 months in part because the blood-brain barrier is generally impermeable to many therapeutic agents. Drugs that target microtubules (MT) have shown remarkable efficacy in a variety of cancers, yet their use as GBM treatments has also been hindered by the scarcity of brain-penetrant MT-targeting compounds. We have discovered a new alkylindole compound, ST-11, that acts directly on MTs and rapidly attenuates their rate of assembly. Accordingly, ST-11 arrests GBM cells in prometaphase and triggers apoptosis. *In vivo* analyses reveal that unlike current antitubulin agents, ST-11 readily crosses the blood-brain barrier. Further investigation in a syngeneic orthotopic mouse model of GBM has revealed that ST-11 activates caspase-3 in tumors to reduce tumor volume without overt toxicity. Thus, ST-11 represents the first member of a new class of brain-penetrant antitubulin therapeutic agents.

In addition to GBM, antitubulin agents are efficacious antineoplastic agents against a variety of cancers. A common drawback to their clinical use is the acquisition of drug resistance. The mechanisms governing cellular sensitivity to antitubulin compounds are complex. In particular, alterations in MT dynamics have been found to correlate with increased resistance to antitubulin compounds. Heterotrimeric G protein signaling has been implicated in the regulation of MT dynamics. However, research focusing on the effect of G proteins or heptahelical G protein coupled receptors (GPCRs) on sensitivity to antitubulin agents is lacking. Using multiple unbiased screens, biochemical analyses and live cell imaging techniques, we identified the orphan GPCR GPR124 as a novel coordinator of MT dynamics in cancer cells

that regulates cellular sensitivity to MT-targeted agents, including ST-11. GPR124 associates with the MT plus end binding protein ch-TOG and increases its expression. Consequently, GPR124 increases spindle and interphase MT dynamics and the prevalence of lagging chromosomes during anaphase, which are evidence of increased chromosomal instability (CIN). High levels of CIN can lead to decreased tumor growth. Accordingly, overexpression of GPR124 significantly reduces the growth of U87MG xenograft tumors *in vivo*. Thus, our research supports a model in which GPR124 associates with ch-TOG to alter MT dynamics and increase lagging chromosomes that can lead to CIN and decreased tumor growth. Together, these studies describe a new brain-penetrant antitubulin agent and reveal novel MT regulatory components that affect antitubulin drug efficacy and tumor growth.

Table of Contents

List of Abbreviations

Abbreviation	Full name
GBM	Glioblastoma multiforme
TMZ	Temozolomide
GSC	Glioma stem cell
RTK	Receptor tyrosine kinase
GPCR	G protein coupled receptor
TTFields	Tumor treatment fields
MT	Microtubule
SAC	Spindle assembly checkpoint
CIN	Chromosomal instability
PLC	Phospholipase C
PKA	Protein kinase A
GRK	GPCR regulated kinase
MAPK	Mitogen activated protein kinase
MMP	Matrix metalloprotease
GF	Growth factor
PI3K	Phosphoinositol-3-kinase
SHH	Sonic hedgehog
AEA	Anandamide
2-AG	2-arachydonoylglycerol
THC	Δ^9-tetrahydrocannabinol
CP	CP55,940
WIN-2	WIN55,212-2
AI	Alkylindole
PK	Pharmacokinetics
LC-MS	Liquid chromatography-Mass spectrometry
i.p.	Intraperitoneal
PARP	Poly ADP ribose polymerase
MTD	Maximal tolerated dose
TEM5	Tumor endothelial marker 5
C2-CM	C2-ceramide
Stauro	Staurosporine

List of Figures

List of Tables

Acknowledgements

First, I would like to thank Nephi Stella for mentoring me through my years in graduate school. Nephi, you have guided me through a particularly demanding project, and your mentorship has taught me not only to have confidence in myself, but never to give up when things become challenging. With this project, I have learned just how difficult science can be and also how rewarding it is. I am profoundly grateful for your unwavering support, encouragement, advice, and guidance.

I would also like to thank my graduate committee for their support and guidance on a project that changed directions several times over the five and a half years I worked on it. I am particularly grateful to my reading committee, Nephi, Sandy, and John, for taking the time to read this dissertation.

Outside of my advisor and my graduate committee, several faculty members have shared expertise and advice during my time in the Department of Pharmacology. Shao-En Ong provided ample guidance and spent a great deal of time teaching me the basics of SILAC and mass spectrometry. I am additionally grateful to Chris Hague for the scientific and career advice he has given me over the years. John Scott has been particularly invested in both my scientific and career development. His advice has helped me through challenging times during my graduate school career. Despite the huge advancements we have made, it is still challenging to be a woman in science. Sandy Bajjalieh and Gwenn Garden have not only encouraged me as a scientist, but they have been phenomenal role models. Lastly, I would like to thank Linda Wordeman for taking me under her wing as a budding microtubule biologist. I am extremely grateful for the guidance and generosity she has shown me as I have finished this work.

As my project progressed and changed over the years, many post doctoral scientists worked with me to lend scientific expertise. Dave Canton and Donelson Smith in the Scott lab spent a tremendous amount of time teaching me molecular biology and helping me come up with new hypotheses and ways to test them. Additionally, I am extremely grateful to Juan Jesus Vicente in the Wordeman lab. Juanje has spent ample time expounding the biology of microtubules and cell division to me. He has been indispensable in helping me with come up with hypotheses, plan and execute experiments, and analyze and interpret data.

I have many friends that have been central to my life during the time I worked on this dissertation. Specifically, Katie Swinney, Alipi Naydenov, Susan Fung, Jon Coy, Will Marrs, Brian Haas, Jessie Cao, and Eric Horne in the Stella lab were there for me through all the difficult as well as the successful times. I was always able to bounce ideas off of them. I have many fond memories of working with them, and I am glad that our lab functioned as a social as well as a professional environment. I am also especially grateful to Jen Whiting, Patrick Nygren, Jaci Saunders, Sharri Zamore, and Sean Knecht who have been important friends outside of the Stella lab. Having a support network of fellow graduate students has been instrumental to my success and general wellbeing over the years. Living with Jaci and her dog Edie for the first several years of graduate school was especially valuable for support, celebrations, and puppy cuddles. Outside of science, I have a wonderful group of people that I am proud to call my friends. I can always count on Katie Swinney, Cesar Viray, Sean Knecht, Josh Dorothy, Leah Adams, Vince and DeAnna Martinez, Kaila Montero, Dom Marion, Al Mark, Allen Lee, Jeremy

and Staphanie LaDuke, and Chani Bare to be around for dinner parties (DWF), a night out (Konaroke Roulette), or a night in playing games (Settlers of Chris Catan, Settlers of Westeros). Additionally, I have enjoyed going skiing with Jeremy and Cesar (NW GNARPOW KILLAZ) virtually every free weekend during the winter. Our annual summer (Chelan OH!12 – OH!15) and winter (Chronicles of GNAR-nia '13 – '14) vacations have helped me get away and take a break. Johnny Deng, Mel Nguyen, Gordon Sumioka, and Adam Alsabery have introduced me to a new world of climbing and taken me on many outdoor adventures. My friends from afar, including Amie Calhoun, Alex Klug, Alyssa Kurkoski, Ari Fram, Krish Maharaj, Jordan Hart, Ross Thompson, Kim Roth, and Kelly McDonald have all been supportive, given me places to sleep when I go on vacation, and most importantly, kept in touch as close friends from so far away for so many years.

Finally, I would like to thank my family. Mom and Dad have been the most supportive parents I could hope for throughout my entire life. They have encouraged me to follow my dreams, always expressed to me that I can accomplish anything I set my mind to, and been phenomenal role models to me. My mom has listened to many emotional phone calls when my project was especially challenging, for which I am extremely grateful. My dad shared his Ph.D. experience with me, which helped me navigate my own. I consider both of them to be academics at heart, and I believe that is where I get my love of research and learning. Thanks for making me the person I am and for supporting me. My brother Adam has always been an amazing sibling. He has helped me through some difficult times both personally and professionally. I am happy that we are friends in addition to family, and I am looking forward to many skiing, hiking, camping, and climbing trips in the future.

"I'm not trying to prove anything, by the way. I'm a scientist and I know what constitutes proof. But…a scientist must also be absolutely like a child. If he sees a thing, he must say that he sees it, whether it was what he thought he was going to see or not. See first, think later, then test. But always see first. Otherwise you will only see what you were expecting. Most scientists forget that."
Douglas Adams

"So long and thanks for all the fish"
Douglas Adams

Preface

Portions of the text and data from *Chapter 1* are reproduced from the following previously published work under fair use:

Cherry A.E., Stella N. (2014) G protein coupled receptors as oncogenic signals in glioma: emerging therapeutic avenues. *Neuroscience* **278,** 222-236

Portions of text and data from *Chapter 2* and *Chapter 3* are reproduced from the following manuscripts in preparation:

Cherry A.E., Haas B.R.*, Naydenov A.V.*, Fung S., Xu C., Swinney K., Wagenbach M., Freeling J., Canton D.A., Coy J., Horne E.A., Rickman B., Scott J.D., Ho R.J.Y., Liggitt D., Wordeman L., and Stella N. (2016) ST-11: a new brain-penetrant microtubule-destabilizing agent with therapeutic potential for glioblastoma multiforme. *In submission to Molecular Cancer Therapeutics*

Cherry A.E., Vicente J.J., Xu C., Swinney K., Ong S.E., Wordeman L., and Stella N. (2016) The orphan seven transmembrane receptor GPR124 regulates microtubule dynamics through ch-TOG. *In preparation*

CHAPTER 1
Introduction

GBM: From histology to driver mutations

Gliomas are a brain neoplasm and account for 80% of primary central nervous system tumors diagnosed between 2004 and 2008 in the United States (1). The largest subset, comprising well over 50% of gliomas, is the astrocytomas, which is so-named because these tumors share histological features with astrocytes. The World Health Organization stratifies astrocytomas into four grades (I-IV) based on several histological criteria: cellularity, nuclear pleomorphism, mitotic activity of tumor and the presence of necrosis and neovasculature. Grade IV astrocytoma, or Glioblastoma Multiforme (GBM), is the most common primary glioma diagnosed in adults and occurs at an incidence of approximately 3 per 100,000 people per year in the United States alone (1). The median survival of patients diagnosed with GBM is only 14.2 months when treated with the standard of care, which consists of surgical resection followed by a combination of radiotherapy and the alkylating agent temozolomide (TMZ) (2). With the exception of the addition of TMZ to the standard of care in 2005, which increased median survival of GBM patients by a mere 2 months, very little progress has been made to treat this cancer in decades (2). The 5-year survival rate of GBM patients is only 4.7% owing to the inevitability of recurrence. The eventual resurfacing of this cancer is likely due in part to glioma stem cells (GSCs) within the tumor that resist radiation and chemotherapy (3, 4) and are capable of propagating heterogeneous tumors (5-8). Thus, the prognosis for patients

diagnosed with GBM is dismal, and despite the clinical testing of several novel therapeutic approaches, little progress has been made to help these patients.

Classification of gliomas

The current classification system that divides gliomas by malignancy has not been effective in estimating prognosis, most notably between grades III and IV (9). Therefore, The Cancer Genome Atlas (TCGA) research network dedicated a significant amount of effort to stratify gliomas by driver mutations, first with GBM and more recently with lower grade gliomas (10, 11). The initial genetic subclassification proposed by Verhaak et al. included four GBM subtypes: Classical, Mesenchymal, Proneural, and Neural (12).

The classical subtype is primarily defined by an amplification of the *epidermal growth factor receptor* (*EGFR*) and deletion of the *tumor suppressor protein phosphatase and tensin homolog* (*PTEN*) genes. The *EGFR* amplification in this subtype often co-occurs with a mutation that gives rise to a constitutively active receptor (*EGFRvIII*) (13-16). EGFR is an oncogenic receptor tyrosine kinase (RTK) that activates both pro-migratory and proliferative pathways, and when amplified or mutated, it plays a role in the development of various neoplasms (17). The *EGFR* amplification, though not strictly defining the other genetic subtypes, is also commonly present in the proneural and neural subtypes, which makes it the most frequent genetic mutation in GBM. Thus, although 27% percent (18) of these cancers are characterized as the classical subtype, approximately 40% of all diagnosed GBMs contain an *EGFR* amplification, many of which also contain the *EGFRvIII* mutation (16, 19-21).

The mesenchymal and proneural subtypes comprise 29% and 28% of GBMs, respectively (18). The mesenchymal subtype is characterized by deletion or mutation of the tumor suppressors *neurofibromin 1* (*NF1*) and *PTEN*. NF1 is a negative regulator of the oncogenic protein RAS, and PTEN antagonizes phosphoinositol-3-kinase (PI3K), which are two important signaling molecules downstream of RTKs. The proneural subtype typically have a *platelet derived growth factor receptor A* (*PDGFRA*) amplification and mutations in the tumor suppressor *TP53*. Like EGFR, PDGFRA is an RTK that activates mitogenic growth pathways.

Lastly, the neural subtype is the least common, and it comprises 16% of diagnosed GBMs. This subtype is not defined by a dysregulation of oncogenic or tumor suppressor pathways but instead defined by the presence of neuronal markers, such as neurofilament light polypeptide (NEFL), GABA receptor subunit alpha 1 (GABRA1), and synaptotagmin-1 (SYT-1).

Current therapeutic strategies to treat GBM

During neoplastic transformation, cells typically acquire six attributes that allow for unchecked growth and spread: uncontrolled proliferative signaling, evasion of growth suppressors, activation of invasion and metastasis, replicative immortality, ability to induce angiogenesis, and resistance to cell death (22). The genetic characteristics that define the GBM subtypes feature common dysregulations in RTK signaling, which are major drivers behind several of the acquired hallmarks of malignancy. Accordingly, many of the newly developed GBM therapies are designed to target RTK signals. Three main classes of drugs have been developed to accomplish this task: vascular endothelial growth factor (VEGF) inhibitors, EGFR inhibitors, and non-specific tyrosine kinase inhibitors. Bevacizumab is an antibody designed to neutralize the signaling of the pro-angiogenic protein VEGF and was approved by the FDA for the treatment of GBM in 2009. Results were promising in early phase II clinical studies that involved small groups of patients; bevacizumab in combination with the topoisomerase inhibitor irinotecan or with TMZ and radiotherapy improved the 6-month progression free survival and overall survival (23). However, in a recent large study involving 637 patients, bevacizumab had no significant effect on overall survival, and it prolonged progression-free survival by merely 3 months in patients with newly diagnosed GBM (24). Furthermore, evidence suggests that bevacizumab promotes tumor cell infiltration into the brain parenchyma (25, 26). Efforts to treat GBM with small molecules targeting EGFR, such as erlotinib and gefitinib, have also fallen short of expectations in clinical trials. While gefitinib is used successfully to treat patients with non-small cell lung cancer, clinical trials evaluating this drug in GBM have failed to report any therapeutic benefit (27). Several clinical trials evaluating erlotinib in GBM patients have reported similar negative results (27-29). Imatinib and sunitinib, both non-specific tyrosine kinase inhibitors that block PDGFR activity, have also have not produced therapeutic benefits in phase II trials (30-32).

These results suggest that exclusively targeting RTK signals is ineffective to treat GBM and new therapeutic modalities to apply alone or in combination with targeted therapies may improve the success of GBM treatment. From the many studies that have been published on this topic, two strategies have emerged with promising potential. First, gliomas have been found to be hypersensitive to antimitotic agents compared with healthy non-malignant cells (33). Therefore, antitubulin drugs, which are commonly used therapeutic agents for other cancers, are becoming attractive candidates for glioma therapy. Second, oncogenic signals that modulate glioma growth, migration, and angiogenesis may emanate from another class of

receptors, the G protein-coupled receptors (GPCRs). Preclinical studies evaluating the efficacy of several GPCR-based therapies have produced encouraging results for glioma treatment. New therapies aimed at targeting GPCRs independently or in conjunction with RTK-inhibiting drugs should be considered for GBM treatment.

Promising new targets for GBM treatment

Mitotic effector proteins and microtubules

Most classical chemotherapeutic agents, such as DNA damaging agents, take advantage of aberrant cell cycle progression by targeting hyperproliferative cells; however, these agents also target fast-dividing populations of healthy cells, leading to unfortunate, and often dangerous, side effects. A recent study demonstrated that GBM cells are particularly sensitive to mitotic disruption compared with healthy tissue, indicating that antimitotic agents might display a promising therapeutic index for this type of cancer (33). For example, antimitotic devices that generate electromagnetic fields known as tumor treatment fields (TTFields) have shown promise as novel GBM treatments. TTFields target hyperproliferative cells in a specific region of the body, and thus, have less widespread negative effects than classical chemotherapeutics. One such device, the NovoTTF-100A System, was approved for use on GBM patients in 2011 and had equivalent efficacy and a favorable safety profile compared with standard chemotherapeutics in clinical trials (34).

Antimitotic agents function by inhibiting mitosis, leading to apoptotic cell death. The cell cycle is divided into 2 primary phases: interphase (growth and DNA replication), and mitosis (M phase, cell division). Interphase is further divided into G_1 (first gap), S (DNA synthesis), and G_2 (second gap). Additionally, cells can enter a quiescent phase known as G_0. Progression through the 3 stages of interphase and subsequent mitosis is controlled by cyclin-dependent kinases. These proteins are activated by cyclins, and each phase of the cell cycle is controlled by expression of a different cyclin. In turn, cyclin-CDK pairs are inhibited by CDK inhibitors (CDKIs), and thus, cell cycle progression is the result of a balance between “on” signals (cyclins) and “off” signals (CDKIs). Additionally, checkpoints during G_1, G_2, and M phase arrest the cell cycle if a problem is encountered. These processes are frequently dysregulated in cancer, leading to unchecked cellular growth and division [reviewed in (35)]. Mitosis is a rapid process compared with the much slower interphase. Populations of rapidly dividing cells, such as tumors, enter mitosis with a higher frequency than slower dividing cell types, exposing them

to drugs that act during mitosis. Accordingly, similar to DNA damaging agents, antimitotic agents target rapidly dividing cells by arresting the cell cycle when they reach M phase and triggering apoptosis.

Mitosis is a complex mechanism centered on tightly regulated dynamic microtubules (MTs) to ensure the equal separation of chromosomes into daughter cells. This mechanism occurs in 6 main stages: 1. The DNA condenses in *Prophase*; 2. The nuclear envelope breaks down, freeing the condensed DNA inside the nucleus in *Prometaphase*; 3. The sister chromatid pairs attach to the spindle MTs and align along the center of the cell known as the metaphase plate in *Metaphase*; 4. The sister chromatids are pulled to opposite poles in *Anaphase*; 5. The new daughter cells form nuclear envelopes around recently separated chromosomes in *Telophase*; 6. The plasma membrane is divided along the center of the cell, separating it into 2 new cells through *Cytokinesis* (Figure 1.1). Each chromatid has a kinetochore complex that attaches the chromatid to dynamic spindle MTs. During early mitosis, the kinetochore-MT attachments are weak and transient, allowing chromatid pairs that are not properly attached to opposite spindles (known as biorientation) to detach from spindle MTs and reattach elsewhere. The mitotic checkpoint (also known as the spindle assembly checkpoint, SAC) prevents entrance into anaphase until the condensed sister chromatids are properly bioriented, ensuring that each daughter cell receives only 1 copy of every chromosome after division. Upon proper biorientation, the SAC is deactivated, and kinetochore-MT attachments become stable, marking the entrance into anaphase.

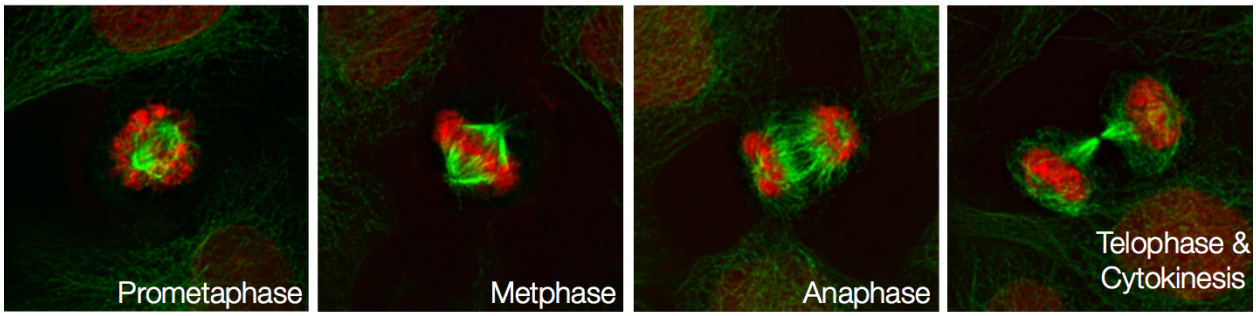

Figure 1.1: Cells in mitosis
Representative images of cells in each stage of mitosis illustrating the dynamics between microtubules and chromosomes in each phase. Microtubules are visualized in green and DNA is shown in red.

Antimitotic agents can trigger the SAC, which can leave cells susceptible to apoptosis. A properly functioning SAC is essential to prevent mitotic errors and preclude chromosomal instability (CIN). CIN increases the risk of lethal chromosomal imbalances. However, at

controlled levels, CIN can increase the mutational capacity of cancer cells, leading to rapid tumor evolution and progression (36-39). Thus, CIN is a hallmark of solid tumors (40). Although the SAC prevents CIN, many cancers, including GBM, often have increased SAC protein activity (33, 41, 42). The prevailing hypothesis to explain this counterintuitive phenomenon is that the upregulated SAC activity seen in many tumors contains CIN within a limit that allows tumor cells to survive and evolve (41, 43, 44). Therefore, targeting SAC processes may hold therapeutic value for treating cancers such as GBM.

Recently, researchers discovered that core SAC proteins, including BUBR1, PLK1, and MPS1, are specifically required for cancer cell viability, uncovering valuable therapeutic targets (33, 45, 46). Six PLK1 inhibitors have been tested in phase I or II clinical trials for various cancers (44). Volasertib (BI-6727) is effective against GBM *in vitro* and received a breakthrough therapy designation from the FDA for acute myeloid leukemia (44, 47). Small molecule inhibition of MPS1 is also effective in a variety of cancers *in vitro* and *in vivo* (48-50). These studies substantiate the presence of a cancer-specific susceptibility to mitotic perturbation that can be exploited for targeted cancer treatment.

In addition to SAC protein inhibitors, antitubulin agents also disrupt mitotic processes and are frequently used to treat cancer. These agents promote spindle defects that prolong the activation of the SAC, leading to cell cycle arrest and apoptosis (51). Antitubulin drugs are divided into 2 classes: MT stabilizing agents that prevent depolymerization at high concentrations (*i.e.* paclitaxel), and MT destabilizing agents that increase MT breakdown or prevent growth at high concentrations (*i.e.* vincristine, and colcemid). Given that these compounds non-specifically target dynamic MTs, antitubulin drugs have less selectivity towards tumor cells than SAC protein inhibitors. However, due to the delicate balance that exists in tumor cells between hyperactive SAC proteins and mitotic defects, tumor cells may be more sensitive to additional insults to the spindle machinery. Accordingly, MT disruption has been found to synergize with MPS1 inhibition in HeLa xenograft models and in orthotopic GBM models (49, 50).

Antitubulin agents have several important drawbacks when considering their use as GBM therapies. Specifically, these compounds are generally not brain-penetrant and induce a concerning level of peripheral neurotoxicity, which raises questions regarding their safety if delivered to the brain [reviewed in (52)]. Nonetheless, multi-drug regimens containing vincristine have been used to treat high-grade gliomas, including GBM (53, 54), though their efficacy has been disputed due to a lack of adequate brain penetrance (55). Epothilones, brain-

penetrant MT stabilizing agents, are clinically approved to treat advanced paclitaxel-refractive breast cancer and have been investigated for use in GBM (56-58); however the clinical efficacy of sagopilone has been disputed in patients with recurrent GBM (59, 60). It is clear that safe and effective MT-targeting drugs have not yet been developed for use in GBM. Nonetheless, the success of MT-disrupting TTFields combined with the clinical success of antitubulin agents in other cancers maintains a level of enthusiasm for the identification of chemically optimized MT-targeting agents to treat GBM (34, 61).

GPCRs: Central controllers of cellular signaling

Fifty to sixty percent of all marketed drugs target GPCRs (62), but few such drugs have been tested for their therapeutic potential on GBMs. The GPCR family is composed of over 900 members divided into six classes. All GPCRs share a common heptahelical structure, and different GPCR classes are defined by sequence homology (63). GPCRs control an array of signaling pathways that intimately interact with and modulate RTK signals that can control the migration and growth of tumors.

In addition to affecting oncogenic signaling pathways, GPCRs are involved in regulating the differentiation state of cells and can be overexpressed by GSCs (64, 65). A recent study aimed at profiling GPCR expression in GSCs, healthy astrocytes, neural stem cells, and GBM cell lines identified 8 GPCRs that are exclusively expressed by GSCs (including LPHN2, GPR37, CALCRL, HRH2, GPR73, $S1PR_5$, GPR128, and GPR103), revealing several new therapeutic targets to explore within the GPCR family (66). Accordingly, GPCRs represent valuable molecular modulators to control the cancer stem cell phenotype.

GPCR signaling can be broken down into 3 main branches: the canonical activation of G proteins, the deactivation of the receptor and scaffolding of downstream signaling by β-arrestins, and the non-canonical transactivation of RTKs. In the canonical GPCR signaling pathway, activation of the receptor by its ligand leads to binding and stimulation of a heterotrimeric G protein (Gαβγ). The Gα subunit is activated by GDP/GTP exchange that results in the dissociation of the Gβγ subunit, and both subunits activate downstream second messengers to elicit a cellular response. The Gα subunit is divided into four main subtypes: $G\alpha_s$, which stimulates cAMP production; $G\alpha_{i/o}$, which inhibits cAMP production; $G\alpha_{q/11}$, which stimulates phospholipase C (PLC) and calcium mobilization; and $G\alpha_{12/13}$, which regulates actin cytoskeleton remodeling through the activation of small GTPases. The Gβγ subunit can also

directly affect cAMP production, tyrosine kinase and RTK activation, and ion channel activation, which add an additional level of complexity to GPCR signaling (63).

The G protein signal is terminated when Gα hydrolyzes GTP to GDP and re-associates with Gβγ. In addition, GPCRs can be deactivated or internalized through the actions of kinases and β-arrestins. Phosphorylation of serine and threonine residues on the receptor by protein kinase A (PKA), protein kinase C (PKC), or GPCR regulating kinases (GRKs) provides a docking site for β-arrestin. This protein sterically hinders further G protein coupling and mediates the internalization of the GPCR. Therefore, loss of activity or expression of either GRKs or β-arrestins could lead to an increase in GPCR signaling. For example, GRK3 is downregulated specifically in the classical subtype of GBMs, and this loss of GRK expression is thought to be associated with sustained oncogenic signaling of GPCRs (67). Further supporting this hypothesis, the loss of β-arrestin 1 activity is positively correlated with glioma malignancy (68). Alternatively, β-arrestins can initiate mitogenic signaling by serving as adapter proteins for mitogen activated protein kinase (MAPK) signaling components, such as ERK, JNK, and p38 (69). GRK5 is upregulated in GBM and GSCs, and knockdown of this protein reduces the proliferation of these cells, a phenomenon that could result from increased MAPK signaling through recruited β-arrestins (70). The complexity of GPCR signaling brands these receptors as **“**molecular hubs” that control a wide array of downstream effectors.

Recent advances in our understanding of GPCR signaling mechanisms have led to the realization that these receptors are involved in multiple non-canonical signaling pathways. For example, the transactivation of RTKs, such as EGFR, by GPCRs is instrumental in controlling cellular processes, such as growth, migration, and angiogenesis. This crosstalk has been shown to contribute to the progression of many cancers (71-73). RTKs are single pass membrane proteins that dimerize upon ligand binding, allowing each monomer to transphosphorylate key tyrosine residues on the receptor. These phosphorylated residues serve as docking sites for adaptor proteins containing a Src Homology 2 (SH2) or phosphotyrosine binding domain (PTB) that anchor downstream signaling components of mitogenic pathways, such as MAPK, RAS, and PI3K (Figure 1.2). GPCRs activate growth factor receptors via two mechanisms: 1) extracellularly, by promoting the release of growth factors that provide autocrine or paracrine stimulation or 2) intracellularly, through phosphorylation cascades (Figure 1.2) (74-76). In the first scenario, GPCR signaling leads to the activation of the matrix metalloproteinase (MMP) tumor necrosis factor alpha-converting enzyme (TACE), which then cleaves growth factors from the membrane and results in the autocrine activation of

growth factor receptors that can mediate a variety of tumorigenic responses (72, 77-79). Alternatively, in the second scenario, GPCRs activate non-receptor tyrosine kinases, such as SRC, by direct interaction with by Gα or Gβγ (80, 81), which can phosphorylate tyrosine residues on RTKs (82). This evidence indicates that through a combination of classical G protein signaling and RTK transactivation, GPCRs can regulate crucial oncogenic pathways.

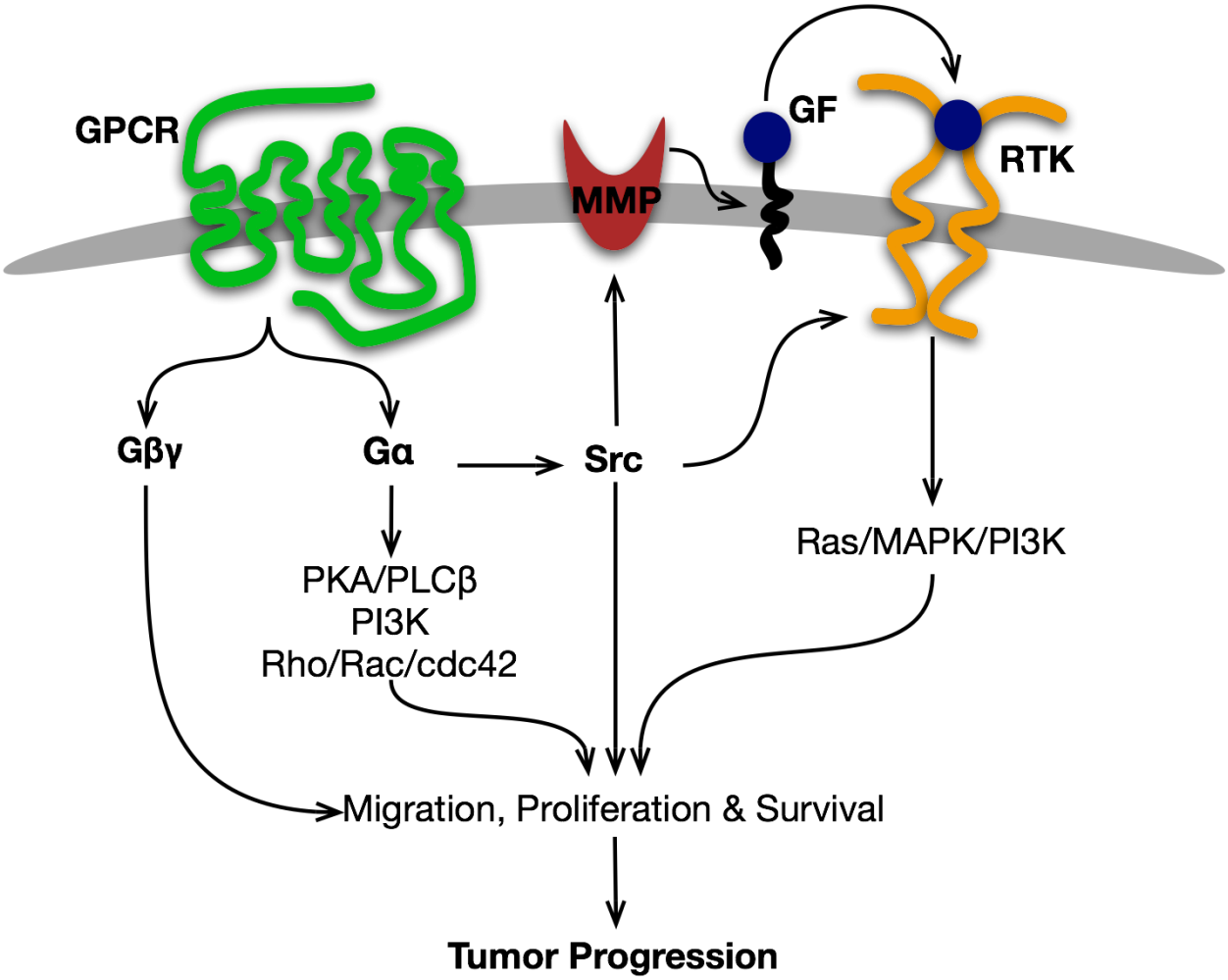

Figure 1.2: GPCR regulation of tumor growth processes
GPCRs activate heterotrimeric G proteins containing an α and a βγ subunit that separate upon activation. Gα proteins can stimulate pro-growth signaling through protein kinase A (PKA) and phospholipase Cβ (PLCβ), pro-survival signaling through phosphoinositol-3-kinase (PI3K), and pro-migration signaling through Rho, Rac, and cdc42. Moreover, Gα proteins can stimulate additional tumorigenic processes through activation of Src-family kinases. Src can activate RTKs directly through intracellular phosphorylation or indirectly by promoting matric metalloprotease (MMP)-dependent release of growth factors (GFs) from the plasma membrane. RTKs activate oncogenic Ras, mitogen activated protein kinase (MAPK), and PI3K pathways that can affect tumor growth and progression. Gβγ can additionally stimulate PKA, tyrosine kinases, and RTK activation via distinct mechanisms.

There are several examples of GPCR-targeted therapies that show promise for cancer treatment. The Smoothened receptor antagonist vismodegib has been clinically approved to treat basal cell carcinoma and is undergoing clinical trials for GBM (83, 84). This receptor is a member of the sonic hedgehog (SHH) signaling pathway that is normally vital to neural stem cell maintenance and the formation of therapy-refractive GSC populations (85). While multiple studies have shown that SHH signaling is activated in low-grade gliomas, whether it is hyperactive in GBM is still debatable (65, 86). This discrepancy likely arises from the heterogeneous nature of GBM and the comparatively small populations of GSCs that rely on SHH signaling (65). Additional support for the anti-glioma efficacy of Smoothened inhibition is found in studies using a distinct antagonist, cyclopamine, in xenograft models. Cyclopamine reduced GSC sphere formation, growth, and tumor engraftment as well as conferred a survival benefit in xenograft models of high-grade gliomas (65, 87). The concept of targeting the Smoothened receptor for glioma treatment is relatively new. However, because SHH signaling maintains populations of GSCs that are resistant to conventional therapy, this treatment modality shows considerable promise.

The chemokine receptor CXCR4 antagonist plerixafor is additionally undergoing clinical trials to treat GBM and has shown remarkable efficacy in preclinical models (88-91). CXCR4 expression correlates with tumor grade and is overexpressed by GBM cell lines and patient tissues (89, 92-95). Like mitogenic and oncogenic signals emanating from RTKs, CXCR4 and its endogenous ligand CXCL12 control invasiveness and tumor growth (95-97). Accordingly, comparative studies between plerixafor and RTK inhibitors have underscored the clinical promise of targeting CXCR4 to treat gliomas. For example, while the non-specific RTK inhibitors vatalanib and sunitinib increased tumor volume and cell invasion, respectively, in *in vivo* glioma models, plerixafor remained highly effective at reducing these indices of tumor severity (90). Additionally, plerixafor combined with radiotherapy prevented tumor recurrence and neovascularization more effectively than the VEGF neutralizing antibody DC101 (91). These preclinical studies combined with the favorable safety profile of plerixafor in humans (98) provide clear incentive to continue to elucidate CXCR4/CXCL12 signaling in GBM.

Significant advances in the standard of care for cancer treatment have occurred through the addition of therapies targeting driver mutations. Indeed, this effort fueled the development of breakthrough cancer treatments, including imatinib for chronic myelogenous leukemia and tamoxifen for breast cancer. Because RTKs function as prominent oncogenes in GBM, significant efforts have been dedicated to developing therapies that target these overactive

signaling pathways. Unfortunately, these efforts have yet to produce remarkable increases in survival. Owing to the ability of GPCRs to modulate RTK signaling and other parallel signaling pathways, GPCRs represent a promising class of therapeutic targets for the treatment of GBM.

Cannabinoid compounds in GBM

The cannabinoid GPCRs are of particular interest in the field of tumor biology. These 2 molecularly identified receptors, CB_1 and CB_2, have the remarkable ability to regulate several fundamental components of tumor cell biology. These processes include cell cycle arrest, loss of cell viability, reduction in tumor cell invasion, and GSC differentiation (64, 99, 100). Notably, despite their antineoplastic effects, compounds acting on cannabinoid receptors are not toxic to healthy cells (101). Cannabinoid receptors are activated by the endogenous cannabinoids, arachidonoylethanolamine (AEA, also known as anandamide) (102) and 2-arachydonoylglycerol (2-AG) (103-105); however, this signaling system derives its name from the naturally occurring cannabinoid receptor agonists produced by plants in the *Cannabis* genus, the most well-known of which is Δ^9-tetrahydrocannabinol (THC) (106, 107). A multitude of synthetic compounds, such as CP-55940 and WIN55,212-2 (CP and WIN-2, respectively), have additionally been produced to study the pharmacological effects of cannabinoid receptor engagement.

Cannabinoid compounds have the multifaceted ability to regulate a range of physiological processes including synaptic transmission, pain, and emesis (108-110). However, one of the most intriguing qualities of cannabinoid drugs is their ability to induce apoptosis in tumor cells and reduce tumor growth without apparent toxicity to healthy tissue (101, 111). The first evidence of this notable quality surfaced in 1975 when THC treatment of lung adenocarcinoma tumors implanted in mice inhibited tumor growth by 75% and increased lifespan by 36% compared with controls (111). Since then, cannabinoid treatment has proven to be effective in a number of xenograft tumor models [summarized in (112)]. In a landmark study published by Galve-Roperh et al., THC and WIN-2 eradicated orthotopic tumors in 1/5 (THC) and 1/3 (WIN-2) of the rats in the study. The remaining animals had significantly smaller and less vascularized tumors. Remarkably, there was no detectable cytotoxicity in the healthy brain tissue surrounding the site of original tumor growth, indicating that these drugs selectively kill malignant cells (101). GBM regression was also observed with a selective CB_2 agonist *in vivo* (113). These studies led to a small clinical trial to address the safety and possible therapeutic

efficacy of intratumoral THC injection in 9 patients with recurring GBM (114). The median survival of these 9 patients was 5.7 months after treatment initiation. In contrast, the median survival of patients with recurrent GBM is 7.4 months after re-operation of the recurrent tumor (115); however, the THC regimen remained very well tolerated and overt psychoactive effects were minimal. While a noteworthy improvement to the side effect profile could be regarded as a success, the failure of this treatment strategy to significantly extend survival might be attributed to small sample size and unverified variables such as delivery and dosing.

Mechanistically, THC induces tumor cell apoptosis by increasing ceramide lipid levels. Ceramide accumulation stimulates transcription of the ER stress protein p8, which subsequently inhibits AKT (Figure 1.3). The detailed molecular steps between activation of CB_1 and CB_2 receptors and increases in ceramide remain unclear, although initial evidence points to the involvement of serine palmitoyltransferase, the rate-limiting step in *de novo* ceramide synthesis (116-119). The ability of these receptors to couple to apoptosis is inversely correlated with their expression levels, which contributes further complexity to cannabinoid-induced cytotoxicity. Presumably, this phenomenon results from an increase in pro-survival AKT signaling in gliomas expressing high levels of CB_1 or CB_2, which is important to consider when developing cannabinoid-based therapies for GBM (119). These studies laid the foundation for evaluating the potential of cannabinoid-based drugs as antineoplastic therapies and for elucidating the signaling network mediating their selective killing of tumor cells.

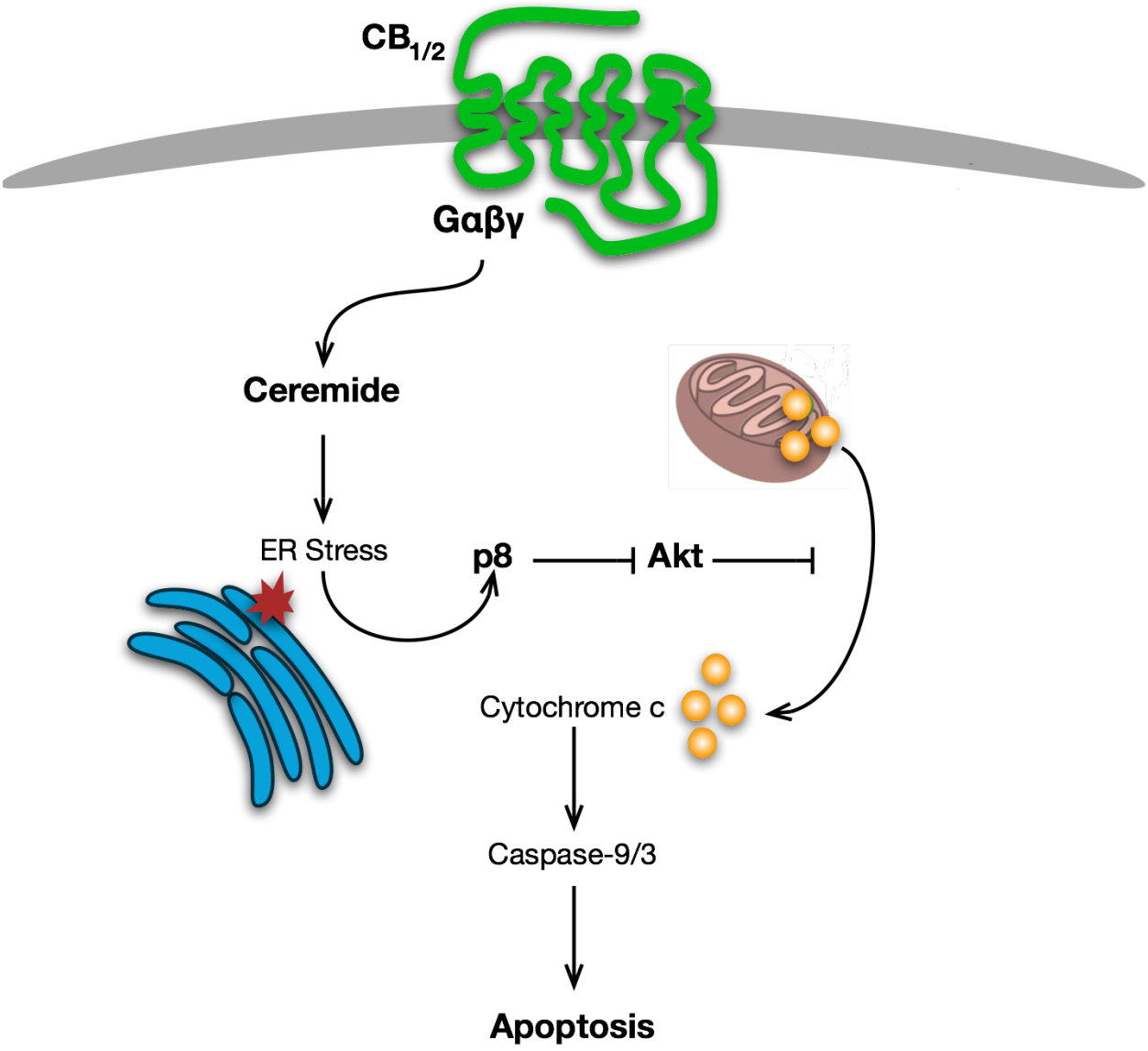

Figure 1.3: Cannabinoid receptor regulation of tumor cell death
Tumor cell death mediated by the cannabinoid receptors is dependent upon an increase in ceramide following the induction of serine palmitoyltransferase, which is the rate-limiting step in de novo ceramide production. Ceramide activates an ER-stress response, causing the upregulation of the stress protein p8, which inhibits the pro-survival factor Akt. Inhibition of Akt promotes cytochrome c release, which activates caspases that mediate apoptosis.

Uncovering the complexity of cannabinoid compounds

Cannabinoid compounds range across a broad spectrum of chemical structures that are defined by their ability to bind to both CB_1 and CB_2 receptors. These compounds can be divided into 5 classes based on their origin (*i.e.* plant-derived, endogenous, or synthetic) as well as their structure. The first class, known as the *classical cannabinoids*, comprises tricyclic-

dibenzopyran derivatives that originate from the plant *Cannabis sativa* and synthetic analogs such as HU-210. The *non-classical cannabinoids* make up the second class and include the synthetic CB_1 and CB_2 full agonist CP55,940. These compounds are structurally similar to members of the first class, however they lack the dihydropyran ring. The third class consists of the *alkylindole* (AI) compounds such as WIN-2 and JWH-015. These compounds are structurally dissimilar to other classes of cannabinoid compounds, although WIN-2 is a full agonist at both CB_1 and CB_2, and JWH-015 is a non-selective CB_2 agonist, illustrating the immense complexity of the cannabinoid system. The *endocannabinoids* 2-AG and AEA make up the fourth class and are derivatives of arachidonic acid. Lastly, the fifth class is composed of *inverse agonists* such as SR141716A and AM251. While the chemical structures of these compounds are structurally dissimilar, they share common features such as their hydrophobic nature that allows them to pass the blood-brain barrier, and their biological cannabimimetic effects.

The AI class of cannabinoids is particularly interesting owing to the fact that several effects of these compounds have yet to be attributed to CB_1 or CB_2 activity (120-122). Specifically, the mechanisms governing the antineoplastic activity of these compounds remain unclear. Several studies suggest that AI-based cannabinoids kill tumor cells through the activation of CB_1 and CB_2 receptors (123, 124); however, this response occurs at micromolar concentrations despite the fact that these compounds activate CB_1 and CB_2 receptors with nanomolar potencies (125). Additionally, antagonists for both CB_1 and CB_2 receptors only partially block the antineoplastic activity of AI-based cannabinoids. Together, this evidence suggests that AI-based cannabinoids kill tumor cells via a non-CB_1/CB_2-mediated mechanism.

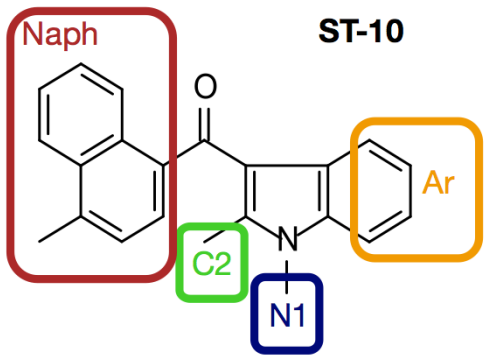

Figure 1.4: ST-10, the ST compound prototype. Naph: Naphthalene; Ar: Aromatic.

Development of novel AI compounds to study their antineoplastic activity

In an effort to characterize the mechanism employed by AI cannabinoids to kill tumor cells, our laboratory created a library of compounds that are structurally analogous to WIN-2, referred to as ST compounds (Figure 1.4). Because little is known about the antineoplastic activity of AI compounds, the Stella laboratory performed a structure activity relationship analysis of 25 AI compounds in T98G

cells using WST-1, a reagent that measures mitochondrial output, to assess viability. This small library of compounds combines 9 commercially available AI compounds with 16 newly developed ST compounds (Table S1) (126, 127). These analogs are derived from a prototypical compound, 1,2-dialkyl-3-aroylindole (ST-10) that contains an indole ring linked to a naphthalene group (Figure 1.4). Our AI analogues test modifications to the aromatic group as well as to the C-2 and N-1 positions on the indole ring. We observed that 8 of the compounds (JWH-015, JWH-148, ST-11, ST-24, ST-25, ST-27, ST-29 and ST-30) killed T98G cells with a greater potency than WIN-2 (Table S1, highlighted with **), revealing key chemical moieties necessary for antineoplastic activity. Specifically, the 10- and 7-fold changes in EC_{50} between ST-21 and ST-26 and between ST-23 and ST-31, respectively, indicate that modification of the aromatic moiety is likely to affect activity. Moreover, the loss of activity measured with JWH-120 and JWH-200 suggests that the C-2 position is exquisitely sensitive to modifications. Conversely, the minor changes in EC_{50} measured between ST-10, ST-11, ST-29, ST-30 and JWH-148 (1.0–2.9 μM) imply that the length of the chain appended to N-1 is not critical for potency. Finally, the 15-fold change in EC_{50} between ST-11 and ST-47 suggests low flexibility in naphthalene modifications. ST-11 was selected to confirm that neither CB_1 nor CB_2 receptor engagement contributes to the antineoplastic activity of AI compounds. Treatment of T98G glioma cells with antagonists to each receptor subtype (SR141716 for CB_1, SR144528 for CB_2) produced no effect on ST-11-mediated cell killing (Figure 1.5A). Additionally, T98G cells do not express CB_1 or CB_2 receptors (Figure 1.5B). Thus, ST-11 represents a novel cannabinoid-based AI compound that selectively kills glioma cells through a non-CB_1/CB_2-dependent mechanism.

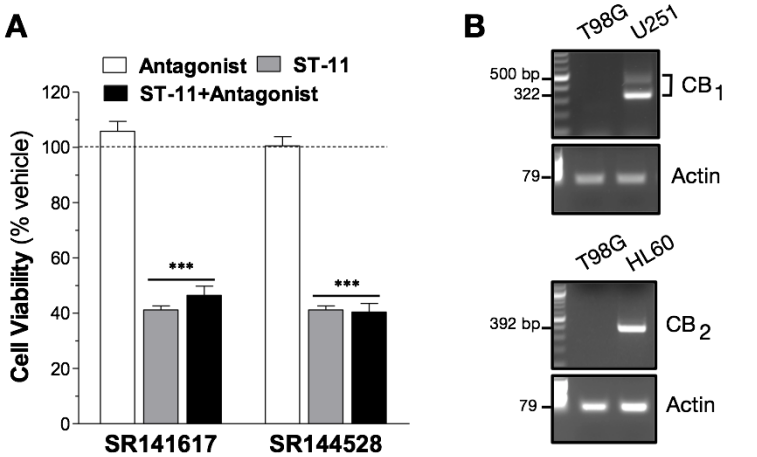

Figure 1.5: ST-11 does not kill GBM cells through cannabinoid receptor engagement.
(A) Pretreatment of T98G cells with antagonists to CB1 (SR141617, 30 nM) or CB2 (SR144528, 300 nM) for 10 min did not affect the reduction in cell viability induced by ST-11 (3 μM). (B) CB1 and CB2 mRNA expression in T98G, U251 (positive control for CB1), and HL60 (positive control for CB2) cells. Bands represent an intron-spanning region of each receptor mRNA, and primers were designed to recognize multiple mRNA variants. Beta-actin was used as a loading control.

Our lab has identified a novel agent, ST-11, that kills glioma cells through an unknown mechanism. The following chapters outline two studies designed to identify the novel molecular mechanism of this compound in glioma cells. This work led to the discovery of new proteins involved in the regulation of MT dynamics and cancer cell sensitivity to antitubulin agents. Mechanistically, ST-11 was found to permeate the cell to act directly on MTs to arrest cell division and induce apoptosis in gliomas. The orphan GPCR GPR124 was additionally identified as a key regulator of the efficacy of this compound, revealing a link between MT-dependent processes and GPCR signaling. I determined that GPR124 reduces tumor growth by directly interacting with the MT polymerizing enzyme ch-TOG to increase the dynamics of spindle MTs during mitosis. The functional consequence of raising spindle MT dynamics is the promotion of mitotic errors that reduce overall tumor growth. Thus, I have identified a novel molecular and functional interaction between GPR124 and MTs that disrupts mitotic processes, leading to inhibited proliferation and differential cellular sensitivity to antitubulin agents. My discovery of GPR124 as a controller of MT dynamics provides evidence that GPR124 has tumor suppressive properties and relevant therapeutic value. This research will bring new light to the field of cancer cell division, adding an additional GPCR-regulated branch to our understanding of mitotic mechanisms. The continued chemical optimization of ST compounds that will be aided by our new mechanistic understanding of their function will lead to promising new therapeutic candidates for GBM treatment.

CHAPTER 2

Alkylindole compounds target microtubules

Introduction

GBM is a devastating and intractable type of cancer. Current antineoplastic drugs do not improve the median survival of patients diagnosed with GBM beyond 14-15 months in part because the blood-brain barrier is generally impermeable to many therapeutic agents. The standard of care for GBM patients consists of surgery, radiation and the DNA intercalating agent TMZ (Temodar®) (2). Non-selective chemotherapeutics remain the sole drug treatment option for this patient population in large part because recent targeted therapies, such as gefitinib and bevacizumab that block EGFR and VEGF signaling, respectively, have fallen short of expectations (24-27). This realization has underscored the need for novel therapeutics to combat GBM through a distinct mechanism of action; however, the development of new GBM therapeutics is complicated by the necessity for efficient brain penetrance.

A recent study demonstrated that GBM cells are particularly sensitive to mitotic disruption compared with matched nonmalignant cells (33). This finding has led to the notion that innovative therapies that perturb MT assembly may represent a promising strategy to manage this type of cancer. For example, TTFields function by disrupting MTs and show significant efficacy as novel GBM treatments (34, 61). This result indicates that antitubulin agents are likely to show antineoplastic efficacy in patients diagnosed with GBM; however, the

majority of antitubulin agents do not readily cross the blood-brain barrier [Reviewed in (52)]. In fact, of the few brain-penetrant antitubulin agents, only 2, sagopilone (ZK-EPO) and the non-analgesic opioid noscapine, have been evaluated for glioma indications (57, 128). However, sagopilone suffered from a lack of efficacy in clinical trials (60), and noscapine required high doses to elicit an effect (128). Irrespective of the limited success of currently available compounds, the susceptibility of GBM cells to mitotic perturbation holds considerable promise for the treatment of this type of cancer (33). To this end, it is necessary to discover and develop novel brain-penetrant antitubulin agents with high therapeutic potential.

Our lab has recently developed a library of AI compounds with the capacity to kill glioma cells *in vitro* (126, 127). Here, we used a combination of biochemical and cell biology approaches to demonstrate that the AI compound ST-11 arrests the cell cycle and kills glioma cells by directly acting on MTs. To determine the pharmacokinetics (PK) and *in vivo* efficacy of ST-11, we established a stable formulation of this compound in liposomes and developed a liquid chromatography-mass spectrometry (LC-MS) method to quantify ST-11 in blood and brain. Using these tools, we determined that ST-11 readily penetrates mouse brain after intraperitoneal (i.p.) injection and dose-dependently reduces tumor volume in a syngeneic GBM mouse model. Importantly, ST-11 does not produce overt toxicity in mice. Our study highlights the therapeutic potential of AI compounds as novel brain-penetrant antitubulin agents with antineoplastic activity in GBM.

Results

ST-11 inhibits proliferation and kills GBM cells in vitro

A library of 25 AI analogues was screened for activity on the human GBM cell line T98G (Table S1). The first-generation compound ST-11 exhibited a combination of properties requisite for further mechanistic and *in vivo* analyses: it reduced T98G cell number with high potency and efficacy, and it encompasses the basic chemical scaffold of the series (the ST compound library) (Figure 2.1A, Table S1). Thus, ST-11 was selected for further screening on additional human GBM cell lines, including 4 adherent cell lines (U251, A172 and U87MG cells) and 2 stem cell lines (MGG4 and MGG8) (129). ST-11 reduced cell number in all of the GBM lines tested when applied at micromolar concentrations (EC_{50} from 2.4 – 8.6 μM, maximal efficacy from 51 – 96%) (Table 1). A vital and desired feature of any new antineoplastic drug is a

favorable therapeutic index, which is related to the preferential activity of the compound for tumor cells. Thus, we tested the antineoplastic activity of ST-11 on malignant and non-malignant mouse cells. ST-11 killed mouse DBT glioma cells with a potency and efficacy similar to T98G cells (EC_{50} = 2.5 μM, maximal efficacy = 60.7%). Notably, this compound did not affect the viability of primary mouse astrocytes or neurons (Figure 2.1B). Therefore, ST-11 preferentially targets a variety of GBM cell lines, including glioma stem cells, which tend to be refractive to therapy (3, 4).

Cells	Potency (μM)	Efficacy (% Dead)
MGG8	4.6	96.0
BT74	2.4	89.9
A172	5.8	68.2
U251	4.3	67.0
T98G	2.5	65.7
U87	5.5	63.2
MGG4	8.6	51.3

Table 2.1: ST-11 preferentially kills GBM cells over mouse astrocytes and neurons in culture. GBM cell lines were treated with ST-11, and cell number was measured after 72 hrs using WST-1. Dose-response curves were analyzed and data shown are the mean ± SEM from at least 3 independent experiments.

A loss of cell number can result from reductions in cell proliferation and/or increases in cell death. In order to delineate between both outcomes, we initially determined if ST-11 reduces cell viability using a trypan blue exclusion assay. We discovered that ST-11 dose-dependently increased the percentage of dead cells (EC_{50} = 2.9 μM, maximal efficacy = 68%) (Figure 2.1C). We then ascertained whether ST-11 reduces cell proliferation using 2 independent approaches. First, we measured the dose-dependent effects of ST-11 on [^{3}H]-thymidine incorporation in T98G and DBT cells and found that this compound reduced [^{3}H]-thymidine uptake in both T98G and DBT cells within 24 hrs of treatment (Figures 2.1D and S2.1A). Second, we monitored the time-dependent effects of ST-11 action on the accumulation of 2 mitotic markers: cyclin-B1 and phospho-histone H3. Application of ST-11 led to an increase in both cyclin-B1 and phospho-histone H3 levels (Figures 2.1E and 2.1F). Thus, we propose that ST-11 reduces GBM cell number by arresting cells in mitosis and subsequently killing them.

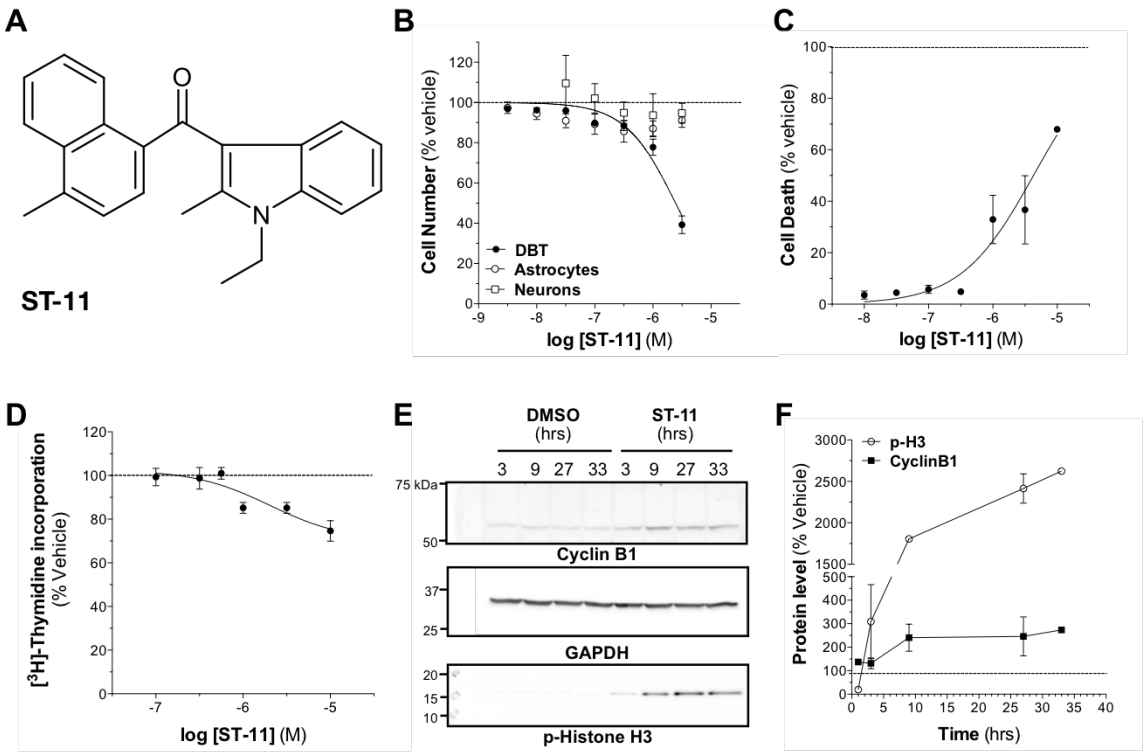

Figure 2.1: ST-11 reduces proliferation and kills T98G cells *in vitro*
(A) Chemical structure of ST-11. (B) Viability of mouse DBT, astrocytes and neurons measured with WST-1 72 hrs after ST-11 treatment. (C) T98G cell death measured with trypan blue 72 hrs after ST-11 treatment. (D) [3H]-thymidine incorporation in T98G cells 24 hrs after ST-11 treatment. (E-F) The time-dependent accumulation of cyclin-B1 and phospho-histone H3 after ST-11 treatment (3 μM) shown by a representative western blot (E) and quantified using GAPDH as a loading control (F). Data are the mean ± SEM of at least 3 independent experiments.

ST-11 arrests cells in prometaphase by directly targeting MTs

To further confirm our hypothesis that ST-11 arrests GBM cells in mitosis, we quantified the proportion of cells in each stage of mitosis after application of ST-11. Our compound increased the percentage of prometaphase T98G and DBT cells in a dose-dependent manner (Figure 2.2A and S2.1B), suggesting that ST-11 arrests cells in mitosis by triggering the SAC [reviewed in (130)]. In line with this observation, we also noted that ST-11 both dose-dependently increased the proportion of cells with multipolar spindles (Figures 2.2B and S2.1C) and induced severe defects in chromosomal biorientation (Figure 2.2C).

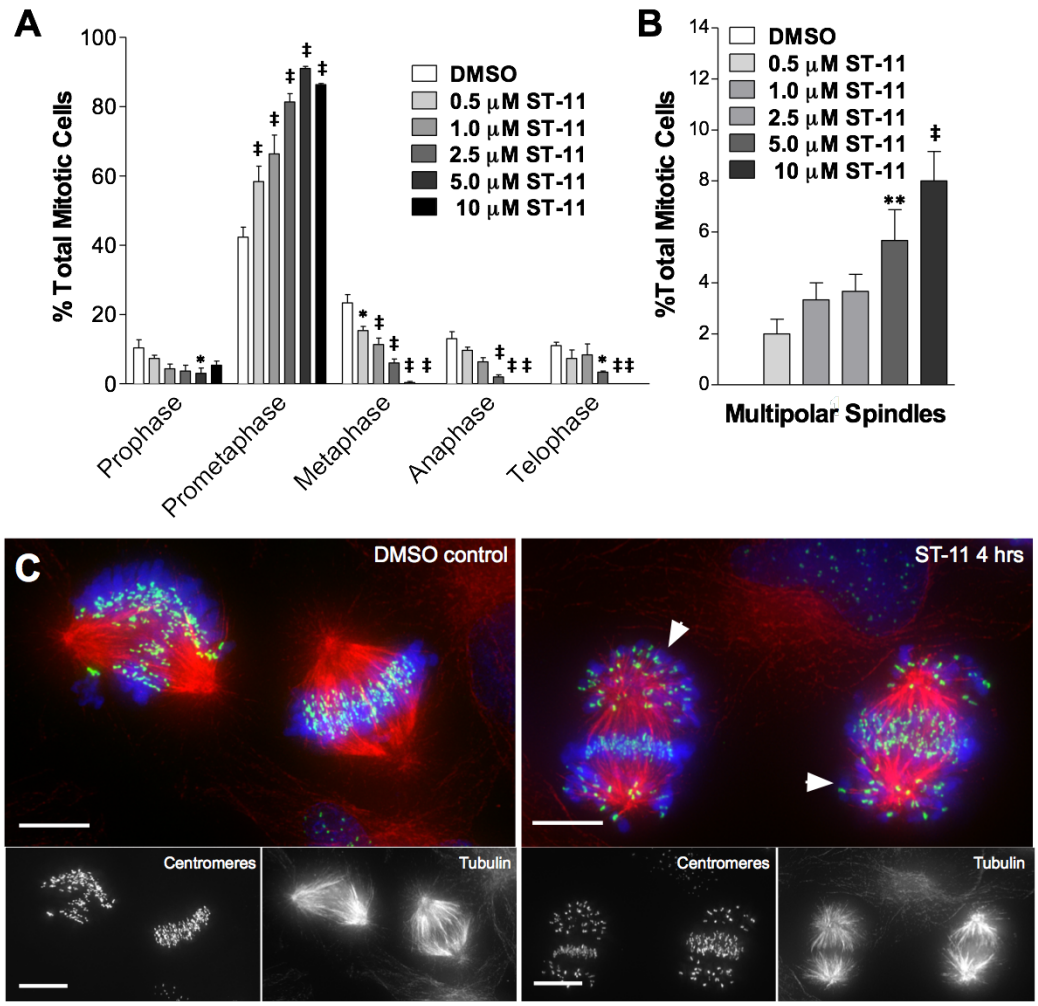

Figure 2.2: ST-11 arrests cultured T98G cells in prometaphase
(A) Percentage of cells in each stage of mitosis after treatment with ST-11. *p<0.05, ‡p<0.001 compared with vehicle, two-way ANOVA with Bonferroni post-hoc test. (B) ST-11 dose-dependently increases the formation of multipolar spindles. **p<0.01, ‡p<0.001 compared with vehicle, one-way ANOVA with Tukey post-hoc test. Data are the mean ± SEM of at least 3 independent experiments. (C) Representative images of ST-11-induced (5 μM) abnormalities in chromosomal alignment (arrowheads). Tubulin is shown in red, centromeres in green, and DNA in blue. Scale bars: 10 μm.

Improper spindle assembly can be attributed to defects in MT dynamics and polymerization. Thus, we used 3 approaches to determine whether ST-11 was acting directly on MTs. First, we used a cell-free assay with purified tubulin to assess the partitioning of MT dimers and polymer. As expected, the MT destabilizing agent nocodazole triggered an increase the free tubulin (Figure 2.3A). Conversely, a decrease in free tubulin levels was observed upon addition of the MT stabilizing agent paclitaxel (Figure 2.3A). Similar to nocodazole, ST-11 dose-dependently increased the level of free tubulin, which corresponds to MT disassembly (Figure

2.3A). Thus, ST-11 destabilizes MTs in a cell-free system containing purified MTs. The EC_{50} of ST-11 on MT destabilization (EC_{50} = 3.7 μM) is similar to its EC_{50} on T98G and DBT cell viability, indicating MTs may be the direct molecular target of ST-11 involved in its antineoplastic effect. Second, we assessed whether ST-11 affected MT polymer levels in T98G cells *in vitro*. MTs were significantly less abundant in T98G cells treated with ST-11, indicating that this compound directly acts on MTs in cells (Figure 2.3B). Lastly, using live cell imaging of EB3-GFP on assembling MTs in T98G cells, we found that sub-micromolar concentrations of ST-11 (0.5 μM) decreased the MT assembly rate by 32% within 10 min of treatment (Figures 2.3C and 2.3D). Together, these results indicate that ST-11 directly acts on MTs to reduce MT assembly, leading to mitotic spindle defects and prometaphase arrest in GBM cells.

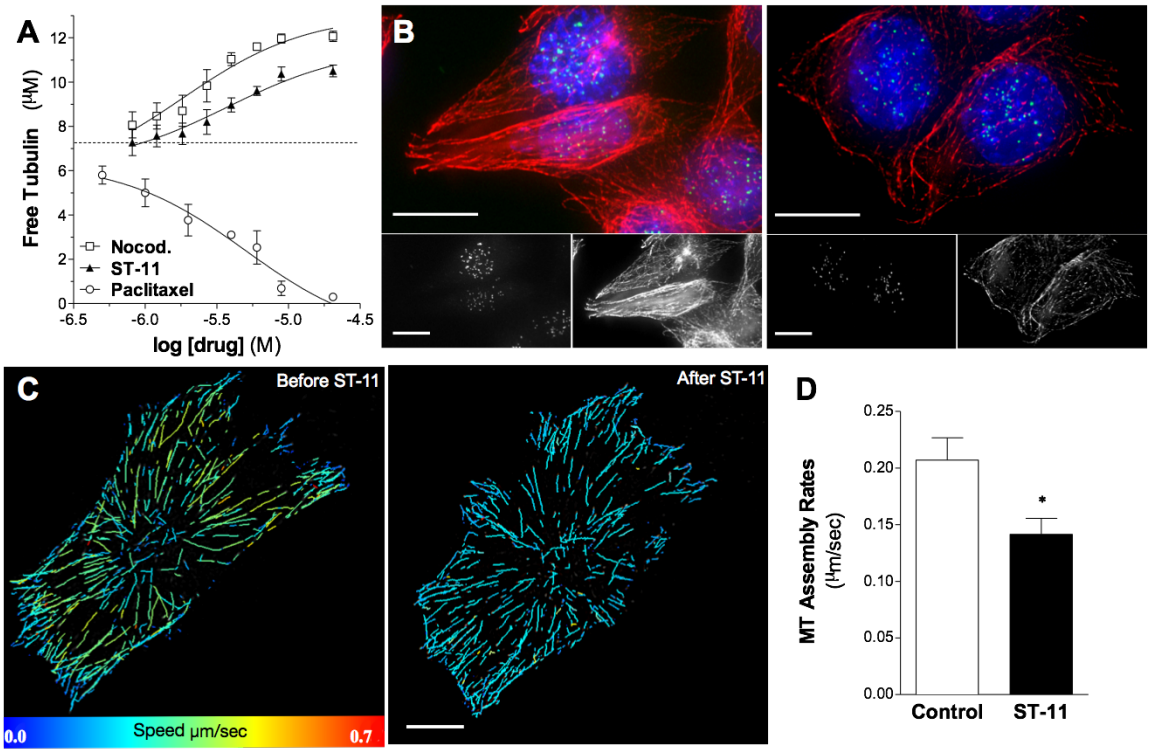

Figure 2.3: ST-11 directly destabilizes MTs and decreases their assembly in cultured T98G cells
(A) Incubation of ST-11 with purified tubulin induced a dose-dependent increase in free tubulin. Paclitaxel and nocodazole were used as positive controls to decrease and increase free tubulin, respectively. The dashed line indicates the steady-state level of free tubulin established prior to the addition of antitubulin agents (7.8 μM). Results are the mean ± SEM of at least 3 independent experiments (B) Representative images of ST-11 (5 μM) disrupting MTs in T98G cells. Tubulin is shown in red, centromeres in green, and DNA in blue. Scale bars: 10 μm. (C-D) ST-11 (0.5 μM) slows MT dynamics within 10 min of treatment (C, quantified in D). *p<0.05, Student's t-test. Scale bars: 10 μm. Data are the mean ± SEM of at least 3 independent experiments.

ST-11 activates caspase-3-dependent apoptosis

Antitubulin agents often promote caspase-dependent apoptosis (51). Therefore, we sought to determine whether ST-11 activated apoptosis in GBM cells *in vitro*. ST-11 induced caspase-3 activation in both T98G and DBT cells as early as 6 hrs after treatment (Figures 2.4A and S2.1D). This result was confirmed by western blot analysis 24 hrs after treatment with ST-11 (Figure 2.4B). Accordingly, this compound induced time-dependent cleavage of poly ADP ribose polymerase (PARP) (Figure 2.4C). Moreover, cells exhibited nuclear condensation and membrane blebbing within 24 and 48 hrs of ST-11 treatment, respectively (Figure 2.4A). Control experiments confirmed that inhibition of caspase-3 with Z-DEVD-FMK blocked the antineoplastic action of ST-11 (Figure 2.4D). Therefore, ST-11 activates caspase-3-dependent apoptosis in GBM cells.

To compare the *in vitro* efficacy of ST-11 with other antitubulin agents, we measured the time-dependent effects of ST-11, paclitaxel and nocodazole on T98G cell number using WST-1. By 12 hrs, all 3 compounds had reduced cell number by 10–15%. However, by 72 hrs, paclitaxel was inactive, whereas cell number was reduced by 34% with nocodazole and by 48% with ST-11 (Figure 2.4E). ST-11 was therefore more effective at reducing cell number than 2 antitubulin compounds, one of which (paclitaxel) is widely used in the clinic as an antineoplastic drug. This result suggests that further research into the *in vivo* safety and efficacy of ST-11 is warranted.

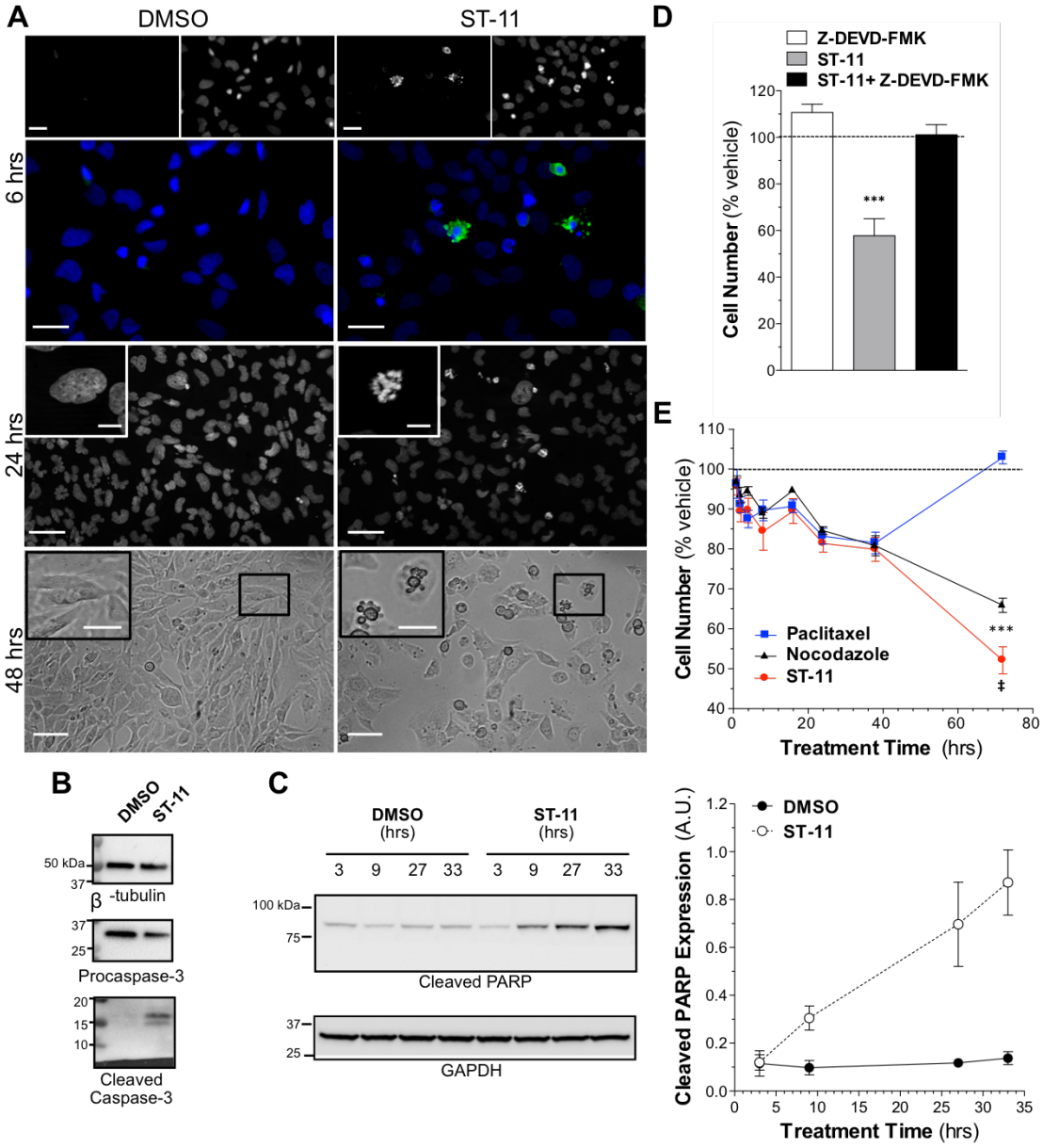

Figure 2.4: ST-11 triggers caspase-3-dependent apoptosis in cultured T98G cells
(A) Caspase-3 activation (green) correlating with condensed nuclei (blue) (upper panels), overt nuclear condensation (middle panels), and plasma membrane blebbing (lower panels) after treatment with ST-11 (10 μM) at the indicated times. Scale bars: upper and middle panels, 50 μm and 10 μm (inset); lower panels, 200 μm and 50 μm (inset). (B-C) Representative western blots showing activation of caspase-3 24 hrs after ST-11 treatment (3 μM) (B) and an increase in cleaved PARP (C, left) after ST-11 treatment (3 μM) for the indicated times. PARP cleavage was quantified using GAPDH as a loading control (C, right). Blots are cropped for conciseness, and molecular weights are indicated. (D) The antineoplastic effect of ST-11 (10 μM) was ablated by a caspase-3 inhibitor (Z-DEVD-FMK, 10 μM, 15 min preincubation). ***P<0.001 compared with vehicle, one-way ANOVA with Tukey post-hoc test. Data are the mean ± SEM of at least 3 independent experiments. (E) Cell number over a 72 hr period measured with WST-1 after treatment with ST-11 (10 μM), nocodazole (10 μM), or paclitaxel (10 μM). ***P<0.001 compared with paclitaxel, ‡p<0.001 compared with nocodazole, two-way ANOVA with Bonferroni post-hoc test. Data are the mean ± SEM of at least 3 independent experiments.

Solubility and safety of ST-11 in vivo

Since ST-11 does not adversely affect the viability non-malignant cells *in vitro*, we sought to study its safety *in vivo* by measuring its maximal tolerated dose (MTD) in mice. The lipophilic nature of ST-11 necessitated the establishment of an alternate formulation prior to delivery to mice. Standard solvents such as 30% mouse serum, 10% ethanol, 1% DMSO, 1% Tween-80, 2% Tween-80, 1:1:18 ethanol:Cremophor® RH40:saline, or 1% Tween-80 + 10% FBS did not solubilize ST-11 (Figure S2.2). Thus, we explored liposome formulations, which are composed of combinations of lipids that form semi-solid nanospheres (131). Our analyses revealed that ST-11 was soluble and stable for at least 14 days in nanospheres composed of 9:1:0.5 (m/m/m) EPC:DMPG:DMPE-mPEG2000 at a final lipid-to-drug ratio of 6:1 (m/m). This formulation was used to administer ST-11 in all subsequent *in vivo* experiments.

Initially, we assessed the MTD of ST-11 in a 5-day pilot dose-range finding study. Mice were treated with ST-11 (15, 40, 80, 160, and 240 mg/kg, i.p.) and monitored for signs of distress (see Materials & methods). No adverse effects were observed when the compound was administered at doses up to 240 mg/kg daily over 5 days, indicating that ST-11 appears to be well tolerated. In addition, tissue damage was assessed using H&E staining of 6 principal organs (heart, liver, kidney, lungs, spleen and brain). No signs of tissue injury were observed in any organ harvested from any ST-11 dosage group. However, we noted small lymphoid hyperplasias in the marginal zone of the spleen of mice treated with both 240 mg/kg ST-11 and the matched liposome-only control. This finding indicates that the large amount of liposomes injected in this condition induced a high rate of liposome phagocytosis in a manner that was independent of ST-11 (data not shown). This pilot safety study indicates that ST-11 is well tolerated at high doses and does not produce overt toxic effects when administered daily over a wide dose range.

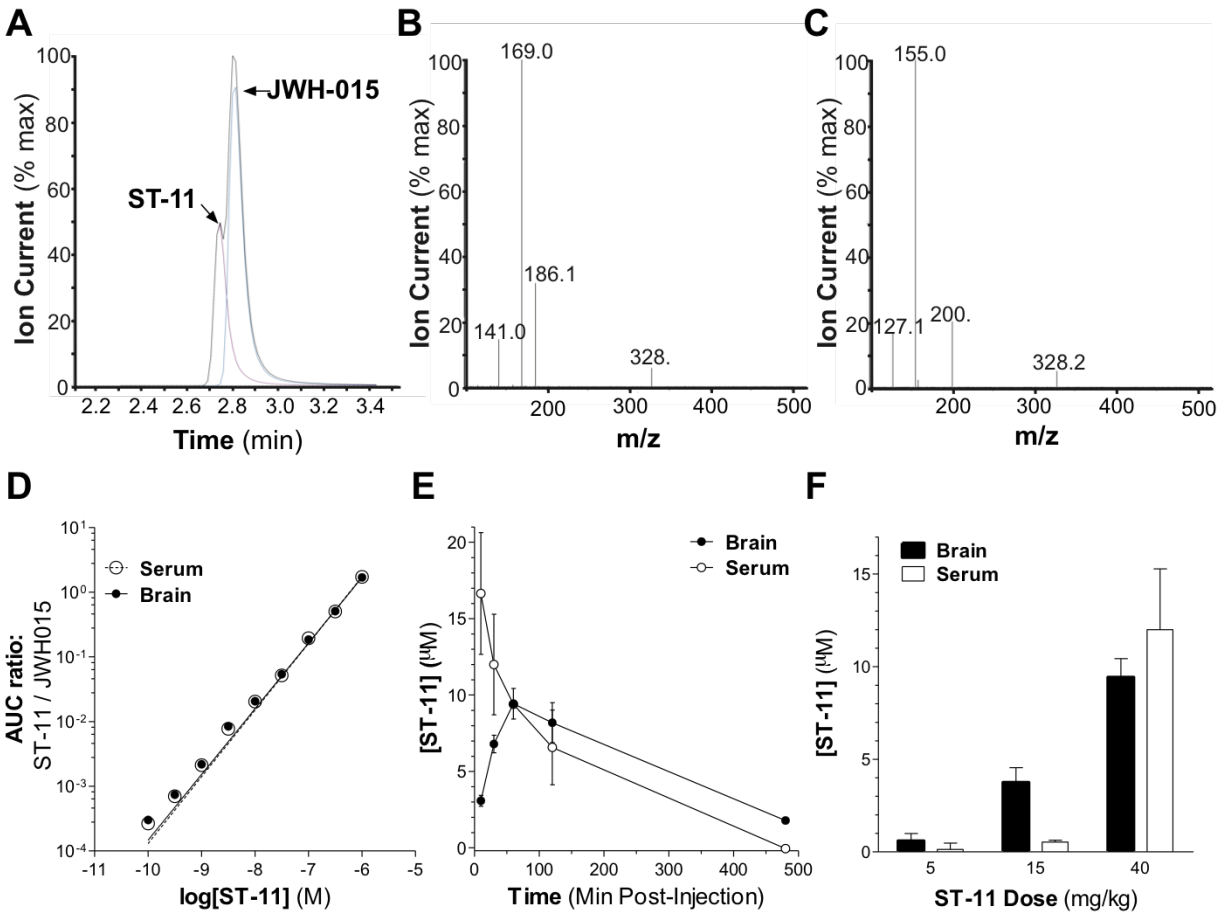

Figure 2.5: LC-MS and pharmacokinetic analysis of ST-11 in mouse serum and brain
(A) Elution time of ST-11 and JWH-015 showing total current (black line) and individual currents from ST-11 and JWH-015. (B-C) Resolution of ST-11 (B) and JWH-015 (C) daughter ions. (D) Quantification of ST-11 extracted from serum and brain matrices shows a linear range of detection from 30 fg – 1 ng. (E) Time course of ST-11 levels in serum and brain after i.p. injection of 40 mg/kg ST-11. (F) Brain and serum levels of ST-11 60 min after i.p. injection of the indicated doses. Results are presented as the mean ± SEM of 3 independent experiments.

Pharmacokinetic profile of ST-11

A limiting factor of the use of many antitubulin agents to treat GBM is their inability to cross the blood-brain barrier [Reviewed in (52)]. Thus, we established the PK profile of ST-11 in mice to evaluate whether this compound reaches the brain at concentrations that could produce antineoplastic activity (*i.e.* above its EC_{50} for killing GBM cells in culture). We developed an LC-MS method that quantifies ST-11 in biological matrices using a related compound, JWH-015, as an internal standard (see chemical structure in Table S1). Both compounds eluted at ~2.8 min (Figure 2.5A) and were independently detected with base peaks of 169.0 (ST-11) and 155.0 m/z (JWH-015) (Figures 2.5B and 2.5C). The quantification of ST-11 was linear from 30 fg to 1

ng (r^2>0.99) upon analyzing the compound when spiked into either blood or brain matrices (Figure 2.5D). The limit of detection was 100 fg and the limit of quantitation was 3 pg (error <10%). Thus, our newly developed method allows for the reliable and precise quantification of ST-11 from 0.1 to 1 ng in samples from mouse blood serum and brain tissue.

To establish the PK profile of ST-11, mice were treated with ST-11 (40 mg/kg, i.p.), and blood and brain tissue were harvested 10, 30, 60, 90, and 480 min after injections. Serum levels of ST-11 peaked after 10 min (C_{max} = 15.3 ± 3.6 μM), declined steadily thereafter and reached undetectable levels within 8 hrs post-injection (Figure 2.5E). By contrast, brain levels of ST-11 peaked after 60 min (C_{max} = 8.7 ± 0.9 μM) and remained above its average antineoplastic EC_{50} (*i.e.* 1.8 ± 0.2 μM) for up to 8 hrs. In a follow-up experiment, mice were treated with 5, 15, or 40 mg/kg ST-11 (i.p.), and blood and brain tissue were harvested 60 min post-injection. Both 15 and 40 mg/kg injections led to brain levels of ST-11 that were greater than the EC_{50} for killing GBM cells (Figure 2.5F). Hence, liposomes deliver micromolar concentrations of ST-11 to the brain within 60 min of i.p. injection that remain above its efficacious concentration for killing GBM cells for 4–8 hrs.

ST-11 induces apoptosis in orthotopic DBT tumors and reduces tumor volume

Finally, to determine if ST-11 affects GBM growth *in vivo*, we used a syngeneic mouse model in which DBT cells were orthotopically implanted into BALB/c mice (Figures 2.6A, S2.3 and S2.4). One week after DBT cell implantation, mice were treated daily with 5, 15 or 40 mg/kg ST-11 or the corresponding liposome vehicle for 2 weeks. The total volume of each tumor after 2 weeks was estimated by slab approximation and adjusted for the abundant invasion of microglia using semi-quantitative IHC analysis of Iba-1 (Figure S2.4). ST-11 treatment promoted a dose-dependent reduction in tumor volume (Figure 2.6B). Importantly, we detected a dose-dependent increase in caspase-3 activation, nuclear condensation and cellular loss within the tumor mass (Figure 2.6C). Collectively, these results indicate that i.p. administration of ST-11 dose-dependently activates apoptosis and reduces the volume of orthotopically implanted DBT tumors.

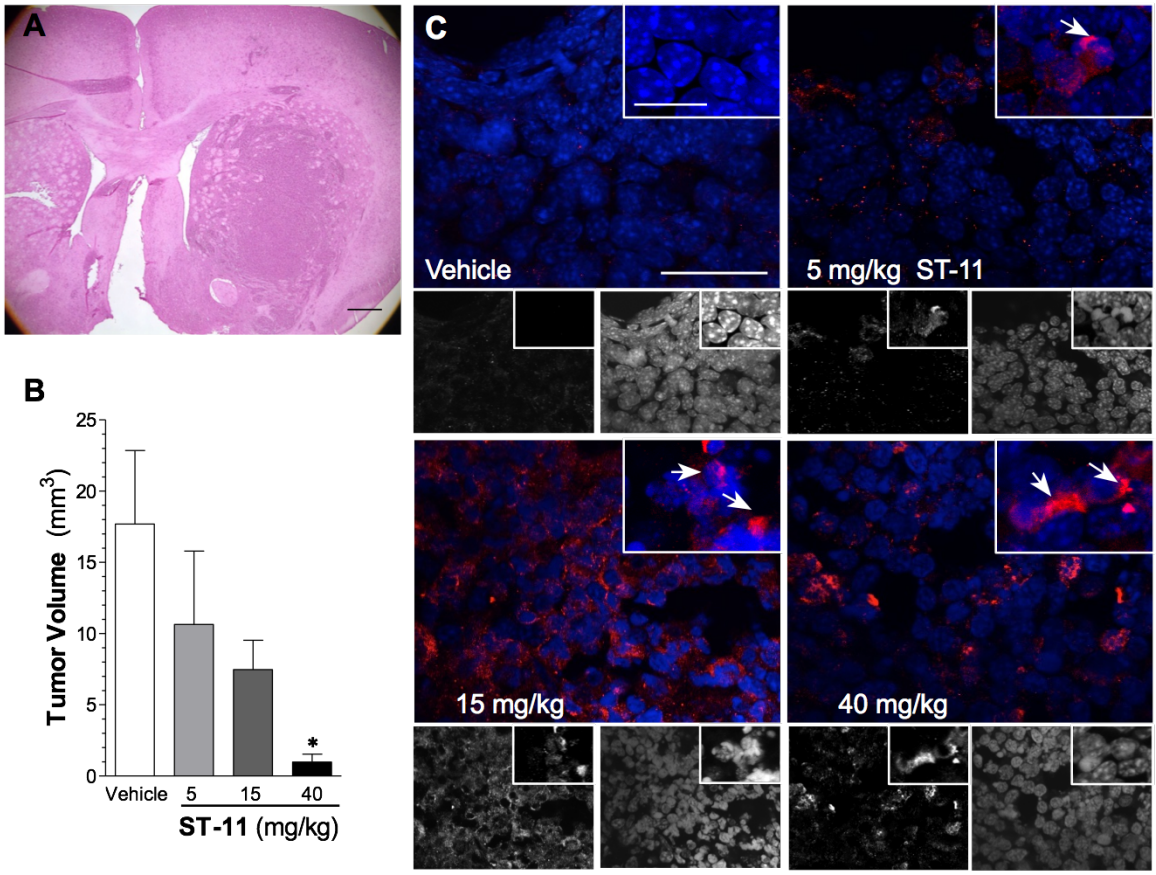

Figure 2.6: ST-11 activates caspase-3 and reduces mouse GBM tumors *in vivo*
(A) Representative image of a BALB/c mouse brain containing a DBT tumor harvested 3 weeks post-implantation and stained with H&E. Scale bar: 500 µm. Additional H&E features are presented in Figure S1. (B) Daily i.p. treatments of ST-11 for 2 weeks dose-dependently decreased tumor volume *p<0.05, one-way ANOVA with Dunnett's post-hoc test. Results are mean ± SEM of at least 5 mice. (C) Representative images of activated caspase-3 (red) and DAPI (blue) staining in DBT tumor slices obtained from mice given the indicated treatments. Scale bars: 25 µm and 10 µm (inset). Arrows show DBT cells with high levels of activated caspase-3 neighboring condensed nuclei.

Discussion

In this study, we describe the pharmacology and mechanism of action of ST-11, a novel AI compound that destabilizes MTs. This new compound displays 3 properties that are requisite for treating GBMs: 1) the ability to cross the blood-brain barrier, 2) preferential selectivity for killing GBM cells and 3) a favorable safety profile when administered at doses above its therapeutic efficacy. Our study not only provides a solid foundation for further chemical optimization of this compound but also launches the pharmacological and biological characterization of this new class of brain-penetrant antitubulin agents. Accordingly, ST-11 and

future derivatives may prove to be efficacious for the treatment of brain cancers such as GBM, which remain both one of the most devastating and therapeutically intractable forms of cancer.

ST-11 reduces GBM cell number by reducing both proliferation and viability. Mechanistically, we have discovered that this compound acts directly on MTs to reduce their assembly. The EC_{50} of the effect of ST-11 on MT destabilization in a cell-free assay is comparable to its EC_{50} for killing GBM cells. Taken together, these findings infer that tubulin is likely the primary target of this compound. Consistent with this result, ST-11 reduced the level of MT polymer and, at lower concentrations, the rate of assembling MTs *in vitro*. In living cells, MTs rapidly interconvert between assembly and disassembly. This dynamic action is essential for the proper spindle assembly, chromosome attachment and segregation during mitosis (132). Accordingly, we concluded that ST-11 suppressed MT dynamics in a manner that leads to aberrant spindle formation, improper alignment of chromosomes and cell cycle arrest in a prometaphase-like configuration. This effect is consistent with mitotic checkpoint arrest produced by the MT destabilizing activity of this compound.

Drugs that disrupt MT dynamics are commonly prescribed therapeutics as they both reduce tumor cell proliferation and trigger apoptosis (51). Our finding that ST-11 kills GBM cells through the activation of caspase-3-dependent apoptosis is evidenced by increases in caspase-3 and PARP cleavage, nuclear shrinkage and plasma membrane blebbing. Further support for this postulate is provided from our investigation of ST-11 on T98G cells where induction of apoptosis was ablated upon pretreatment with the caspase-3 inhibitor Z-DEVD-FMK. Therefore, we conclude that the principle mechanism of action of ST-11 is to directly suppress MT assembly, which leads to defects in mitotic spindle formation and chromosome attachment. This response is known to trigger mitotic checkpoint arrest and ultimately render glioma cells susceptible to apoptotic cell death.

A recent study designed to identify novel therapeutic targets for the treatment of GBM that do not adversely affect healthy brain cells revealed that this type of cancer is particularly sensitive to mitotic disruption (33). Other investigators have examined the efficacy and potency of indole-containing compounds on MT disruption and tumor reduction using different cancer models (133-135). For example, the antitubulin agent BPR0L075 effectively reduces tumor size in flank xenograft models of gastric and cervical carcinomas (134). Importantly, our studies suggest that ST-11 has increased therapeutic potential over other classical antitubulin compounds. Specifically, it has a higher efficacy and more lasting effect than either paclitaxel

or nocodazole on the viability of GBM cells *in vitro.* Thus, as a novel brain-penetrant compound, ST-11 underscores the therapeutic potential of antitubulin agents for the treatment of GBM.

Another feature of our study was the establishment of the PK profile of ST-11. We determined that single injections of 15 and 40 mg/kg resulted in micromolar concentrations of ST-11 in brain that exceed its EC_{50} for killing GBM cells in culture that persists for 4-8 hours. Hence, ST-11 dose-dependently activated caspase-3 and reduced tumor volume when delivered i.p. daily for 2 weeks. Importantly, we did not observe overt signs of toxicity in these mice during the treatment period (data not shown). Moreover, we monitored the MTD of ST-11 in a 5-day dose-range finding study that incorporated clinical and histopathologic assessments. These rudimentary analyses of ST-11 toxicity indicate that this compound does not produce overt side effects when administered chronically at 40 mg/kg or acutely up to 240 mg/kg *in vivo*. Importantly, this result agrees with our *in vitro* finding that ST-11 is nontoxic to non-malignant cells. Thus, we have derived a new delivery method that achieves therapeutic brain-levels of ST-11 and exhibits an encouraging safety profile when assessed in mice.

To conclude, our study introduces ST-11 as a novel brain-penetrant antineoplastic agent with preferential selectivity for GBM cells and no discernible toxicities in mice. The use of antitubulin agents for the treatment of GBM is all the more convincing when one considers that they act in a manner that has been anticipated to be effective for the treatment of this type of cancer (33). We therefore propose that ST-11 belongs to a promising new class of brain-penetrant antineoplastic agents that slow MT assembly, promote cell cycle arrest and trigger apoptosis in GBM. The future development and characterization of ST-11 analogs may ultimately lead to the advent of new drugs for the treatment of this intractable and debilitating form of brain cancer.

CHAPTER 3

GPR124 coordinates microtubule dynamics in cancer cells

Introduction

Antitubulin drugs such as taxanes (*i.e.* Taxol®, also referred to as paclitaxel) and *Vinca* alkaloids (*i.e.* vinblastine) are clinically applied antineoplastic agents that are used successfully to treat a variety of cancers, including breast cancer and GBM. These cancers are particularly sensitive to MT dysfunction, as paclitaxel is commonly prescribed to treat breast cancer, and MT disrupting TTFields are effective against GBM (34, 61). Additionally, GBM cells are differentially sensitive to disruption of MT-dependent processes compared with healthy brain tissue, making these mechanisms valuable potential therapeutic targets (33, 46). The core mechanism of action of antitubulin agents is generally thought to rely on their ability to reduce MT dynamics, promoting prolonged activation of the SAC and activating apoptotic cell death during mitosis (136). Thus, the central concept behind cancer treatment with antitubulin agents is that the uncontrolled cell division exhibited by cancer cells exposes them to cell death induced by MT perturbation (136). Despite the non-targeted nature of antitubulin drugs, their clinical success and efficacy against a broad array of solid and hematological cancers underscores their relevance as antineoplastic agents (136-138).

Regardless of the success of targeting MTs for many malignant diseases, treatment with antitubulin drugs is often complicated by the prevalence of side effects and the development of drug resistance. For example, it is not understood why paclitaxel is effective against many solid

tumors, while *Vinca* alkaloids are often ineffective against solid tumors but commonly used to treat hematological malignancies. The mechanisms behind sensitivity to antitubulin agents are further convoluted by the diverse mechanisms that underlie drug resistance. Resistance can result from loss of drug access to the tumor or changes in molecular components within individual tumor cells. For example, brain penetrance by many MT-targeting agents is hindered by ATP-binding cassette transporters such as P-glycoprotein within the blood-brain barrier that pump drugs out of the brain (139). P-glycoprotein is the predominant efflux pump responsible for multidrug resistance to taxanes and *Vinca* alkaloids. Intracellular components that regulate MT functionality also affect cellular sensitivity to antitubulin drugs. Evidence exists that combining antitubulin agents such as vinblastine or paclitaxel with inhibition or knockdown of the SAC protein MPS-1 results in synergistic tumor cell killing (49, 50). Additionally, because low concentrations of both stabilizing and destabilizing antitubulin agents can kill cells by marginally altering MT dynamics, one can reason that changes in MT dynamics by regulatory proteins might alter drug sensitivity. For example, paclitaxel-resistant lung cancer cells were found to have higher MT polymerization rates (140). Thus, while antitubulin agents are considered nonspecific drugs, their efficacy can be highly dependent on cancer-specific alterations in protein expression. Understanding the complex mechanisms governing cancer cell sensitivity to antitubulin agents could be the key to developing safer and more effective drugs.

Evidence over the past decade has revealed an intimate relationship between tubulin dynamics and heterotrimeric G protein signaling, suggesting that this broad signaling system may yield proteins that regulate antitubulin drug efficacy. Both Gα and Gβγ proteins can directly bind to MTs and regulate their assembly (141, 142). $G\alpha_i$ has specifically been implicated in spindle pole organization during cell division (143, 144). Notably, heterotrimeric G protein activation is required to regulate MTs (145). While G protein-dependent regulation of tubulin function has been studied extensively (141, 142), little is known about the ability of additional molecular components of G protein signaling, such as GPCRs, to regulate MT-dependent processes. Currently, the sphingosine-1-phosphate receptor 5 ($S1PR_5$) has been identified as a centrosomal GPCR that might regulate mitotic MT dynamics (146). Additionally, metabotropic glutamate receptors and melatonin receptors directly bind tubulin (147-150), and activation of GPCRs has been shown to promote tubulin recruitment to the plasma membrane (149, 151). Our current understanding of the molecular components controlling these links between MTs and GPCRs and their functional consequences in cells is limited. Moreover, the

effect of GPCR signaling on sensitivity to antitubulin agents has not been explored. The purpose of this study was to identify novel GPCRs that participate in MT-dependent processes and regulate the efficacy of antitubulin drugs in cancer cells. This research will increase our understanding of the crosstalk between GPCRs and tubulin and build upon that knowledge to develop more effective antitubulin agents.

Our laboratory recently developed ST-11, a novel antitubulin agent that selectively targets cancer cells. We utilized this compound to identify orphan GPCRs that might be involved in MT functionality by determining its efficacy in several human cancer cell lines and developing a functional genetic screen of orphan GPCRs in human T98G glioma cells. From this screen, we identified that the orphan receptor GPR124 (also known as Tumor Endothelial Marker 5, TEM5) is necessary for the activity of ST-11 and controls the growth of tumors *in vivo*. We additionally determined that GPR124 interacts with the MT plus-end binding protein ch-TOG in a dynamic manner that depends on MT polymerization. Overexpression of GPR124 leads to increased MT assembly rates, altered mitotic timing, and lagging chromosomes during cell division. Collectively, our results indicate that GPR124 is a novel GPCR that is involved in MT dynamics in cancer cells and regulates the efficacy of antitubulin agents.

Results

Involvement of GPR124 in the antineoplastic activity of antitubulin agents

To identify orphan GPCRs that regulate the efficacy of antitubulin agents, we designed a functional genetic screen based on differential sensitivity several human cancer cell lines to antitubulin agents. First, four cell lines, T98G glioma, MDA-MB-231 (MDA231) breast, HCT116 colorectal, and HeLa cervical cancer cells, were treated with vinblastine, colcemid, and ST-11. T98G cells were particularly sensitive to ST-11, but resistant to vinblastine and colcemid (Figure 3.1A). In contrast, MDA231, HCT116, and HeLa cells were similarly sensitive to all compounds (Figure 3.1A). We were specifically intrigued by the response of ST-11, which was most efficacious in T98G cells that were resistant to other antitubulin compounds. T98G and MDA231 cells had the largest differential in ST-11 efficacy. We focused on these two cells lines to establish dose response curves of the antineoplastic effect of ST-11. The efficacy of ST-11 was reduced by 42% in MDA231 cells compared with T98G cells (Figure 3.1B). The potency of the compound was similar between both cell lines (1.1 μM in T98G and 0.8 μM in MDA231)

(Figure 3.1B). Thus, ST-11 was found to be effective at killing multiple cancer cell lines with variable efficacy, yielding a system that can be utilized to identify proteins that control sensitivity to anitubulin agents.

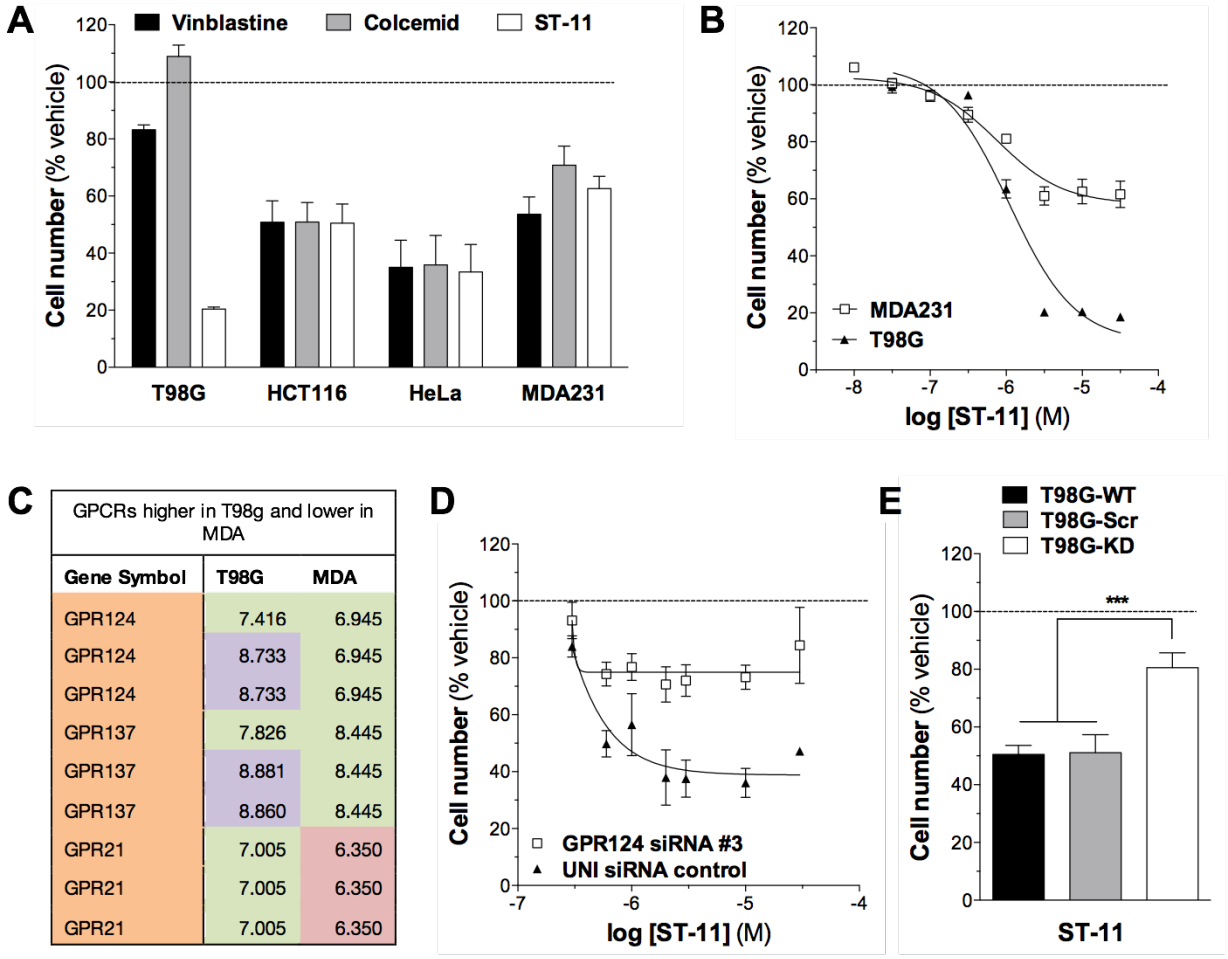

Figure 3.1: GPR124 regulates cellular sensitivity to ST-11
(A) Four cancer cell lines, T98G glioma, HCT116 colorectal, HeLa ovarian, and MDA-MB-231 (MDA231) breast cancer cells were treated with the antitubulin agents ST-11 (10 μM), vinblastine (10 μM), and colcemid (10 μM). Cell number was measured after 72 hrs with WST-1 to obtain a baseline response of these cells to various antitubulin agents. (B) Viability of T98G and MDA231 cells measured with WST-1 72 hrs after treatment with ST-11. (C) The average expression of 3 orphan GPCRs measured with microarray analysis of T98G and MDA231 cells. Data is the $\log_2$ of the background subtracted fluorescence intensity, and the table is color-coded according to normalized expression level. Red = low expression, green = medium expression, and purple = high expression. (D) Viability of T98G cells expressing a GPR124-targeted siRNA (GPR124 siRNA #3) or a non-targeting siRNA (UNI siRNA control) measured with WST-1 72 hrs after ST-11 treatment. (E) Effect of ST-11 (10 μM) on the viability of wild-type T98G cells (T98G-WT), or T98G cells stably expressing a GPR124-targeted shRNA (T98G-KD) or a non-targeting shRNA (T98G-Scr). ***p<0.001, one-way ANOVA with a Tukey *post hoc* test.

In an effort to identify orphan GPCRs that may control MT processes and sensitivity to antitubulin agents, we exploited the differential sensitivity of our cancer cell lines to ST-11. We hypothesized that the increased sensitivity of T98G cells to ST-11 might result from higher expression of an unknown orphan GPCR. Using microarray analysis of T98G and MDA321 cells, we identified only 3 orphan GPCRs that are more highly expressed by T98G cells than by MDA231 cells (Figure 3.1C). We determined whether these receptors were involved in the antineoplastic effect of ST-11 by knocking down each receptor in T98G cells and evaluating the efficacy of ST-11. The expression of each GPCR was reduced in T98G cells using mixtures of 3 siRNA constructs (#1, #2, and #3) to maximize knockdown efficiency. Only knockdown of GPR124 reduced the antineoplastic effect of ST-11 (Figures S3.1A and S3.1B). We validated our microarray results using qPCR and found that GPR124 is expressed at 33.5 ± 16.1 fold higher levels in T98G cells compared with MDA cells (data not shown). Using 1 of the 3 siRNA constructs to knockdown GPR124 (siRNA #3), we found that reduction in GPR124 levels by 72% (Figure S3.1C) in T98G cells reduced ST-11 efficacy by 47% (Figure 3.1D). Moreover, we generated T98G cells with stable knockdown of GPR124 using shRNA and again identified the same trend in ST-11 resistance; stable knockdown of GPR124 by 86% (T98G-KD) (Figure S3.1D) reduced the efficacy of ST-11 on T98G cells by 61% compared with cells stably expressing a scrambled shRNA control (T98G-Scr) (Figure 3.1E). Thus, our unbiased screen revealed GPR124 as an orphan GPCR that regulates the efficacy of the antitubulin agent ST-11.

To ascertain the specificity of the effect of GPR124 on the antineoplastic activity of antitubulin agents, we treated T98G-KD and T98G-Scr cells with 3 additional cytotoxic compounds: staurosporine, C_2-ceremide, and carmustine. GPR124 knockdown had no effect on the antineoplastic activity of these compounds, indicating that this protein does not broadly affect resistance to pro-apoptotic drugs (Figure 3.2A). We then assessed how GPR124 knockdown in T98G affects their sensitivity to additional MT-targeted agents, including paclitaxel, vinblastine, and colcemid. Interestingly, while GPR124 knockdown reduced the efficacy of ST-11 on cell viability, it synergized with the antineoplastic effect of both vinblastine and colcemid, producing a 25% and a 43% increase, respectively, in drug efficacy (Figure 3.2B). Paclitaxel was ineffective against both T98G-Scr and T98G-KD cells. The fact that T98G-Scr cells were resistant to both vinblastine and colcemid (efficacies of 17% and 0%, respectively) is noteworthy and indicates that the absence of GPR124 alone might vastly improve the response to these drugs.

ST-11, vinblastine, and colcemid are known to induce apoptosis by prolonging activation of the SAC during prometaphase. To better understand how GPR124 knockdown reduces ST-11 efficacy, we used time-lapse microscopy of T98G-KD and T98G-Scr cells to observe directly how they are affected by ST-11 treatment. Strikingly, while 80% of T98G-Scr arrested in prometaphase and subsequently died, only 21% of T98G-KD cells died through this mechanism. Instead, 79% of the T98G-KD cells proceeded to anaphase without establishing a fully formed metaphase plate (Figures 3.2C and 3.2D). These data indicate that GPR124 might be involved in cell division processes.

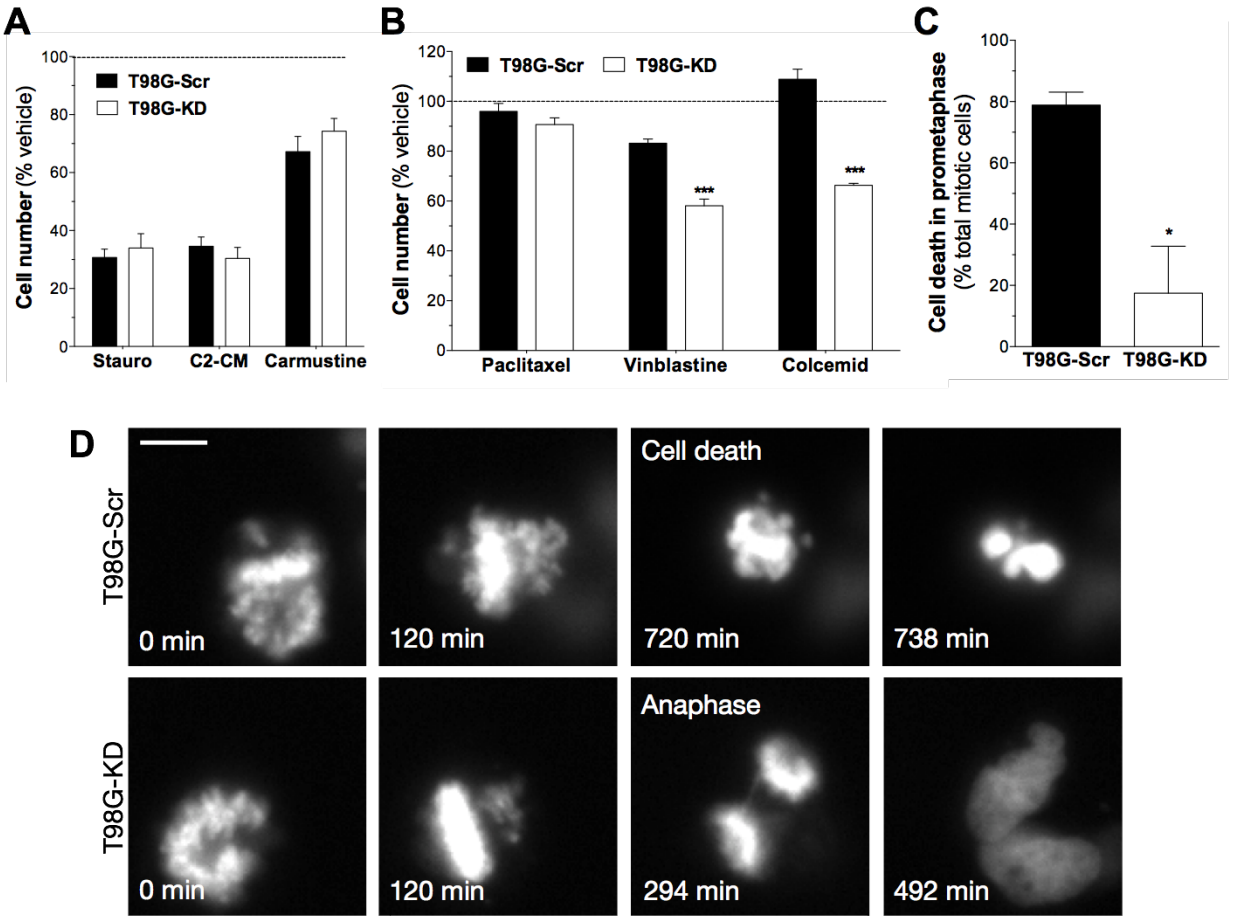

Figure 3.2: GPR124 specifically affects the efficacy of antitubulin compounds
(A) Effect of staurosporine (Stauro, 2 μM), C2-ceremide (C2-CM, 10 μM), and carmustine (1 mM) on the viability of T98G-Scr control and T98G-KD cells measured with WST-1. (B) Effect of the antitubulin compounds paclitaxel (10 μM), vinblastine (10 μM), and colcemid (10 μM) on the viability of T98G-Scr control and T98G-KD cells measured with WST-1. ***$p<0.0001$, Student's t-test. (C-D) Cell death that occured during prometaphase in the presence of ST-11 (10 μM) was measured in T98G-Scr control and T98G-KD cells using time-lapse microscopy. *$p<0.05$, Student's t-test. Data are the mean ± SEM of at least 3 independent experiments. Representative time-lapse frames are shown in (D). Scale = 10 μm.

GPR124 reduces tumor growth in vivo

Little is currently known about GPR124. This protein was identified in colorectal cancer tissues and was found to be involved in the proliferation, survival, and angiogenesis of tumor-associated endothelial cells (152-156). We hypothesized that the intriguing differential effect of GPR124 knockdown on the efficacy of antitubulin agents likely had to do with its role in cell proliferation. However, the mechanistic details of how GPR124 affects proliferation are not well understood, nor has this effect been studied in tumor cells (155). Thus, we first assessed the effect of GPR124 on gross tumor growth by establishing xenograft models with altered GPR124 expression. U87MG human glioma cells overexpressing myc-tagged GPR124 (U87MG-GPR124) or an empty vector (U87MG-pcDNA) were implanted subcutaneously into the flanks of nude mice. GPR124 overexpression significantly reduced the growth rate of U87MG flank tumors compared with expression of a control vector (U87MG-pcDNA) (Figure 3.3A). These tumors were found to have histological markers consistent with typical GBMs, including pseudopalisading, necrosis, and frequent mitotic cells (Figure 3.3B and 3.3C). There was a slight, non-significant reduction of necrotic area in U87MG-GPR124 tumors compared with U87MG-pcDNA tumors of the same size (Figure S3.2A). This difference likely could not account for the significant reduction in tumor size in U87MG-GPR124 xenografts. Thus, we hypothesized that increased GPR124 expression must reduce cell proliferation. We assessed the proliferation index of U87MG tumors using the cell cycle marker Ki67. U87MG-GPR124 tumors contained 50% less Ki67-positive nuclei than control U87MG-pcDNA tumors, indicating that GPR124 overexpression reduces tumor proliferation (Figure 3.3D and 3.3E).

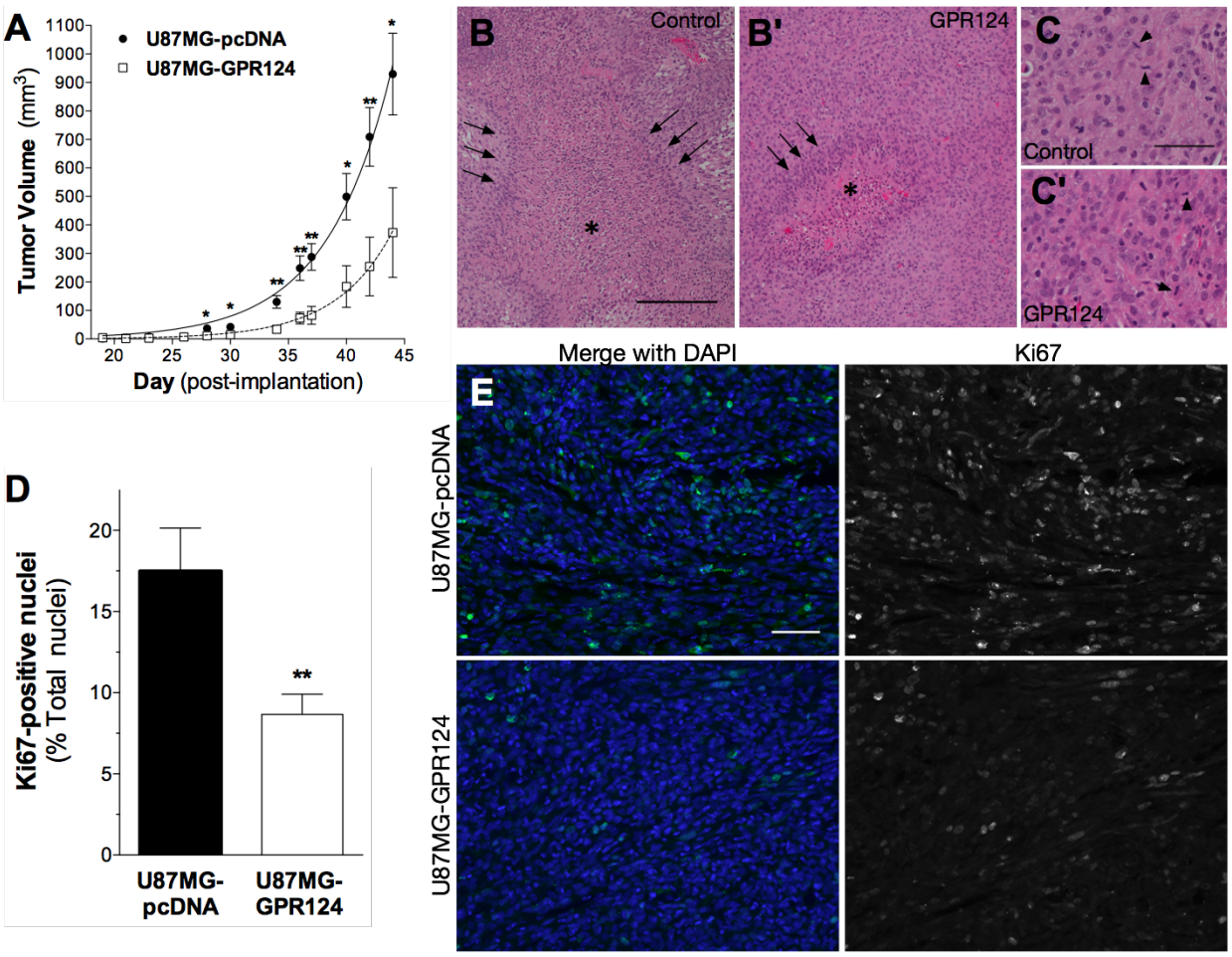

Figure 3.3: GPR124 slows U87MG xenograft tumor growth.
(A) GPR124 overexpression slowed the growth of xenograft U87MG tumors (U87MG-GPR124) compared with control (U87MG-pcDNA). Tumors were measured with calipers every 2-3 days for 42 days post-implantation. *p<0.05, **p<0.01, Student's t-test. (B-C) H&E staining of U87MG-pcDNA (B, C) and U87MG-GPR124 (B', C') tumors reveal features consistent with GBM including pseudopalisading (arrows) and necrosis (stars) (B, B') as well as frequent mitotic cells (arrow heads) (C, C'). Scales 200 μm (B, B') and 50 μm (C, C'). (D-E) Overexpression of GPR124 resulted in U87MG tumors with less Ki67-positive nuclei than control tumors (D). Representative images of U87MG-pcDNA (top panels) and U87MG-GPR124 tumors (bottom panels) with Ki67 shown in green (left) or gray (right), and DAPI shown in blue (left) (E). **p<0.01, Student's t-test. Scale 50 μm. Data are the mean ± SEM of 10 mice per group.

GPR124 regulates mitotic progression in vitro

To dissect the mechanistic details governing GPR124-dependent reduction in tumor cell proliferation, we validated our *in vivo* findings *in vitro* using an [^{3}H]-thymidine incorporation assay to assess the basal rate of cell division in cells expressing different levels of GPR124. As expected, overexpression of GPR124 reduced the [^{3}H]-thymidine uptake of cultured U87MG cells by 32.5%, 34.2%, and 43.2% in 0%, 1%, and 10% serum, respectively, compared with

U87MG-pcDNA control cells (Figure 3.4A). Interestingly, knockdown of GPR124 in T98G cells also reduced ^{3}[H]-thymidine uptake by 42.7% compared with T98G-Scr controls, however this only occurred in culture conditions with 1% serum (Figure S3.2B). The observation that changing GPR124 levels in either direction upsets cellular proliferation is consistent with a role in MT-dependent processes. Our collective findings that GPR124 differentially regulates cellular sensitivity to antitubulin compounds, independently controls cell proliferation *in vitro* and *in vivo*, and does so in a way that indicates that its expression must be tightly controlled suggests that GPR124 might be involved in mitosis. Mitosis is a strictly regulated process that is targeted by antitubulin agents. Many of the mechanisms involved in successful completion of mitosis require a carefully orchestrated balance of events that when disrupted can upset the process as a whole. By quantifying the relative fraction of mitotic cells in each phase of mitosis, we found that GPR124 overexpression in U87MG cells reduces the number of cells in prometaphase by 31.4% compared with U87MG-pcDNA cells. In contrast, knockdown of GPR124 in T98G cells increased the fraction of cells in prometaphase by 41% compared with T98G-Scr cells (Figure 3.4B and 3.4C). These data indicate that mitotic progression is disrupted when GPR124 levels are altered, as the fraction of cells in each mitotic phase may correlate with the speed at which that phase progresses. To quantify mitotic progression with more precision, we used time-lapse microscopy of HeLa cells expressing H2B-GFP (H2B-GFP HeLa) to visualize nuclei. HeLa cells were chosen because mitotic progression is very reliable and well understood in this cell line. As expected, GPR124 overexpression in H2B-GFP HeLa cells using lentiviral transduction decreased the time spent in prometaphase by 40% compared with H2B-HeLa cells infected with a lentiviral control (Figure 3.4D). This finding implies that GPR124 promotes the formation of a metaphase plate by increasing chromosomal congression. In addition, GPR124 slowed progression from metaphase to anaphase by 24%, resulting in no change in the overall mitotic timing compared with control HeLa cells (Figure 3.4D). Mitotic progression is tightly regulated, and both prometaphase and metaphase are critical stages during which the cell establishes proper kinetochore-MT attachments that are vital for accurate chromosomal segregation. Mitotic progression is paused in metaphase by the SAC until the kinetochores have formed accurate bipolar attachments to spindle MTs. Accordingly, we hypothesized that GPR124 overexpression might promote erroneous kinetochore-MT attachments that result in a metaphase delay. A common consequence of improper kinetochore-MT attachments is lagging chromosomes during anaphase. Hence, using time-lapse microscopy of H2B-GFP HeLa cells, we noted a 44% increase in the

prevalence of lagging chromosomes in GPR124-overpexressing cells (Figure 3.4E and 3.4F). Collectively, our findings suggest that GPR124 overexpression alters mitotic progression and promotes erroneous kinetochore-MT attachments. Regulated MT assembly in the spindle is essential to efficient and error-free mitosis, and alterations in spindle MT dynamics has been associated with the presence of lagging chromosomes and increases in CIN (157). Thus, GPR124 may increase MT dynamics in the spindle, promoting lagging chromosomes and delaying metaphase progression.

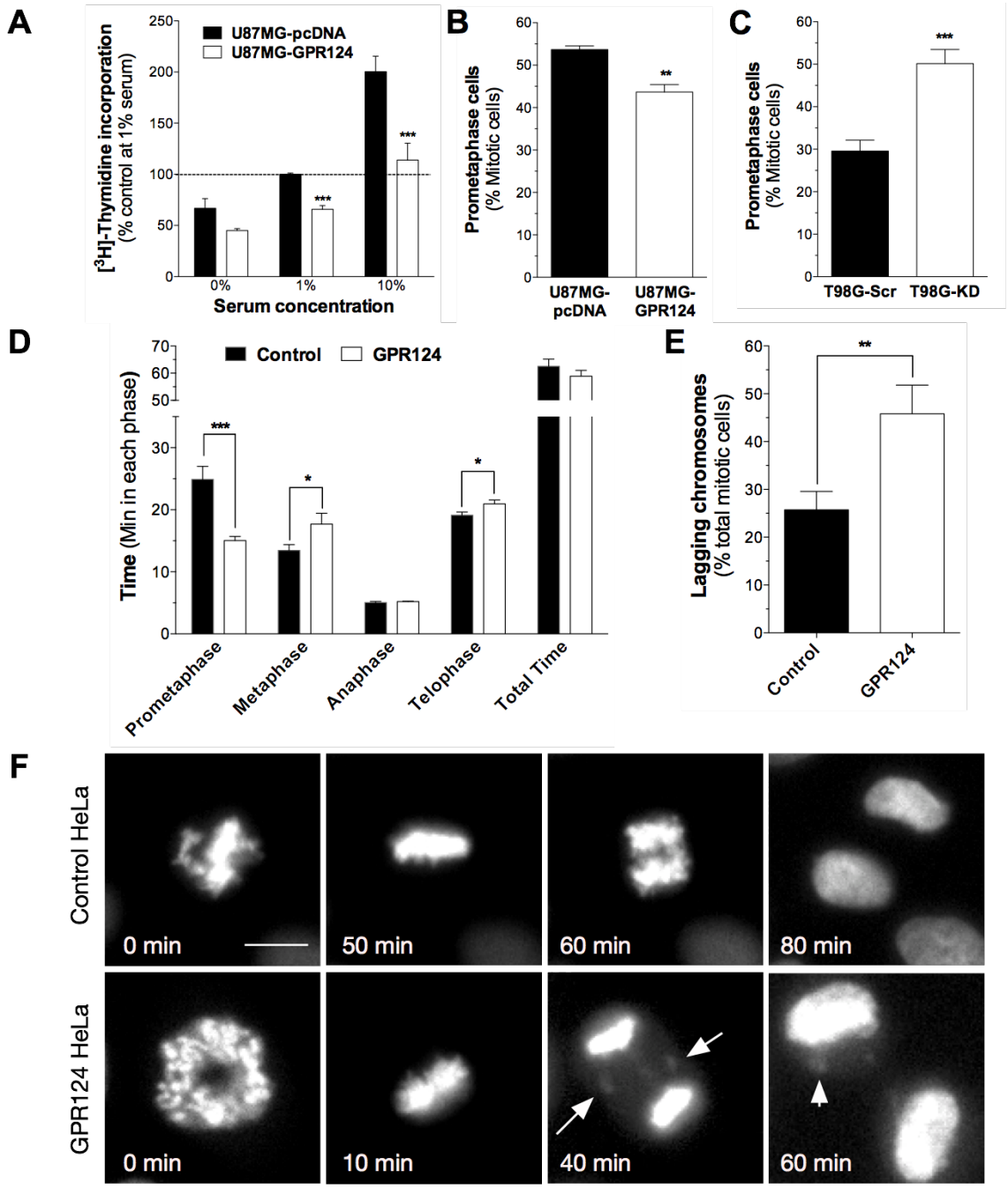

Figure 3.4: GPR124 reduces proliferation and alters mitotic progression

(A) Overexpression of GPR124-myc in U87MG cells (U87MG-GPR124) reduced ^{3}[H]-thymidine incorporation in 3 serum concentrations (0%, 1%, and 10%) compared with cells expressing an empty vector control (U87MG-pcDNA). ***p<0.001 2-way ANOVA. (B-C) Overexpression of GPR124 in U87MG cells reduces the percentage of mitotic cells in prometaphase compared with control (B). Accordingly, knockdown of GPR124 in T98G cells (T98G-KD) increases the percentage of mitotic cells in prometaphase compared with control (T98G-Scr) (C). (D-E) Timeplapse microscopy of HeLa cells shows that overexpression of GPR124 reduces the time spent in prometaphase and increases time spent in metaphase and anaphase (D) while leading to an increase in the prevalence of lagging chromosomes (E). (F) Representative frames from time-lapse microscopty of control and GPR124-overexpressing HeLa cells going through mitosis. Arrows point to lagging chromosomes, arrow head points to a micronucleus. Scale = 10 µm. Data is the mean ± SEM of at least 3 independent experiments.

GPR124 regulates MT assembly and interacts with ch-TOG

Lagging chromosomes can arise from minute changes in spindle MT dynamics. Moreover, changes in MT assembly rate can promote resistance to antitubulin agents (140). We hypothesized that GPR124 alters mitotic progression, promotes lagging chromosomes, and regulates sensitivity to antitubulin agents by controlling MT dynamics. The effect of GPR124 overexpression on MT dynamics was assessed using live cell imaging of EB3-GFP comets in HeLa cells. We observed a slight, but significant, increase in MT assembly rates in interphase HeLa cells overexpressing mCherry-tagged GPR124 (GPR124-mCherry, 6.5% increase over control HeLa cells expressing mCherry) (Figure 3.5A). MT assembly in mitotic cells was measured in both the spindle and astral MTs (Figure S3.3). GPR124 overexpression in HeLa cells promoted a small, but highly significant, increase in spindle MT assembly rates without affecting astral MT assembly rates (8.1% increase over mCherry-expressing HeLa cells in spindle MTs) (Figure 3.5A). While an increase in MT assembly by only 8.1% is modest, small alterations in MT assembly rates have been linked to CIN and mitotic abnormalities (157). Therefore, we suggest that the increase in MT assembly rates induced by GPR124 may be responsible for the observed changes in mitotic timing and the prevalence of lagging chromosomes when this protein is overexpressed.

To understand how a GPCR might affect MT assembly rates in the spindle, we used mCherry-tagged GPR124 to visualize the localization of this protein throughout different stages of the cell cycle. Interestingly, despite the effect of GPR124 on spindle MTs, this protein was present on the plasma membrane throughout mitosis (Figure 3.5B). GPR124 colocalized strongly with actin, as has been shown previously in HEK293 cells (158) (Figures 3.5B and 3.5C). GPR124 did not strongly colocalize with MTs; however, it overlapped with MTs in discreet locations where a MT contacts the plasma membrane (Figure 3.5D). Therefore, contrary to our findings that GPR124 affects MT dynamics and mitosis, we found little overlap between this protein and MTs. However, the discovery that MTs appeared to contact GPR124 at the plasma membrane suggests that this protein might regulate MT dynamics by controlling the association or function of MT plus-end binding proteins. These proteins are instrumental to both MT polymerization and breakdown and together coordinate the dynamic functions of MTs both in interphase and in mitosis.

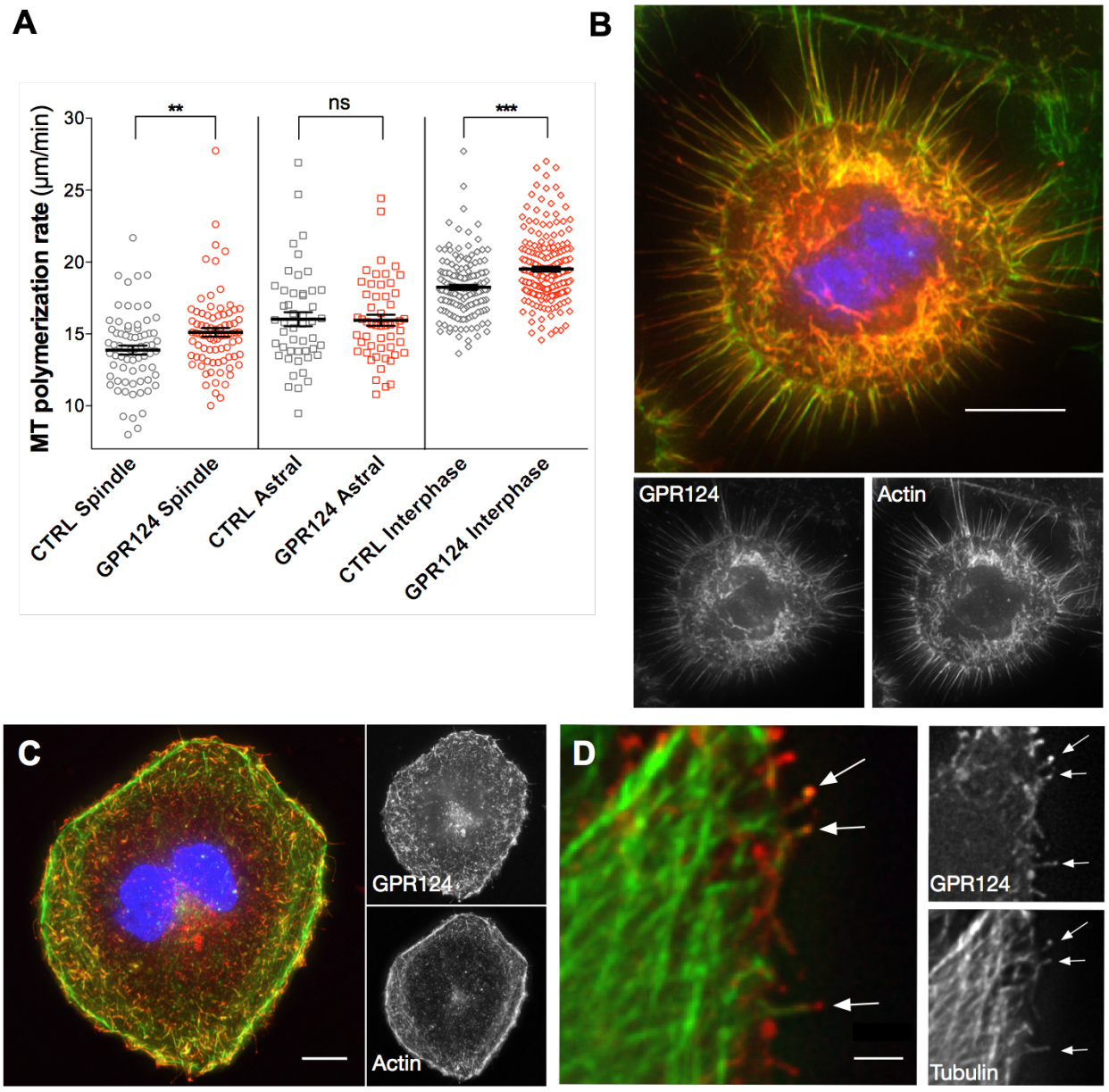

Figure 3.5: GPR124 increases MT dynamics and colocalizes with MT tips at the plasma membrane
(A) Overexpression of GPR124-mCherry in HeLa cells increased MT assembly rates in the mitotic spindle without affecting astral MT assembly rates. GPR124-mCherry also increased MT assembly rates in interphase HeLa cells. **p<0.01, ***p<0.001 Student's t-test. (B) GPR124 is present on the plasma membrane through mitosis in HeLa cells overexpressing GPR124-mCherry. GPR124 is shown in red, actin is stained with phalloidin in green, and DAPI is in blue. Scale = 10 µm. (C) GPR124 is present on the plasma membrane during interphase and colocalizes with actin in HeLa cells overexpressing GPR124-mCherry. GPR124 is shown in red, actin is stained with phalloidin in green and DAPI is in blue. Scale = 10 µm. (D) MT plus end tips colocalize with GPR124 in discreet areas on the plasma membrane (marked by arrows). GPR124 is shown in red, and microtubules are shown in green. Scale = 2 µm.

Very little is known about the components of GPR124 signaling, and no MT-dependent functions have yet been identified. This receptor has recently been found to be involved in Wnt signaling and to function through the small GTPase cdc42 when activating the migration of endothelial cells (159-161), which implies a role in cytoskeletal remodeling. We hypothesized that GPR124 regulates the function of MT plus-end binding proteins. Accordingly, we analyzed the constituents of the GPR124 complex using Stable Isotope Labeling of Amino acids in Cell culture (SILAC), a quantitative and reliable method to analyze protein complexes with mass spectrometry (162, 163). With this technique, we identified several proteins that are involved in regulating MTs, centrosomal function, and cytoskeletal dynamics (Table 3.1).

Protein	Function	Significance (p-value)
GPR124	*Adhesion GPCR involved in cell growth and migration*	*** 0.007*
ch-TOG	MT plus-end binding protein involved in MT dynamics and organization	*** 0.0008
PKA Regulatory subunit II	Regulatory subunit of PKA	** 0.0013
AKAP450	Scaffold for PKA, protein phosphatase 1 and protein phosphatase 2A	** 0.0027
Midline-1	Microtubule binding protein that facilitates anchoring of multiprotein complexes to	0.16
Myosin Light Chain Kinase	Phosphorylates Myosin Light Chain to stimulate actin binding	0.16

Table 3.1: GPR124-associated proteins identified using SILAC and mass spectrometry. Proteins were SILAC labeled *in vitro*, and GPR124-myc was immunoprecipitated. Proteins bound to the GPR124 complex were identified using mass spectrometry, and statistical significance was determined using a one sample Student's t-test against a hypothetical value of 0. For more information, see *Chapter 4: Materials & Methods.*

Notably, we identified ch-TOG, a MT plus-end binding protein that regulates MT polymerization (164-166). Ch-TOG is well known to be indispensable for the proper formation of bipolar spindles (167-169). Ch-TOG knockdown significantly reduces MT assembly rates and chromosome oscillations during prometaphase and metaphase (157, 169, 170). Thus, varying ch-TOG levels can affect MT dynamics and chromosome congression, which we also noted upon overexpression of GPR124. We verified the interaction between these 2 proteins using 3 independent assessments. First, we immunoprecipitated GPR124-myc and identified a clear band for ch-TOG upon analysis by western blot (Figure S3.4A). Second, ch-TOG and GPR124 colocalized on the plasma membrane and GPR124-positive filopodial extensions in interphase

HeLa cells (Figure 3.6A). Interestingly, while the majority of ch-TOG was present in the centrosomes and on spindle MTs, there was clear evidence of this protein on the plasma membrane during mitosis where it colocalized with GPR124 (Figure 3.6B). Lastly, we treated U87MG-GPR124 cells with ST-11 (10 μM) and identified an 80% reduction in the amount of ch-TOG that immunoprecipitated with GPR124 after 4 hrs (Figures 3.6C and 3.6D). This finding suggests that ch-TOG and GPR124 association is a dynamic process that requires MT polymerization. Collectively, our results indicate that GPR124 and ch-TOG form a complex in cells and this complex likely regulates spindle MT dynamics and mitotic progression by modulating ch-TOG activity.

The expression level of ch-TOG is known to affect spindle MT dynamics (157, 169, 170). Because GPR124 induced small, but functionally relevant, changes in spindle MT assembly, we hypothesized that this protein associates with ch-TOG at the membrane and induces a compensatory upregulation in ch-TOG levels. However, we expected this increase to be small, as GPR124 overexpression only induced slight changes in MT assembly. Thus, we elected to employ a sensitive quantitative assessment of ch-TOG levels using immunocytochemistry (ICC). Quantitative ICC analysis of spindle and centrosome ch-TOG levels revealed a 33% increase in the level of ch-TOG in the spindle upon overexpression of GPR124 (Figure 3.6E). Moreover, we identified a 38% increase in whole-cell ch-TOG levels in GPR124-overexpressing HeLa cells compared with control (Figure S3.4B). Therefore, we can conclude that GPR124 interacts with ch-TOG, which leads to a compensatory increase in ch-TOG levels that drive rapid MT assembly in the spindle.

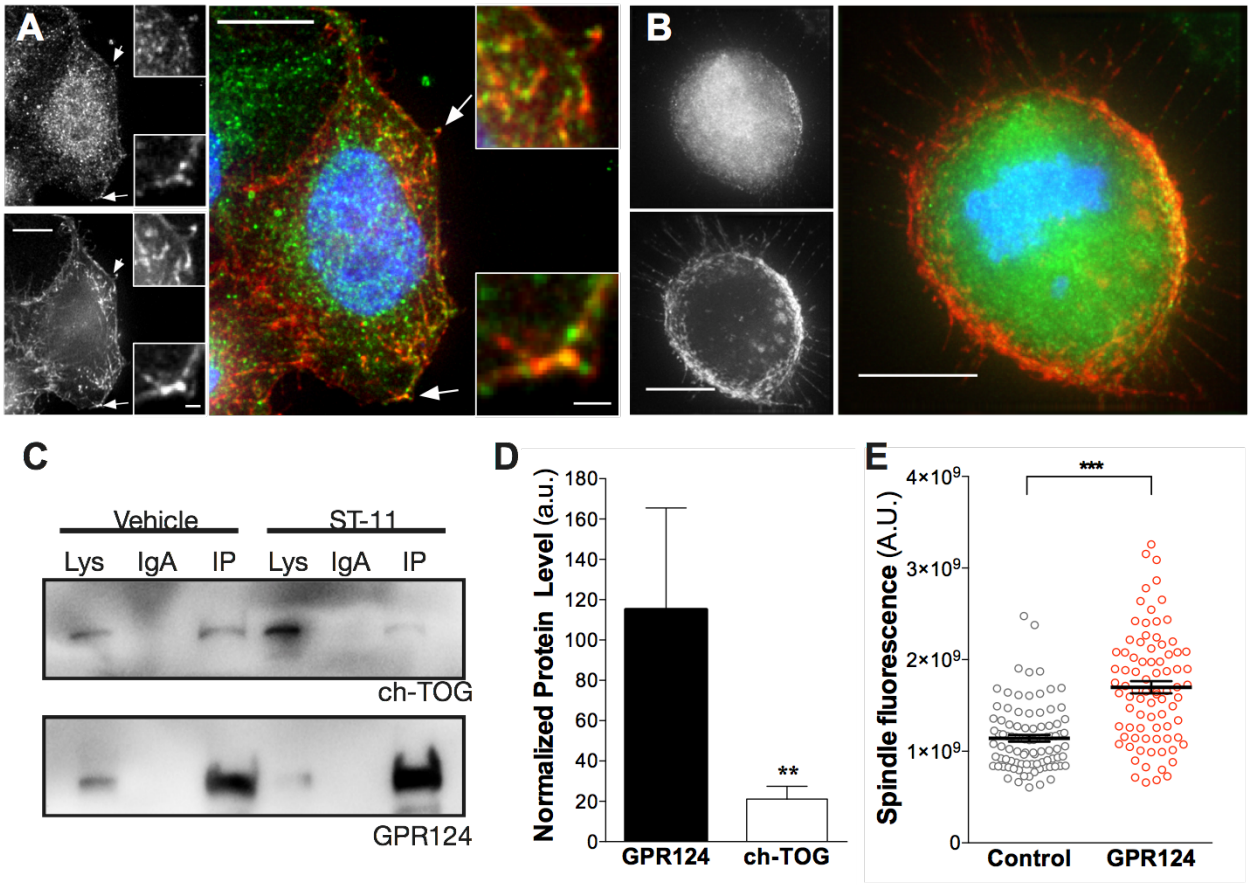

Figure 3.6: GPR124 forms a complex with ch-TOG and increases its levels in the spindle
(A-B) GPR124 co-localizes with ch-TOG in interphase (A) and mitotic (B) HeLa cells. Representative areas of co-localization are shown with arrows and are magnified in insets. GPR124-mCherry is shown in red, ch-TOG is in green, and the nucleus is in blue. Scale bars = 10 μm and 2 μm (*inset*). (C-D) Treatment with ST-11 (10 μM) decreased ch-TOG co-immunprecipitation with GPR124-myc detected by western blot (C). Ch-TOG protein was normalized to the amount of GPR124 in each immunoprecipitation and quantified (D). **p<0.01, Student's t-test. (E) Overexpression of GPR124-mCherry increased the level of ch-TOG present in the spindle. ***p<0.0001, Student's t-test. Data are expressed as the mean ± SEM.

Discussion

Using several unbiased screens, we have identified the orphan receptor GPR124 as a novel component of the MT regulatory system. This protein has known roles in migration and proliferation, however, very little is known mechanistically about these functions. With no identified chemical or endogenous ligand, we used systems in which GPR124 expression was altered to study its function in tumor cells. GPR124 overexpression increases interphase and spindle MT assembly rates, leading to alterations in mitotic timing and increases in lagging chromosomes that can lead to aneuploidy. GPR124 interacts with ch-TOG in a dynamic

manner, and this complex likely promotes its MT-dependent cellular effects. Therefore, we can deduce that GPR124 residing on the plasma membrane has a novel role in fine-tuning MT-dependent processes during mitosis by regulating ch-TOG.

In this study, we set out to identify orphan GPCRs that may affect cellular sensitivity to antitubulin compounds. Using an unbiased genetic screen in MDA231 breast cancer and T98G glioma cells, we discovered that GPR124 controls the efficacy of ST-11, vinblastine, and colcemid. We found that while ST-11 killed most T98G-Scr cells in prometaphase, T98G-KD cells passed into anaphase despite the lack of an established metaphase plate in the presence of this drug, thus reducing ST-11-induced cell killing. Paradoxically, both vinblastine and colcemid treatment was found to synergize with GPR124 knockdown to increase cell killing. While the precise differences in the mechanisms behind these 3 drugs is not currently well understood, it's possible that the cause of this differential effect arises from effects of vinblastine and colcemid on interphase cells. While vinblastine and colcemid can induce cell killing during interphase as well as mitosis (171-173), a high concentration of ST-11 (10 μM) appears to reliably target mitotic cells (data not shown). It's possible that GPR124 may play different mechanistic roles depending on whether cell death occurs during mitosis or interphase. Sensitivity to antitubulin agents can be regulated at a variety of levels. Vinblastine and paclitaxel are both known to synergize with knockdown of SAC components (49, 50), but resistance to antitubulin compounds can arise from alterations in MT stability and dynamics (140). Thus, we hypothesized that GPR124 could conceivably participate in the regulation of MT function during cell division.

While the function of GPR124 is starting to be uncovered, there is still very little information available regarding its cellular role. In cancer, this protein has only been evaluated in tumor-associated endothelial cells during angiogenesis. In this paradigm, GPR124 was found to mediate contact inhibition, begging the question of how it might regulate tumor growth (155). Our finding that GPR124 affected the sensitivity of T98G cells to antitubulin compounds strongly suggested that it might be involved in the regulation of cell division. This hypothesis was supported by 2 independent findings. First, overexpression of GPR124 substantially decreased the growth of xenograft U87MG tumors, implying that this protein is involved in overall tumor growth and proliferation. The expression of mitotic regulators is tightly controlled, and disruption of this balance by overexpression or knockdown has the potential to upset mitosis and reduce proliferation. GPR124 overexpression and knockdown both reduced proliferation *in vitro*, suggesting that this protein may regulate mitosis. Second, the cell

acquires proper kinetochore-MT attachments during prometaphase and metaphase, which is vital to prevent chromosome missegregation and aneuploidy. Notably, GPR124 altered progression through both of these phases. The increase in prometaphase progression that we observed upon overexpression of GPR124 suggests that this protein allows for rapid chromosomal congression; however, these cells additionally spent more time in metaphase, which implies that perhaps GPR124-overexpressing cells are not able to satisfy the SAC as quickly as control cells despite the visual presence of a metaphase plate. One possible explanation for this lag in metaphase progression is that the cells are not acquiring proper bipolar chromosomal attachments. Accordingly, we show here that overexpression of GPR124 increases the prevalence of lagging chromosomes, which result directly from erroneous kinetochore-MT attachments, and are evidence of increased CIN (174). CIN, which is generally defined as frequent chromosomal missegregations that result in aneuploidy, can have paradoxical effects on the growth of tumors. On the one hand, low levels of CIN can promote tumor growth by allowing for enhanced tumor cell evolution and adaptation [reviewed in (175)]. However, on the other hand, high CIN can be detrimental to cell viability and ultimately result in reduced tumor growth (157, 175). Together, our data support a model in which GPR124 promotes high levels of CIN as evidenced by the prevalence of lagging chromosomes, which leads to a reduction in tumor growth and proliferation.

MT dynamics has been implicated in lagging chromosomes and CIN as well as in sensitivity to antitubulin agents (140, 157). Therefore, it follows that GPR124 increases spindle and interphase MT dynamics as well as lagging chromosomes. Our finding that GPR124 associates with the MT plus-end binding protein ch-TOG is significant for several reasons. The GPR124/ch-TOG complex is functionally relevant, as GPR124 overexpression increases whole-cell and spindle ch-TOG levels and promotes cellular effects that would be expected upon increasing ch-TOG activity. Moreover, given that GPR124 is a membrane-associated protein that increases MT polymerization rates, an intracellular MT polymerizing enzyme would be expected to facilitate this response. Thus, it is likely that ch-TOG mediates the cellular effects of GPR124 that we have identified.

The association of ch-TOG with a plasma membrane-bound protein has not been shown before, and thus, brings forth new concepts to our understanding of ch-TOG. Most of what is currently known about ch-TOG is in regards to its role in centrosomal MT nucleation and dynamics (167-169). Little is known about the function of this protein during interphase beyond that it binds to MT plus ends and promotes increased MT dynamics (164-166). We found that

GPR124 associated with ch-TOG on the plasma membrane during interphase and mitosis, which presumably affects the function of ch-TOG during mitosis. Determining the precise mechanism by which ch-TOG encounters GPR124 would greatly expand our understanding of how these two proteins function. Our finding that treatment with a MT depolymerizing agent substantially decreases ch-TOG association with GPR124 suggests that ch-TOG is present on the end of assembling MT tips and gets deposited when it encounters GPR124 at the membrane. This mechanism would support the hypothesis that GPR124 serves as a sensor for ch-TOG expression in the cell and regulates its level accordingly to prevent over- or underexpression of this critical mitotic protein.

The identification of ch-TOG as a novel binding partner of GPR124 greatly enhances our growing understanding of the cellular function of this orphan GPCR. Not only does GPR124 function to regulate proliferation, but most of the available research on this protein examines its role in promoting endothelial cell directional migration (156, 158, 161). The presence of a GPR124/ch-TOG complex on the plasma membrane and in filopodial structures is highly suggestive that GPR124 might maintain this pro-migratory role in tumor cells. It is conceivable that GPR124 on the plasma membrane could localize and anchor ch-TOG to leading edges where it can polymerize MTs and prevent deviations from the established directional movement. Moreover, we show here that GPR124 may associate with an AKAP450 complex, which is known to coordinate the proper orientation of the centrosomes and Golgi during directional migration (176, 177). Hence, it is possible that GPR124 anchors and localizes the molecular machinery involved in properly polarizing and maintaining directionality of migrating cells. These hypotheses support the current literature on GPR124 and should be formally evaluated to enhance our understanding of these coordinated molecular mechanisms.

Together, the model proposed by this research indicates that GPR124 associates with ch-TOG at the plasma membrane, leading to increased ch-TOG activity in the spindle during mitosis. Increased MT assembly rates in the presence of GPR124 can affect several processes, including the cellular response to antitubulin agents as well as CIN and tumor growth. Ultimately, it is likely that through its interaction with ch-TOG, GPR124 overexpression tips the scales in favor of increased CIN and decreased tumor growth. Its effect on antitubulin agents therefore may also result from the ability of GPR124 to regulate MT assembly rates and CIN.

To conclude, the orphan receptor GPR124 is a novel regulator of MT dynamics through its interaction with the MT plus-end binding protein ch-TOG. High levels of GPR124 were found to increase MT dynamics, chromosomal congression, and mitotic errors including lagging

chromosomes. The complex relationship between GPR124, ch-TOG, and CIN leaves many open questions. For example, it is unclear whether GPR124 expression level could be used as a prognostic marker for cancer progression or response to therapeutic antitubulin drugs. Nonetheless, this study lays a foundation for expanding our knowledge of cellular components that influence MT dynamics, CIN, and tumor growth. The identification of GPR124 as a novel regulator of MT dynamics in cancer will uncover new mechanisms for tumor progression and lead to the discovery of novel therapeutic targets.

CHAPTER 4

Conclusions & future directions

Looking Forward

In this work, we have identified ST-11 as a new brain-penetrant MT-destabilizing agent that preferentially kills tumor cells by arresting them in mitosis and activating apoptosis. This compound appears to exert its antineoplastic effects through a similar general mechanism as other MT destabilizing agents such as vinblastine and colcemid; specifically, ST-11 was found to induce cell cycle arrest during mitosis and activate apoptosis. Using ST-11, we went on to discover that the orphan 7-transmembrane receptor GPR124 affects the cellular sensitivity to MT-targeting agents, and these effects likely occur through the ability of this protein to regulate ch-TOG activity and MT dynamics. Thus, this work adds to our understanding of cancer cell division and MT regulation and frames a new avenue of study that bridges the gap between plasma membrane proteins and MT functionality.

Several aspects of this work have clinical relevance in the field of cancer biology, which, if expanded upon, could lead to new therapeutics and improvements in patient response to antitubulin treatments. Three qualities of ST-11 mark this compound as an important contribution to the field of cancer biology. First, ST-11 is one of few available brain-penetrant antitubulin agents. The medicinal optimization of this compound could expand antitubulin treatment to patients with intracranial malignancies including GBM and brain metastases. Second, ST-11 was found to be safe to administer to healthy mice at doses up to 6 times what was required to elicit therapeutic efficacy. Thus, studying the detailed molecular mechanism by which this compound exerts its tumor specificity could lead to more effective and targeted

cancer therapeutics. Lastly, ST-11 was found to be highly effective against T98G glioma cells that are resistant to other antitubulin agents. Because the development of drug resistance complicates the use of antitubulin agents, this unique property of ST-11 sets it apart from traditional antitubulin drugs. Studying the means by which ST-11 evades drug resistance mechanisms could lead to improved therapeutics to treat patients with multi-drug resistant tumors. Thus, ST-11 is a novel compound that exhibits properties that are requisite for treatment of a variety of neoplasms. This compound should be studied and continually optimized to produce new therapeutic antitubulin agents that can be applied clinically.

In this work, we have outlined a new cellular role for GPR124 in tumor biology. This protein was found to exert tumor suppressive effects and to control MT dynamics through a functional interaction with ch-TOG. There are several clinically relevant contributions of this work to our understanding of cancer cell biology. First, GPR124 was found to regulate the efficacy of antitubulin agents. Multi drug resistance to MT-targeted agents is a pervading difficulty with antitubulin therapy. Mechanistic studies on how GPR124 regulates sensitivity to antitubulin agents could lead to its use as a prognostic marker for patient response to antitubulin therapy. Likewise, the molecular components of the GPR124 pathway that mediate its control over cellular sensitivity to antitubulin agents could reveal new molecular targets to combat drug resistance. Second, we identified that GPR124 reduces tumor cell growth when expressed at high levels, indicating that this protein has tumor suppressive properties. Thus, correlating GPR124 levels with tumor progression could confirm GPR124 as a *bona fide* tumor suppressor, uncovering a novel pathway for future targeted therapies.

Many questions remain regarding how GPR124 controls the cellular sensitivity to antitubulin compounds. T98G glioma cells that are generally resistant to other antitubulin agents were particularly sensitive to ST-11, and the efficacy of this drug was lost upon knockdown of GPR124. In contrast, GPR124 knockdown sensitized T98G cells to vinblastine and colcemid, underscoring the complexity in both the mechanism of action of these drugs and in the molecular role of GPR124. We identified that GPR124 overexpression increases MT polymerization rates, which would be expected to decrease sensitivity to antitubulin compounds that function by reducing MT dynamics (140). Thus, in this paradigm, the efficacy of antitubulin compounds would inversely correlate with the expression level of GPR124. These conclusions are supported by our data that GPR124 knockdown improves the efficacy of vinblastine and colcemid. However, the loss of ST-11 efficacy upon knockdown of GPR124 contradicts our expectations based on the hypothesis that GPR124 mediates sensitivity to

these agents solely owing to its effects on MT dynamics. Several conclusions can be drawn from the differential effect of GPR124 expression on the efficacy of these 3 antitubulin compounds. First, the fact that ST-11 alone is inhibited by loss of GPR124 supports an intriguing notion that the mechanistic details governing ST-11 action are quite distinct from those of vinblastine and colcemid. Second, it is likely that GPR124 is mediating further effects on mitosis than have been identified by this work. Specifically, time-lapse microscopy of T98G-Scr and T98G-KD cells in the presence of ST-11 revealed that when GPR124 levels are reduced, the cells are able to complete mitosis despite significantly prolonged prometaphase arrest and the absence of a fully formed metaphase plate. Thus, GPR124 knockdown does not likely reduce sensitivity to ST-11, but instead renders cells more resistant to activation of apoptosis following significant mitotic distress. Thus, GPR124 may be involved in the SAC and the molecular mechanisms that govern the activation of apoptosis upon prolonged activation of this checkpoint. Future mechanistic studies of GPR124 should focus on how it affects the progression from prolonged SAC arrest to apoptosis.

To conclude, this work contributes a new compound that can expand antitubulin treatment to intracranial malignancies and additionally proffers a novel GPCR-regulated branch of MT functionality to the field of cancer biology. My primary contribution to the field of cancer cell biology lays in my discovery that GPR124 regulates the growth of tumors by affecting MT dynamics through a MT polymerase. I hope and predict that the work outlined in this dissertation will lay the foundation for a more detailed exploration of GPCR-mediated control of MT dynamics and MT-dependent cellular functions in cancer.

Q.E.D.

CHAPTER 5

Materials & methods

Chemicals

All chemicals and drugs were purchased from Sigma (St. Louis, MO) unless otherwise noted. SR141716A and SR144528 were provided by the National Institute of Drug Abuse Drug Supply Program (RTI International, Research Triangle Park, NC). WIN 55,212-2, WIN 55,212-3, JWH-015, and JWH-200 were obtained from Cayman Chemical (Ann Arbor, MI). JWH-370, JWH-120, JWH-148, JWH-043, and JWH-042 were a kind gift from John W. Huffman (Clemson University, Clemson, SC), and pravadoline was obtained from Enzo Life Sciences (Farmingdale, NY). The synthesis of the novel AI compounds used in this study has been described elsewhere (126, 127). The caspase-3 inhibitor Z-DEVD-FMK was obtained from Santa Cruz Biotechnology (Santa Cruz, CA). L-α-Phosphatidylcholine (derived from egg containing mixed length fatty acyl chains, EPC) was purchased from Avanti Polar Lipids (Alabastar, AL). 1,2-Dimyristoyl-*sn*-glycero-3-phosphoglycerol, sodium salt (DMPG) and N-(Carbonyl-methosypolyethyleneglycol-2000)-1,2-dimyristoyl-*sn*-glycero-3-phosphoethanolzmine, sodium salt (DMPE-mPEG2000) were purchased from Corden Pharma (Plankstadt, Germany). All components were analytical grade or higher. All cell culture materials were purchased from Life Technologies (Thermo Fisher Scientific, Waltham, MA).

Cell culture

All cells were cultured at 37°C in a 5% CO_2 humidified atmosphere unless otherwise noted. The DBT, T98G, U251, A172, U87MG, and HeLa cell lines (ATCC, Manassas, VA) were cultured with DMEM supplemented with 10% FBS, 2 mM L-glutamine, 5 mM $NaHCO_3$, 5 mM HEPES, 100 U/mL penicillin, and 100 µg/mL streptomycin. The MGG4 and MGG8 glioma cell lines were a generous gift from Samuel Rabkin and Hiroaki Wakimoto (Massachusetts General Hospital and Harvard University, Boston, MA) and maintained as floating spheroid cultures in Neurobasal-A medium according to a previously established protocol (178), except using mechanical dissociation. Primary mouse neuron and astrocyte cultures were prepared as previously described (179, 180) in accordance with the Institutional Animal Care and Use Committee of the University of Washington.

Vectors and generation of stable and transient transgenic cell lines

Stable GPR124 knockdown cells were generated in T98G cells using MISSION® pLKO.1-puro lentiviral constructs purchased from Sigma-Aldrich (GPR124 targeting sequence: 5'—ATGTGGAAGCACAAGTTCAGC—3'). The pLKO.1-puro non-target shRNA plasmid (Sigma-Aldrich) was used as a control plasmid. Stable cell lines were grown as single clones generated under puromycin selection (2 µg/ml). Clones were grown and individually assessed for GPR124 expression using qPCR. These clones were kindly generated by Brian Haas. Stable U87MG cells with GPR124-myc overexpression were generated by transfecting pcDNA3.1-GPR124-myc (kindly provided by Brad St Croix, Tumor Angiogenesis Section, Mouse Cancer Genetics Program, National Cancer Institute, National Institutes of Health, Frederick, MD) into U87MG cells using the Lipofectamine® 2000 reagent (Thermo). An empty pcDNA3.1™ (Invitrogen) vector was used as a control. Stable lines were grown as single clones generated under G418 selection (1 mg/ml) and individually assessed for the presence of GPR124-myc by qPCR and ICC. Transient overexpression of GPR124-myc was conducted using lentiviral transduction. GPR124-myc was cloned into a lentiviral construct (referred to as pBS-4821) containing GFP under an IRES promoter generated by Bryce Sopher in the laboratory of Richard Morrison (Department of Neurology, University of Washington. Lentiviral particles were generated by Chizuru Kinoshita in the laboratory of Richard Morrison. An empty pBS-4821 vector was used as a control. Transient overexpression of GPR124-mCherry was conducted using the Amaxa Nucleofector™ system according to the manufacturer's recommendations (Lonza, Basel, Switzerland). GPR124-mCherry was generated by cloning mCherry into the pcDNA3.1-

GPR124-myc vector. An empty mCherry vector used as a control was created by cloning mCherry into the pEGFP-C1 (Clontech) vector. These vectors were generated by Michael Wagenbach.

In vitro drug treatments

Due to the lipophilic nature of the compounds used in this study, DMEM supplemented with 10% FBS was replaced with DMEM supplemented with 1% FBS after rinsing cells with PBS 1 day prior to all AI compound treatments on adherent cells unless otherwise stated in the methods. Phenol red-free medium was used for all WST-1 assays. All drugs were diluted to 1000× DMSO stocks to maintain 0.1% DMSO content, further diluted 1:10 in culture media, and spiked onto cells to obtain a 1× final concentration.

Cell viability and proliferation

Cell viability was assessed with the WST-1 reagent (Roche, Pleasanton, CA) according to the manufacturer's protocol. To measure cell proliferation, [^{3}H]-thymidine (5 μCi/ml, Perkin-Elmer, Waltham, MA, USA) was added to cells 30 min after drug treatments. WST-1 was evaluated 1 hr prior to [^{3}H]-thymidine incorporation, which was measured at the indicated times by adding 1M NaOH for 10 min on ice and quantifying radioactivity. For proliferation and cell death using trypan blue exclusion, cells were trypsinized and counted in the presence of trypan blue (1:10 dilution, Sigma, St. Louis, MO). These studies were completed by Brian Haas and Cong Xu.

Microtubule assembly

MTs were polymerized in BRB80 (80 mM PIPES-KOH pH 6.85, 1 mM $MgCl_2$, 1 mM EGTA) supplemented with 4% DMSO, 2 mM GTP, 1 mM DTT, 2.5 mM $MgCl_2$, and 60 μM bovine brain tubulin for 30 min at 37ºC. Polymerized MTs were diluted to 13 μM with BRB80 supplemented with 1 mM DTT and 0.5 mM GTP and sheared by 6 passes through a 30 G×12.5 mm syringe needle. Aliquots of sheared MTs were added to paclitaxel, nocodazole, or ST-11 to a 1% final DMSO concentration, incubated at 37ºC for 15 min, and centrifuged for 10 min at 42,000 rpm at 37ºC. Free tubulin from supernatants and pellets was separated on 4-12% polyacrylamide gels (Thermo-Fisher Scientific, Waltham, MA) and stained with Coomassie G-250. Peak intensities were quantified using ImageJ. All reagents were obtained from Sigma except for tubulin [purified in-house (181)] and ST-11. MT assembly was assessed by Michael Wagenbach

Cell lysates and western blotting

Western blotting was performed as described previously (182) with the following primary antibodies: cleaved poly ADP ribose polymerase (1:1000, Asp214), cyclin B1 (1:1000, Val152), phospho-histone H3 (1:1000, Ser10), β-tubulin (1:1000), activated caspase-3 (1:500), myc (1:1000) (all from Cell Signaling Technologies, Danvers, MA, USA), GAPDH (1:1000, Sigma), and ch-TOG (1:1000, BioLegend, San Diego, CA, USA). Western blots were performed in part by Brian Haas and Dave Canton.

Reverse transcription PCR and real time qPCR

RNA was extracted from T98G, U251 and HL60 cell pellets using the PerfectPure RNA kit (5-Prime, Gaithersburg, MD). For reverse transcription PCR, mRNA was reverse transcribed using RevertAid™ First Strand cDNA Synthesis Kit (Fermentas/Thermo Fisher Scientific) using random hexamer (for CB_1) or oligo-dT (for CB_2) primers. Intron-spanning primer sets were generated and used to amplify CB_1 (Forward: 5'—CTCCGCCTCTTCTTGTCTCC—3'; Reverse 5'—ATTTGAGCCCACGTACAGGA—3') and CB_2 (Forward: 5'—TCCTGGGAGAGGACAGAAAA—3'; Reverse: 5'—CTGCATGCAAAGACCACACT—3') using the GoTaq Flexi DNA polymerase (Promega, Madison, WI). Beta-actin was used as a loading control (Forward: 5'—ATTGGCAATGAGCGGTTC—3'; Reverse: 5'—CGTGGATGCCACAGGACT—3'). For real time qPCR, the mRNA concentration was determined using a NanoDrop ND1000 spectrophotometer (Thermo). 100 ng of total RNA was used in each reaction generated with the Roche LightCycler® 480 Probes Master kit and Universal Probe Library (UPL) system (Roche, Indianapolis, IN), according to the manufacturer's instructions. Intron-spanning primers for GPR124 (Forward: 5'—GGCTCCTTCCTGGGACTG—3'; Reverse: 5'—GCACTGTGCTGATGATGTTGTT—3', UPL probe #67) and GAPDH (Forward: 5'—AGCCACATCGCTCAGACAC—3'; Reverse: 5'—GCCCAATACGACCAAATCC—3', UPL probe #60) were designed using the Roche UPL Assay Design Center. The PCR reactions were carried out with a Stratagene MX3000P qPCR machine (Stratagene, San Diego, CA).

Immunocytochemistry

Cells were plated on glass coverslips (Thermo Fisher Scientific). For bright field images, cells were imaged in culture dishes prior to fixation with 4% paraformaldehyde (Electron Microscopy Sciences, Hatfield, PA). For DAPI and activated caspase-3 staining, cells were fixed at room temperature for 10 min and permeabilized with Triton X-100 (0.2%) in PBS at RT for 10 min.

The activated caspase-3 antibody (1:200, Abcam, Cambridge, MA) was incubated overnight at 4ºC and then visualized with AlexaFluor 488-conjugated secondary antibody (1:500, Life Technologies, Carlsbad, CA). DAPI (11 μM, Life Technologies) was used to visualize DNA. Coverslips were mounted with Fluoromount™ (Sigma), and images were acquired on a Zeiss Axio Observer Z1 inverted microscope fitted with an Apotome and a 20×/0.8 lens using AxioVision software (Carl Zeiss, Oberkochen, Germany).

For images of MTs and mitotic spindles, cells were plated on glass coverslips in RPMI medium with 10% FBS and treated with 5 μM ST-11 for 4 hrs prior to fixation in 4% paraformaldehyde at 37ºC. Cells were labeled with DM1 alpha (1:500, Sigma) and human anti-centromere primary antibodies (1:100, ACA, Antibodies Inc., Davis, CA). Donkey anti-mouse Alexa Fluor 594 and donkey anti-human Fluorescein secondary antibodies (Jackson ImmunoResearch Laboratories, Inc., West Grove, PA) were used to visualize DM1 alpha and anti-centromere staining, respectively. Coverslips were mounted in Vectasheild® containing DAPI (Vector Labs, Burlingame, CA). For ch-TOG staining, cells were transfected with GPR124-mCherry and fixed in 4% paraformaldehyde at 37ºC. Cells were permeabilized in 0.5% Triton X-100 for 5 min at room temperature. The anti-ch-TOG antibody (1:1000, BioLegend) was applied overnight at room temperature. Staining was visualized using a donkey anti-rabbit Alexa Fluor 647 antibody (Invitrogen). Coverslips were mounted using ProLong® Gold containing DAPI (Molecular Probes, Eugene, OR, USA). Fluorescent images were collected as 0.5 μm Z-stacks on a Deltavision microscope system (Applied Precision/GEHealthcare, Issaquah, WA) using a 60× 1.42 NA lens (Olympus, Tokyo, Japan). Selected images were deconvolved using SoftWorx 5.0 (Applied Precision/GEHealthcare), and representative images are presented as a flat Z-projection (using ImageJ). Mitotic spindles were imaged by Linda Wordeman.

For quantitative analysis of ch-TOG in mitotic cells, cells transfected with GPR124-mCherry or a CMV-mCherry empty vector were treated with the CDK1 inhibitor RO3306 (10 μM, Sigma) overnight to increase mitotic index and stained with the anti-ch-TOG antibody as above. Images were collected as 0.5 μm Z-stacks using consistent settings for quantitative analysis on a Deltavision microscope system and deconvolved using Softworx 5.0. For quantification, regions containing the entire cell, or the mitotic spindle were created on sum slices Z projections. The pixel intensity was quantified and normalized to the area of each region. The background was subtracted by quantifying the pixel intensity in a region outside of

the cell and subtracting from the pixel intensity measured inside the cell. Ch-TOG levels were imaged and quantified by Juan Jesus Vicente.

Spindle profiles and assessment of multipolar spindles

T98G cells were plated on 12-mm glass coverslips and cultured overnight in RPMI medium with 10% FBS. Cells were treated for 4 hrs with ST-11, and MTs and centromeres were labeled as above with DM1 alpha and anti-centromere antibodies. Mitotic stages were scored using a Nikon FX-A microscope with a 60× 1.4 NA lens (Tokyo, Japan) at room temperature. Spindle profiles were collected by Linda Wordeman.

Live cell imaging of MT polymerization

Cells were transfected with EB3-GFP and RFP-CenpB to label assembling MTs and centromeres, respectively (183). For GPR124 experiments, cells were transfected with GPR124-mCherry or CMV-mCherry empty vector. Interphase cells were imaged at a single Z-plane at 500-ms intervals at on a Deltavision microscope system (Applied Precision, Issaquah, WA) using a 60× 1.42 NA lens (Olympus, Tokyo, Japan). ST-11 (0.5 μM) was added, and cells were imaged at 10 min and every 4 hrs after drug application. Mitotic cells were imaged at 37ºC using 3×1.0 μm sections at 2-sec intervals and deconvoluted using SoftWorx 5.0 (Applied Precision). MT assembly rates were scored in interphase cells using Fiji TrackMate (184). To image MT polymerization in mitotic cells, cells were treated with the CDK1 inhibitor RO3306 (10 μM, Sigma) overnight to increase mitotic index. Cells were imaged at 3 Z-planes separated by 0.5 μm at 1 sec intervals for 45 seconds as above. Spindle and astral MT assembly was measured with Fiji by generating kymographs of the EB3-GFP channel. The Fiji Directionality plugin was used to calculate the angles of the EB3-GFP tracks. Speed was calculated using the equation $velocity = \frac{\mu m}{t\,(\tan\theta)}$, where μm = distance per pixel, t = frame time, θ = angle of the EB3-GFP comet in the kymograph (Figure S3.3). Data were expressed as the average of the spindle or astral MT assembly rates for each cell. MT polymerization was measured by Linda Wordeman and Juan Jesus Vicente.

ST-11 nanoparticle formulation

ST-11 nanoparticles were formulated by Jennifer Freeling in the laboratory of Rodney Ho in the Department of Pharmaceutics (University of Washington). For our initial small scale characterization studies, lipid nanoparticles composed of EPC:DMPG:DMPE-mPEG2000 (9:1:0.5 m/m/m) with or without 15 mM ST-11 were prepared by first mixing EPC (20 mg/mL) in

chloroform, DMPE-mPEG2000 (50 mg/mL) in chloroform:ethanol (3:1 v/v), DMPG (50 mg/mL) in chloroform:ethanol:water (65:35:4 v/v/v) and ST-11 (10 mg/mL) in chloroform. The solvent was removed by evaporation under nitrogen gas followed by vacuum desiccation overnight. The dry lipid film was rehydrated at 60°C for 2 hours with 200 µL sterile rehydration buffer consisting of 0.9% sodium chloride and 20 mM sodium bicarbonate at pH 7.8 to a final drug concentration of 15 mM ST-11. The particle size of ST-11 lipid nanoparticles was reduced with a bath-type sonicator (Avanti, Alabastar, AL, USA) at 55°C for 10-15 mins. The ST-11 lipid nanoparticles were allowed to cool to room temperature.

To determine the degree to which ST-11 stably associated with the lipid nanoparticles, 80 µL of the above sample was dialyzed (molecular weight cutoff 6,000-8,000 Da) against 500 mL of 0.9% sodium chloride with 20 mM sodium bicarbonate (pH=7.2) for 20 hrs. Drug concentrations before and after dialysis were analyzed with mass spectrometry (see Materials & methods). The diameter of ST-11 lipid nanoparticles was determined by photon correlation spectroscopy using a Malvern Zetasizer 5000 (Malvern Instruments, Worcestershire, UK). The osmolality of ST-11 nanoparticles was determined using a Vapro 5520 vapor pressure osmometer (Wescor, Logan, UT, USA) and pH was determined using Hydrion pH paper.

For large-scale production for *in vivo* studies, DMPE-mPEG2000 powder was initially added to EPC dissolved in chloroform at the appropriate ratio and mixed. DMPG was dissolved in chloroform:ethanol:water (65:35:4 v/v/v) and added to the chloroform-lipid mixture. For drug-loaded nanoparticles, ST-11 was dissolved in chloroform to a concentration of 13.3 mg/mL and added to the lipid mixture. The final lipid-to-drug ratio was 6:1 (m/m). Solvent was removed under reduced pressure by rotary evaporation using a Büchi Rotavapor R-124 with a Büchi Waterbath B-481 set to 45°C. The lipid film was left under vacuum for 2 days to ensure complete solvent removal. The dry lipid film was rehydrated under aseptic conditions with sterile 0.9% sodium chloride containing 20 mM sodium bicarbonate at 60°C for 3 hrs. The rehydrated mixture was loaded into an Emulsiflex C-5 homogenizer (Avestin, Ottowa, Canada) and homogenized at 11,000-15,000 PSI for 5-12 cycles to reduce the particle size. The size reduction with Emulsiflex C-5 was completed aseptically at 60°C. Particle diameter was determined by photon correlation spectroscopy using a Nicomp 380 ZLS (Particle Sizing Systems, Santa Barbara, CA, USA). Osmolality and pH were determined as described above.

Pilot safety studies

All animal experiments followed the guidelines established by American Association for Accreditation of Laboratory Animal Care, and all procedures were approved by the University of Washington Institutional Animal Care and Use Committee. Following screening for maximum tolerated dose, a 5-day dose-range finding study was performed to gain a preliminary assessment of safety. CD-1 mice were assigned to groups for evaluation following once daily i.p. dosing with 15, 40, 80, 160 or 240 mg/kg ST-11 or the corresponding volume of liposome vehicle. Mice were monitored for signs of general distress, including ataxia, squinting, piloerection, hunching, bradykinesia and dyspnea. Additionally, mice were monitored for organ system dysfunction and/or moribund state. After completion of the study, mice were euthanized and organs were harvested for histopathological analysis by a board-certified veterinary pathologist who was blinded to group assignment. Safety studies were conducted by Brian Haas and Katie Swinney in conjunction with H. Denny Liggitt (Department of Comparative Medicine, University of Washington).

Tissue extraction and ST-11 quantification by LC-MS

Lipids were isolated from blood and whole brains of CD1 mice using a Folch extraction (185). Blood was collected from CD1 mice and immediately centrifuged at 8,160×g to harvest plasma. Whole brains were collected after perfusion with PBS and were immediately homogenized in 10 volumes of $CHCl_3$ and stored at -20°C. Lipids were extracted from 1 mL of each sample using 2 mL $CHCl_3$, 1 mL methanol, 0.5 mL PBS, and 1 µg of JWH-015 as an internal control. Samples were vortexed for 1 min, sonicated for 5 min, and centrifuged at 500 ×g for 5 min at 4°C. Two hundred microliters of the $CHCl_3$ phase was removed, dried down under nitrogen, and resuspended in 1 mL of acetonitrile. Ten microliters of each sample was injected into a Waters Micromass Quattro Premier XE (Milford, MA) equipped with a C18 LC column (AQUITY UPLC BEH C18 1.7 µm 2.1×100mm, Waters, Munich, Germany) to analyze lipid composition. The following protocol was established using a fixed flow rate of 0.3 mL/min: 1) Initial - 70% acetonitrile, 30% H_20; 2) 2.5 min - ramp to 90% acetonitrile/10% H_20; 3) 3.5 min - return to 70% acetonitrile/ 30% H_20. Both ST-11 and JWH-015 have a parent mass/charge ratio (m/z) of 328.2 and elute at 2.7 and 2.9 min, respectively. Compounds were distinguished by their ES+ daughter ions with ST-11 at 169 m/z and JWH-015 at 155 m/z. Quantitation was performed by taking a ratio of the area under the curve (AUC) of ST-11/AUC of JWH-015, and

then calculating the weight of ST-11 using a standard curve. LC-MS quantification was performed by Alipi Naydenov.

Orthotopic DBT tumors and treatment regimen

Eight week old male BALB/c mice were anesthetized with ketamine/xylazine (0.02 mL/g body weight i.p., 130 mg/kg ketamine/8.8 mg/kg xylazine) and placed in a stereotactic apparatus (David Kopf Instruments, CA) on an isothermal pad (Deltaphase®, Braintree Scientific, Inc, Braintree, MA). After midline incision of the scalp, a craniotomy was performed at 2 mm cranial from bregma and 1.5 mm left lateral, and a 25-G needle was used to inject DBT cells (2×10^4 in 1 µL PBS) over 3 min using a microinjector. The needle remained in place for 2 min after injection and was then removed slowly, followed by gentle irrigation with 0.9% saline to flush residual cells. The craniotomy and scalp were closed with bonewax (Ethicon, NJ) and silk suture (no. 3-0, Ethicon), respectively. Animals were allowed to recover from anesthesia on the heating pad. Tumors exhibited features of aggressive progression within 3 weeks, including frequent mitotic figures, multifocal necrosis, edema, and densely arranged neoplastic cells with enhanced cellular atypia, anisocytosis and anisokaryosis (Figure S2.3). For the assessment of ST-11 on glioma progression, mice were divided into 4 arms 1 week after implantation: vehicle (liposome-only), 5 mg/kg, 15 mg/kg, and 40 mg/kg ST-11. Mice received daily i.p. injections of vehicle or ST-11 for 2 weeks. Mice were euthanized and perfused with 4% paraformaldehyde, and whole brains were harvested. DBT tumors were established and treated by Susan Fung, Katie Swinney, and Brian Haas.

Immunohistochemistry (IHC) and H&E

Mice were euthanized with a euthanasia dose of ketamine/xylazine solution, transcardially-perfused with 25 mL of cold PBS, followed by 25 mL of paraformaldehyde (4%). Brains were removed and placed in paraformaldehyde (4%) overnight. IHC was performed as described previously (186), with the following primary antibodies: anti-activated caspase-3 (1:200, Abcam), anti-Iba-1 (1:1000, Abcam), and anti-Ki67 (1:1000, Abcam). Iba-1 and activated caspase-3 images were collected as 0.4 µm Z-stacks with FluoView 10 imaging software (v3.1) on an Olympus FV-1000 Confocal Microscope (Tokyo, Japan) using a 60× 1.35 NA or a 100× 1.4 NA objective. Representative images are presented as maximum intensity Z-projections. Ki67 images were collected using a Marianas Imaging System (Intelligent Imaging Innovations, Inc. Denver, CO, USA) using a 100× 1.4 NA objective. Ten regions were selected at random by stereology using the Slidebook 5 imaging software (Intelligent Imaging Innovations), and total

and Ki67-positive nuclei were hand-counted by an investigator blinded to the experimental group. Representative images were collecting using an AxioObserver Z1 Microscope (Zeiss, Oberkochen, Germany) fitted with an Apotome and a 20× 0.75 NA objective. Images are presented as maximum intensity Z-projections. For H&E staining, fixed brains were either sent to Histology Consultation Services (Everson, WA), or processed in-house. For in-house H&E staining, briefly, brains were soaked in sucrose at 4°C (15%, followed by 30% in PBS for 24 hrs each) and then embedded in Tissue Tek O.C.T. media (Sakura, CA) and slowly frozen over dry ice. Thirty-micron coronal sections were cut using a cryostat (Reichert-Jung 2800 Frigocut E) and air-dried overnight. The slides were dehydrated using increasing concentrations of ethanol, then defatted using xylenes and rehydrated using decreasing concentrations of ethanol. Hematoxylin stain was applied and then slices were rinsed with water and dipped in Eosin (5 sec in concentrated Mayer's hematoxylin and 60 sec in concentrated Eosin Y). Slices were again dehydrated with increasing concentrations of ethanol and rinsed with xylenes before mounting with Permount (Thermo Fisher Scientific). Images were acquired on a Nikon Optiphot-2 microscope (Tokyo, Japan) or a Nikon Eclipse 80i microscope using 4× 0.2 NA, 10× 0.45 NA, or 40× 0.95 NA objectives.

In vivo *xenograft tumor generation*

5×10^6 U87MG-pcDNA or U87MG MC1 cells suspended in 100µl of PBS + 0.1% glucose were implanted subcutaneously into six week old male nu/nu mice (Jackson Labs, Bar Harbor, ME). Mice were housed as 5 per cage, and U87MG tumors appeared approximately 14 days post-implantation. Tumor volume was measured with calipers every two days and calculated with the formula Tumor Volume (mm^3) = length (mm) x width (mm) x height (mm) x 0.5236. Tumors were harvested at 1 of 3 size categories to examine histological markers at different growth stages: 1. Small (500–700 mm^3), 2. Medium (750–950 mm^3), or 3. Large (1000–1200 mm^3). Mice were sacrificed and tumors were removed and divided for either H&E or IHC staining. In preparation of H&E staining, tumors were immediately placed in 10% neutral buffered formalin for 1 week and then sent to Histology Consultation Services for paraffin embedding and staining (Everson, WA, USA). In preparation for IHC, tumors were immediately placed in 4% paraformaldehyde for 24 hrs, 15% sucrose for 24 hrs, and 30% sucrose for 24 hrs prior to being slow frozen over dry ice and stored at -80°C until use.

Tumor volume and necrotic area

Tumor volume was estimated by slab approximation (187). Briefly, whole brain serial sections were visually analyzed for the presence of the tumor and three sections were selected for analysis: one in the middle of the tumor mass and 1 located 1 mm to each side. The sections were stained with H&E and the tumor was hand-traced in each section. The tumor volume was calculated by multiplying the total cross-sectional area of the slabs by the distance between each slab. A number of studies have shown that large numbers of microglia invade GBM tumor masses [Reviewed in (188)] (Figure S2.4). Therefore, to obtain a more precise index of DBT tumor volume, we used semi-quantitative IHC of Iba-1 (186) to calculate the relative percentage of infiltrating microglia for each tumor. We subtracted this value from the calculated tumor volume to obtain the final adjusted tumor volume.

Necrotic area was measured in U87MG-GPR124 and U87MG-pcDNA xenograft tumors on H&E stained slices taken from the center of each tumor. Each slice was overlaid with a grid, and total slice area was calculated by hand using the "measure" tool on the Nikon NIS Elements software connected to a Nikon Optiphot-2 microscope with a 4× 0.2 NA objective. Necrotic area was traced by hand and determined using the same tool.

Microarray analysis of MDA and T98G cells

Microarrays and analysis were performed in conjunction with Theo Bammler (Functional Genomics & Proteomics Facility Core, Center for Ecogenetics and Environmental Health, University of Washington). Integrity of RNA samples from MDA cells was assessed with an Agilent 2100 Bioanalyzer (Agilent Technologies Inc., Santa Clara, CA), which is the method of choice and the recognized standard in the field. RNA integrity was judged by observing distinct and sharp 18S and 28S ribosomal RNA peaks that were baseline separated. RNA quantity was determined by measuring OD_{260} with a Thermo Scientific NanoDrop™ 1000 Spectrophotometer (Thermo Fisher Scientific, Inc.). The NanoDrop instrument was also used to determine purity of RNA samples by measuring $OD_{260/280}$ and $OD_{260/230}$ ratios. Only samples with $OD_{260/280}$ and $OD_{260/230}$ ratios > 1.8 were further processed for Affymetrix Human Gene 1.0 ST arrays. Processing of the RNA samples was performed according to the Affymetrix GeneChip Whole Transcript Sense Target labeling protocol [see (189) for a more detailed description]. The arrays were scanned with an Affymetrix GeneChip® 3000 scanner. Image generation and feature extraction were performed using Affymetrix GeneChip Command Console Software. Please note that we performed processing of RNA samples derived from the MDA cell line only.

Microarray data of T98G cells were obtained from the publicly accessible Gene Expression Omnibus (GEO) data repository ((http://www.ncbi.nlm.nih.gov/gds).

Raw microarray data were processed and analyzed with tools from Bioconductor (190). We normalized the data using the RMA method (191) from the Bioconductor affy package. The quantile normalization step of the RMA normalization was performed at the probeset level. The major goal of this analysis was to characterize the relative expression of orphan GPCR genes in 2 cell lines (MDA, T98G). The data for the MDA cells were generated by our group. The data for the T98G cells were obtained from the publicly accessible data repository Gene Expression Omnibus (http://www.ncbi.nlm.nih.gov/geo), GEO accession number GSE1692. Given that the MDA data were generated by our group and the T98G data by another group, we did not compute contrasts between these independent data sets directly to avoid confounders. Instead, the average normalized fluorescent intensity values for the 25, 50, and 75 percent quartiles were determined for each group. These values were used to divide the GPCR genes with normalized log2 RMA expression values in the 0 to 25, 25 to 50, 50 to 75, and 75 to 100 percentile bins. The bin assignment was used as a surrogate to determine the approximate level of expression of a gene, and this in turn was used to compare expression of GPCR genes across the different cell lines. Identification of the 3 GPCRs with higher expression in T98G cells was validated in-house using qPCR (described above).

SiRNA knockdown and validation of GPR124

SiRNA knockdown of individual GPCRs was conducted in collaboration with the Quellos High Throughput Screening Core at the Institute for Stem Cell & Regenerative Medicine (University of Washington). Sets of 3 siRNA constructs were used to maximize genetic targeting efficacy and knockdown efficiency (Sigma). The Universal control #1 siRNA (UNI, Sigma) was used as a control. The knockdown efficiency of all siRNA sets was validated using qPCR (data not shown). SiRNAs were transfected into T98G cells using Lipofectamine® RNAiMAX reagent (Invitrogen), and ST-11 was added to the cells at 1, 2, and 8 μM. Cell number was assessed after 72 hrs using the WST-1 reagent (described above). GPR124 was identified based on a slight rightward shift in the dose response curve (IC_{50} UNI siRNA = 1.6 μM, IC_{50} GPR124 siRNA = 2.2 μM). By contrast, the IC_{50}'s of GPR21 and GPR137 were both 1.8 μM. All subsequent experiments using siRNA to knockdown GPR124 were conducted using one siRNA construct (#3, targeting sequence: 5'—CCGACUAAACAUAUCUGGA—3').

Time-lapse microscopy

T98G-Scr, T98G-KD, and H2B-GFP HeLa cells were plated in HiQ4 4 chamber glass bottom imaging dishes at a density of 10,000 cells per chamber in DMEM supplemented with 10% FBS. For overexpression experiments, H2B-GFP HeLa cells were infected with pBS-GPR124-myc or pBS-2841 control lentiviruses for 30 hrs prior to imaging. Immediately before imaging, DMEM media was replaced with CO_2-independent media supplemented with 10% FBS. Images were acquired on a Nikon Biostation IM-Q (Nikon) as stacks of 4 3 μm Z-steps every 5–10 min for 24-30 hrs. Time-lapse movies were analyzed by hand using Fiji.

Membrane solubilization

All steps were performed on ice or at 4ºC. Cells were grown to confluence in 10-15 100mm^2 cell culture dishes and harvested by scraping into TME buffer (25mM Tris-HCl pH 7.4, 5 mM $MgCl_2$, 4mM EDTA) containing a cocktail of protease inhibitors (Sigma). Cells were lysed by homogenizing with 40 strokes in a dounce homogenizer, and then centrifuged at 100 × g in a tabletop centrifuge for 10 min to pellet nuclei. The supernatant was collected and diluted with TME containing 2x digitonin (100 mg/ml, diluted to 50mg/ml final concentration, Sigma). Lysates were placed on a rotator at 4 ºC for 2 hrs. Lysates containing cytosolic and solubilized membrane proteins were centrifuged at 15,700 × g and supernatants were collected. Protein concentration was determined using the DC™ Protein Assay (Bio-Rad, Hercules, CA, USA). Lysates were subsequently used for immunoprecipitation or western blot analysis.

Immunoprecipitation

To isolate GPR124 complexes, lysates containing at least 1 mg of protein were incubated with myc antibody (1:100, Cell Signaling Technologies) at 4ºC for 2 hrs. For competition with myc peptide, myc antibody and myc peptide (5 μg/ml, Sigma) were pre-incubated for 30 minutes at room temperature. Agarose beads conjugated to mouse IgA were spiked into lysates and incubated for 1 hr at 4ºC. Beads were washed 5x with TME buffer. For subsequent western blotting, proteins were eluted by heating to 70ºC in 4× LDS sample buffer (Invitrogen) containing 10 % β-mercaptoethanol. For subsequent analysis by mass spectrometry, proteins were reduced with 10 mM DTT and alkylated with 600 mM chloracetamide (Sigma). Proteins were eluted by heating to 70ºC in 4× LDS sample buffer containing 20 mM DTT. Beads were pelleted by centrifugation, and supernatant was loaded into a 4–20 % Bis-Tris polyacrylamide gel for western blotting (described above) or mass spectrometry.

Stable Isotope Labeling of Amino acids in Cell culture (SILAC)

Metabolic labeling of amino acids using SILAC was completed as described previously (163, 192, 193) with DMEM-formulated SILAC media supplemented with 10% dialyzed FBS (Sigma) and either light [L-lysine and L-arginine (Fisher)] or heavy [[$^{13}C_6$, $^{15}N_2$] L-lysine (Sigma-Isotec, St Louis, MO) and [$^{13}C_6$, $^{15}N_4$] L-arginine (Cambridge Isotope Laboratories, Andover, MA)] isotope enriched amino acids. Cells were split into 2 groups regarded as "heavy" and "light". SILAC media was applied to cells for at least 5 cell doublings to ensure complete labeling of the proteome, which was verified by mass spectrometry. Membranes were solubilized as above in preparation for immunoprecipitation and mass spectrometry. Each SILAC labeling experiment consisted of 2 parts completed in parallel: 1. the forward experiment in which a competing myc peptide (5 µg/ml, Sigma) was applied to the light condition, and 2. the reverse experiment in which the myc peptide was applied to the heavy condition. Full competition of the GPR124 complex by the myc peptide was verified by western blot analysis (data not shown). Protein "hits" were identified as described previously (192). Statistical significance was determined using one sample Student's t-tests of the absolute value of the normalized heavy:light peptide ratios of the forward and reverse experiments. A protein was considered statistically relevant if the normalized ratios of each experiment were significantly different from 0.

LC-MS analysis of SILAC reactions

Following immunoprecipitation described above, proteins were separated on a 4–20% polyacrylamide gel and stained with SimplyBlue™ SafeStain (Invitrogen). Lanes were cut into 5 pieces by protein molecular weight. Proteins were digested with trypsin, and samples were extracted and desalted on C18 StageTips (193). Peptides were analyzed on an Orbitrap Elite nanoLCMS (Thermo, Bremen Germany) using 90 min gradients of 3–35% acetonitrile at 200 nL/min (Thermo Dionex RSLCnano, Sunnyvale, CA) as described previously (163). Proteins were identified using MaxQuant [version 1.3.0.5 (195, 196)]. Mass spectrometry was performed in conjunction with Shao-En Ong (Department of Pharmacology, University of Washington).

Statistical Analysis

The GraphPad Prism software (v5.01, La Jolla, CA) was used for statistical analysis. Data are presented as the mean ± SEM, and statistical significance was determined using Student's t-test, a one-way ANOVA followed by a Dunnet's or Tukey *post-hoc* test, or a two-way ANOVA followed by a Bonferroni *post-hoc* test.

APPENDIX

Table S1: Response of T98G cells to 25 AI analogues as measured with WST-1. AI analogues were either commercially available or synthesized in-house. Analogs with a higher potency than WIN-2 are highlighted with **. Data are the mean ± SEM from at least 3 independent experiments performed in triplicate.

Compound	Structure	Potency	Efficacy
WIN55212-2	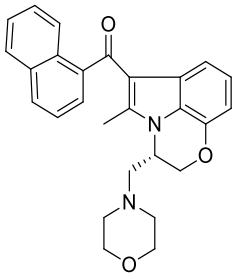	**2.1 μM**	**87.1 ± 1.0%**
WIN55212-3	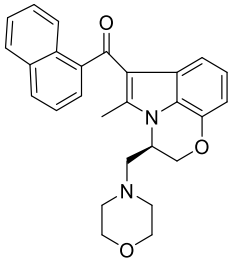	*30 μM inactive*	*N.A.*
Commercially Available Compounds			
JWH-120	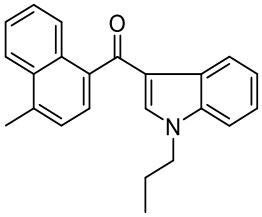	*30 μM inactive*	*N.A.*

Pravadoline	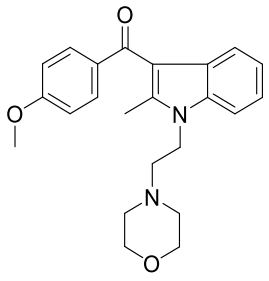	**23 μM**	**87.7 ± 0.5%**
JWH-200	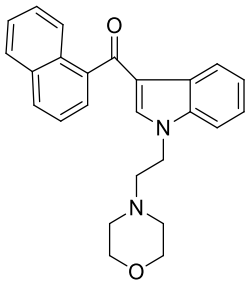	**23 μM**	**48.2 ± 2.0%**
JWH-043	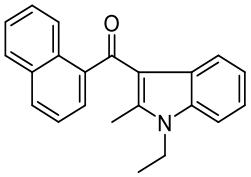	**7.9 μM**	**84.5 ± 0.4%**
JWH-042	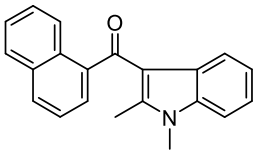	**3.1 μM**	**71.8 ± 2.6%**
****JWH-148**	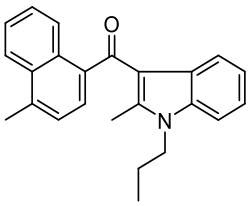	**1.9 μM**	**58.1 ± 4.0%**

****JWH-015**	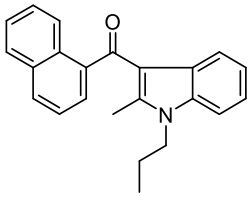	**1.5 μM**	**58.9 ± 1.6%**
ST Compounds			
ST-10	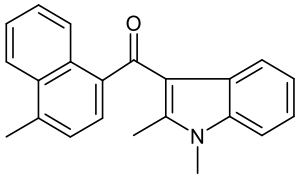	**2.9 μM**	**66.5 ± 2.6%**
N1-Substituted Compounds			
ST-56	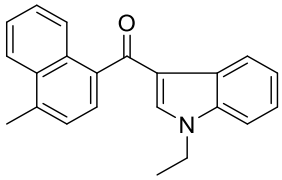	**9.1 μM**	**58.9 ± 6.5%**
ST-48	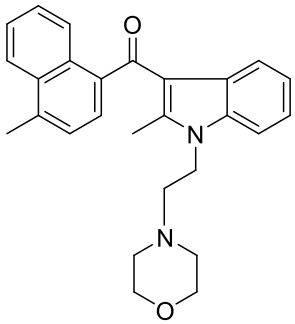	**6.7 μM**	**75.6 ± 2.2%**
****ST-11**	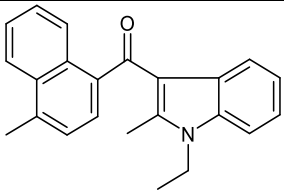	**1.3 μM**	**65.7 ± 6.2%**

****ST-29**	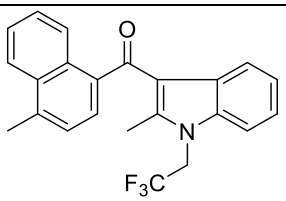	**1.0 µM**	**87.5 ± 0.6%**
****ST-30**	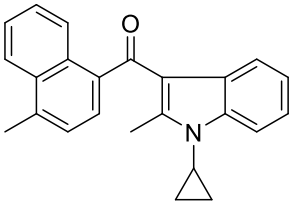	**1.0 µM**	**86.2 ± 0.7%**
N1 + C2-Substituted Compounds			
ST-28	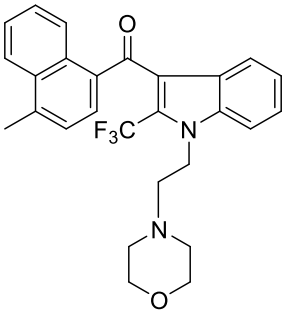	**2.7 µM**	**94.9 ± 1.2%**
****ST-25**	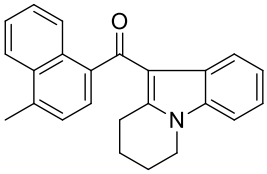	**634 nM**	**64.8 ± 2.3%**
N1 + Aromatic-Substituted Compounds			
ST-21	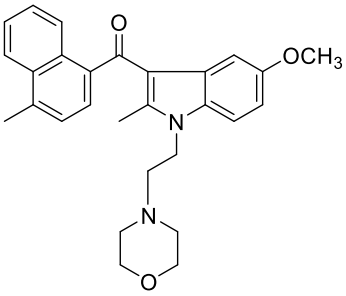	**29 µM**	**66.3 ± 7.8%**

ST-31	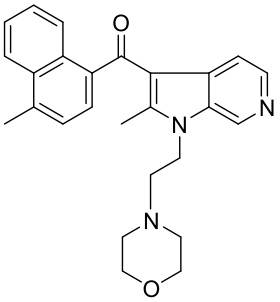	**20 µM**	**73.9 ± 3.9%**
ST-22	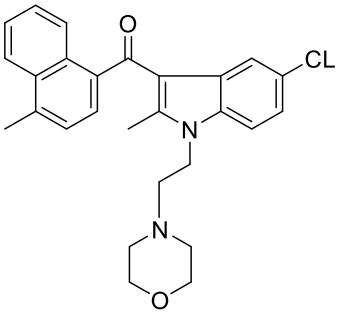	**5.4 µM**	**52.1 ± 2.3%**
ST-23	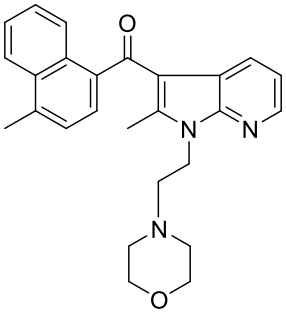	**3.0 µM**	**75.5 ± 4.2%**
ST-26	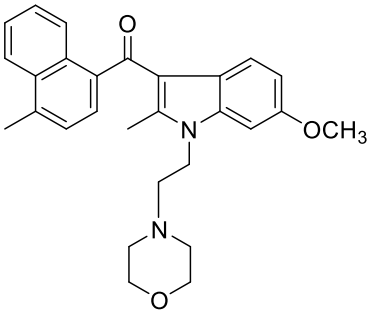	**2.5 µM**	**66.1 ± 9.8%**
****ST-24**	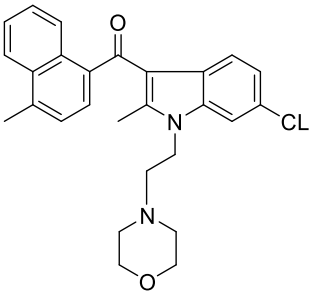	**1.4 µM**	**69.0 ± 1.1%**

****ST-27**	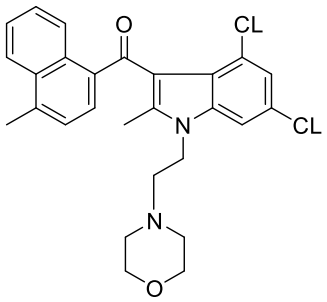	**409 nM**	**78.1 ± 4.1%**
N1 + Naphthalene-Substituted Compounds			
ST-47	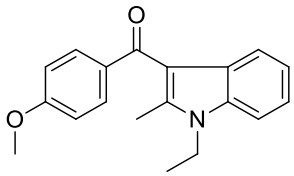	**20 µM**	**54.9 ± 2.1%**

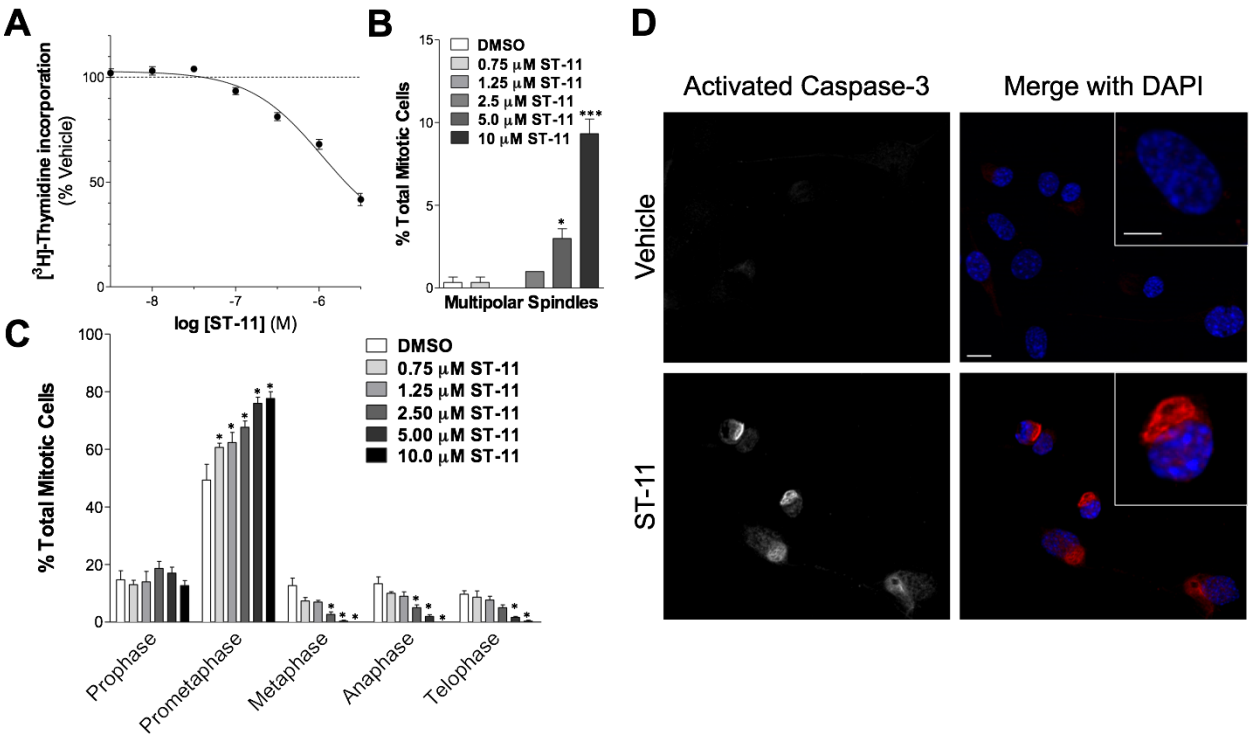

Figure S2.1: ST-11 reduces proliferation and triggers apoptosis in DBT cells *in vitro*.
(A) Increasing doses of ST-11 reduces [3H]-thymidine incorporation after 24 hrs compared with DMSO vehicle control. (B) ST-11 dose-dependently increases the formation of multipolar spindles. *p<0.05 ***P<0.001, one-way ANOVA with a Tukey post-hoc test. (C) ST-11 dose-dependently increases the percentage of mitotic cells in the prometaphase stage. *p<0.05 two-way ANOVA with a Bonferroni post-hoc test. (A-C) Data are the mean ± SEM of at least 3 independent experiments. (D) Representative image of ST-11 (10 μM for 6 hrs) increasing cleaved caspase-3 (red) and inducing nuclear condensation (blue), indicating the activation of apoptosis. Scale bars: 10 μm.

Solubility of ST-11

	1 day	14 days
30% mouse serum	N	N
10% EtOH	N	N
1% DMSO	N	N
1% Tween-80	N	P
2% Tween-80	N	P
EtOH:Cre:Sal (1:1:18)	P	P
1% Tween-80 + 10% FBS	N	P

Key	
S	remained in solution
N	not soluble
P	partially dissolved

Figure S2.2: Solubility and stability of ST-11.
ST-11 was formulated as indicated, and its solubility and stability at 4°C for 1 and 14 days was visually inspected. Each formulation was evaluated 3 independent times. Nomenclature of visual inspections: (S) remained in solution (i.e. clear solution), (N) not soluble (i.e. precipitates) and (P) partially soluble (i.e. cloudy solution).

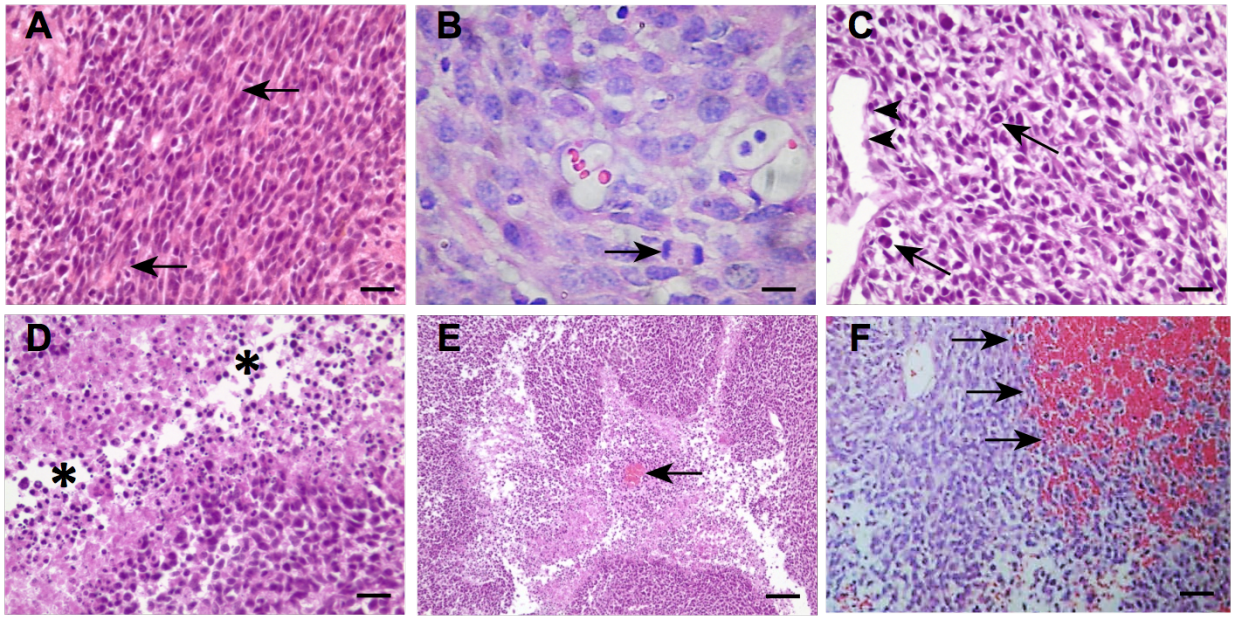

Figure S2.3: Representative histological features of orthotopic DBT tumor 3 weeks after implantation

(A) Arrows point to regions of neoplastic cells that are pleomorphic to spindloid Scale bar: 100 µm. (B) Arrow points to a mitotic cell. Scale bar: 25 µm. (C) Arrows point to mitotic figures and arrowheads point to a blood vessel characteristic of this tumor. Scale bar: 100 µm. (D) Asterisks mark large necrotic area Scale bar: 100 µm. (E, F) Arrows point to focus of hemorrhage surrounding individual necrotic cells. These areas show clear evidence of edema. Scale bars: 400 µm (E) and 100 µm (F).

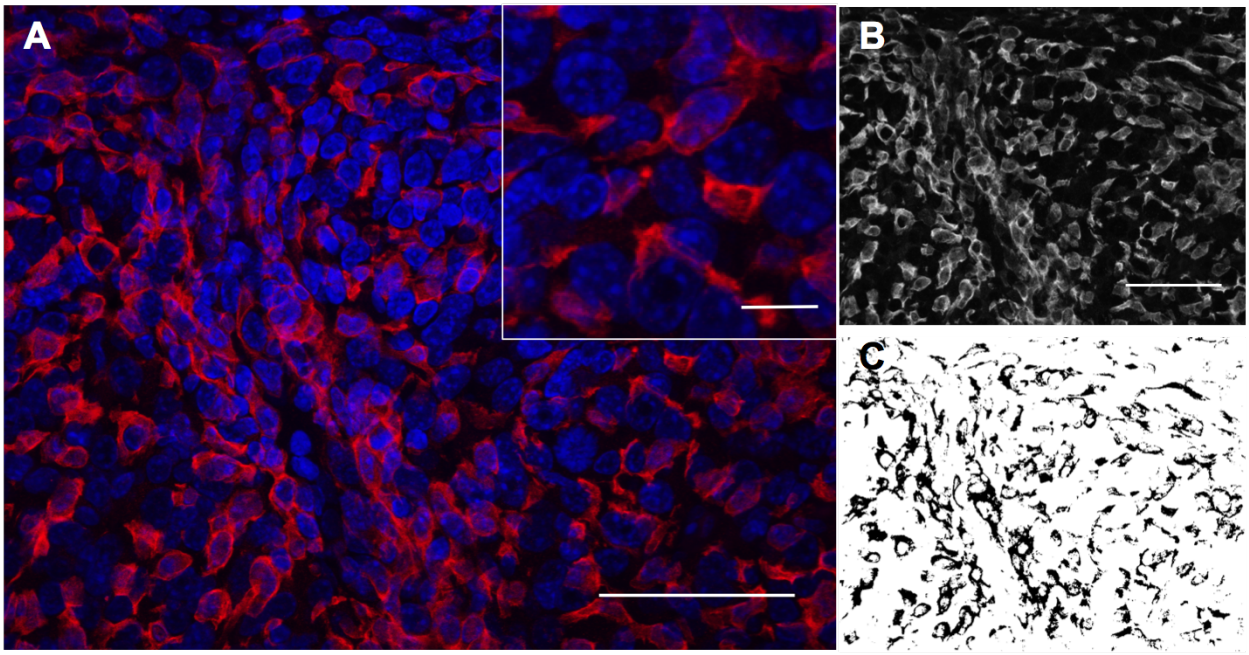

Figure S2.4: Semi-quantitative analysis of microglial invasion of DBT tumors
(A) Representative image of Iba-1 (red) and DAPI (blue) staining of DBT tumor slices showing dense microglia. (B-C) Semi-quantitative analysis of Iba-1 staining: the red channel was isolated (B) and thresholded to obtain a mask of positively stained pixels (C). Regions of interest were generated off this mask to measure the mean intensity of Iba-1 staining in each tumor as a proportion of total cell nuclei. Scale bars: 50 μm, inset: 10 μm.

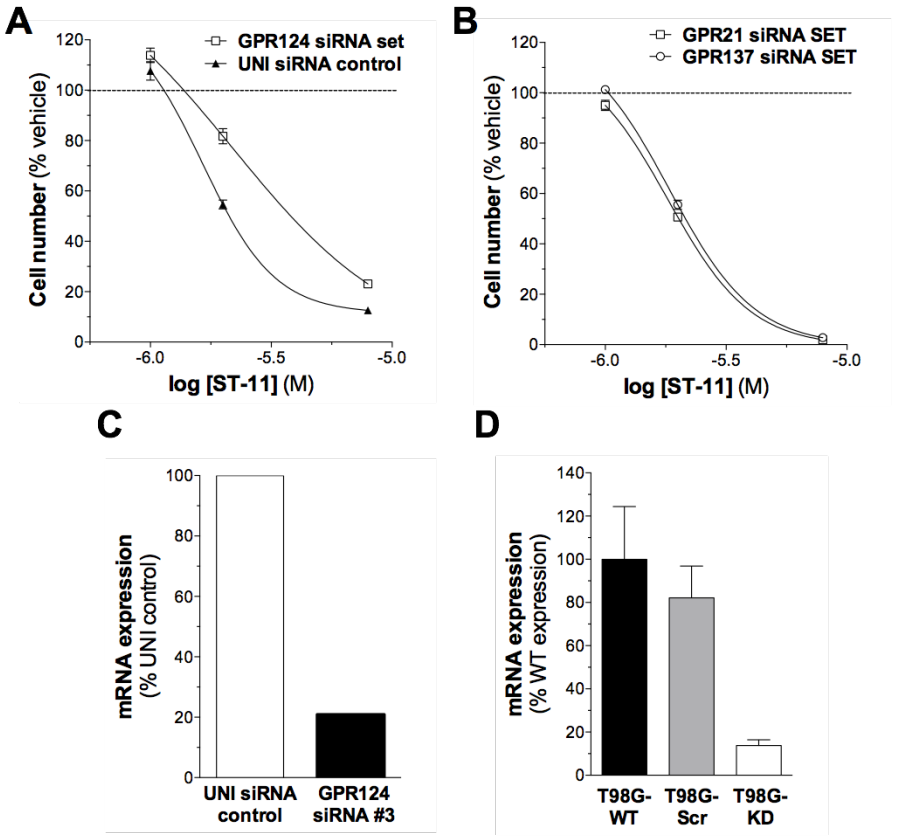

Figure S3.1: GPR124 regulates the cellular response to antitubulin agents.
(A-B) GPR124 (A), GPR21, and GPR137 (C) were knocked down with siRNA and treated with ST-11. Cell number was measured with WST-1 after 72 hrs. A scrambled siRNA (UNI siRNA) was used as a control [shown in (A)]. (C-D) SiRNA (C) and shRNA (D) knockdown of GPR124 in T98G cells was validated using qPCR.

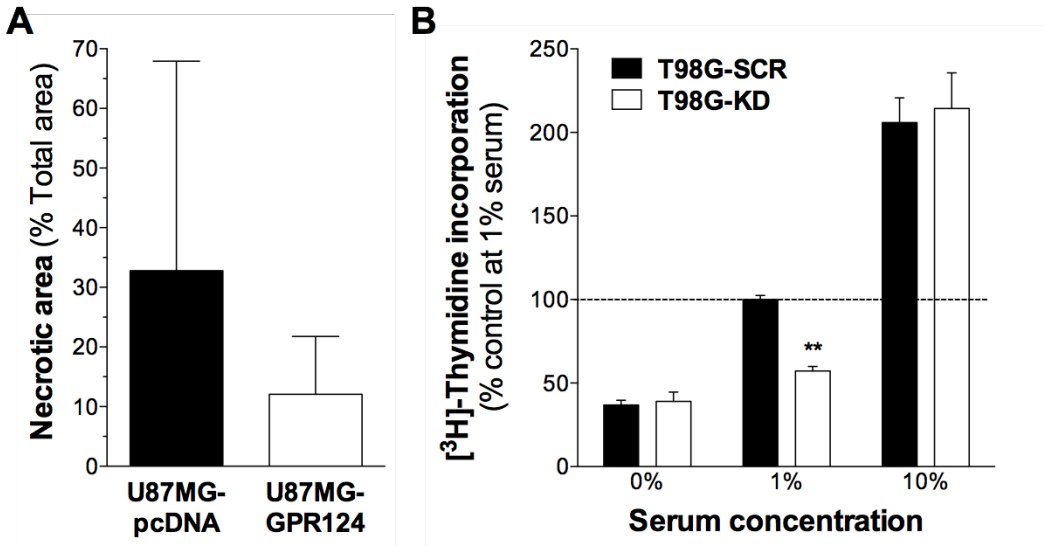

Figure S3.2: GPR124 regulates tumor proliferation and not tumor necrosis.
(A) The total necrotic area was measured in xenograft tumors established with U87MG cells overexpresing GPR124 (U87MG-GPR124) or U87MG cells expressing an empty vector control (U87MG-pcDNA). Results are presented as a mean of all tumors in each group, regardless of tumor size. (B) ^{3}[H]-thymidine uptake was assessed in T98G cells stably expressing a GPR124-targeted shRNA (T98G-KD) or a scramble shRNA control (T98G-Scr) in 3 serum conditions (0%, 1%, and 10%). **p<0.01, two-way ANOVA.

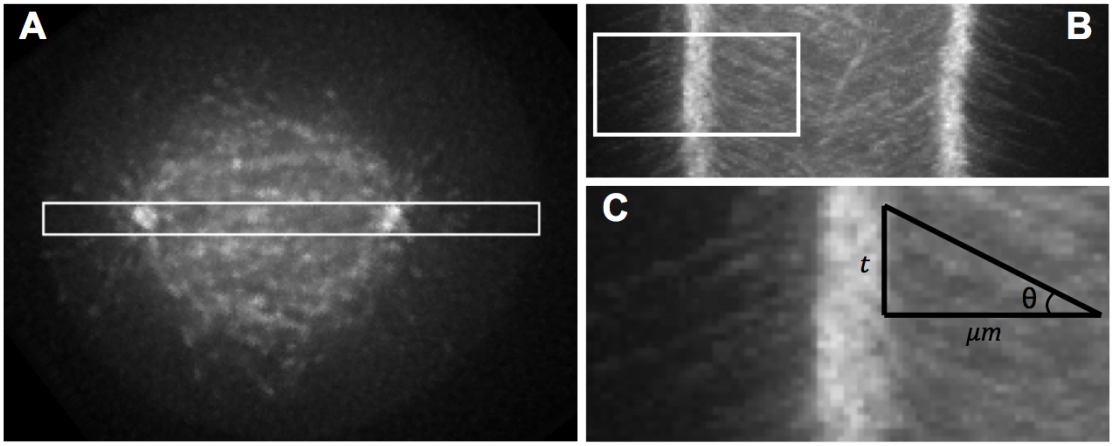

Figure S3.3: Measuring MT assembly rates in mitotic cells.
(A) Cells were transfected with EB3-GFP to label assembling MT tips. Mitotic cells were identified by the presence of a bipolar mitotic spindle and filmed every sec for 60 sec. A region of interest was highlighted surrounding both centrosomes. (B) Kymograph of the region of interest defined in (A). (C) The region defined by the box in (B) is enlarged to show EB3-GFP comet tracks. The velocity of the EB3-GFP comets is defined by the equation velocity=μm/(t*tanθ).

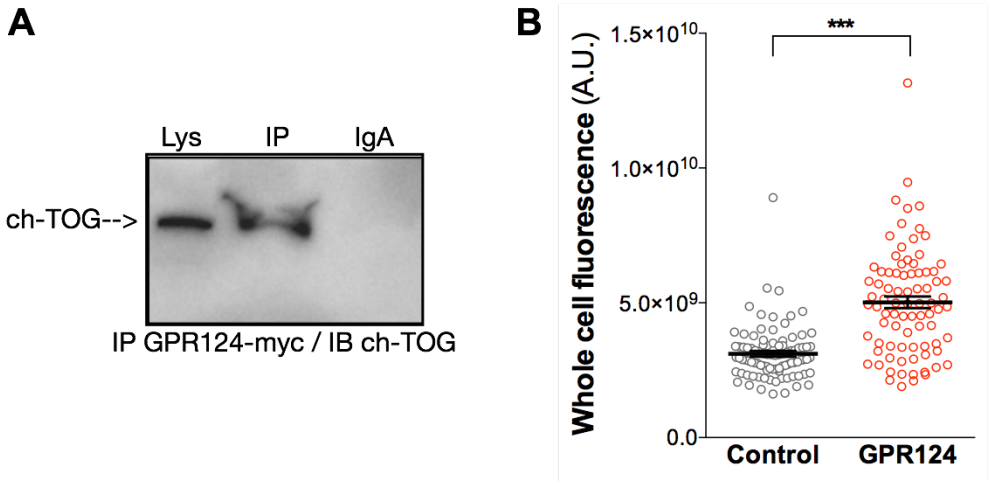

Figure S3.4: GPR124 interacts with ch-TOG and increases ch-TOG levels
(A) Ch-TOG is detected by western blot when GPR124-myc is immunoprecipitated. No ch-TOG band was detected using an IgA-only control. Lys: Lysate, IP: Immunoprecipitation. (B) Overexpression of GPR124-mCherry increased the level of ch-TOG present in mitotic cells. ***p<0.0001, Student's t-test. Data are expressed as the mean ± SEM.

References

1. Central Brain Tumor Registry of the United States [CBTRUS] (2012) CBTRUS Statistical Report: Primary Brain and Central Nervous System Tumors Diagnosed in the United States in 2004-2008 (March 23, 2012 Revision). *http://www.cbtrus.org/2012-NPCR-SEER/CBTRUS_Report_2004-2008_3-23-2012.pdf.* **2013,** 58

2. Stupp, R., Mason, W.P., van den Bent, M.J., Weller, M., Fisher, B., Taphoorn, M.J., Belanger, K., Brandes, A.A., Marosi, C., Bogdahn, U., Curschmann, J., Janzer, R.C., Ludwin, S.K., Gorlia, T., Allgeier, A., Lacombe, D., Cairncross, J.G., Eisenhauer, E., Mirimanoff, R.O., European Organisation for Research and Treatment of Cancer Brain Tumor and Radiotherapy Groups, and National Cancer Institute of Canada Clinical Trials Group (2005) Radiotherapy plus concomitant and adjuvant temozolomide for glioblastoma. *N.Engl.J.Med.* **352,** 987-996

3. Bao, S., Wu, Q., McLendon, R.E., Hao, Y., Shi, Q., Hjelmeland, A.B., Dewhirst, M.W., Bigner, D.D., and Rich, J.N. (2006) Glioma stem cells promote radioresistance by preferential activation of the DNA damage response. *Nature.* **444,** 756-760

4. Liu, G., Yuan, X., Zeng, Z., Tunici, P., Ng, H., Abdulkadir, I.R., Lu, L., Irvin, D., Black, K.L., and Yu, J.S. (2006) Analysis of gene expression and chemoresistance of CD133+ cancer stem cells in glioblastoma. *Mol.Cancer.* **5,** 67

5. Lapidot, T., Sirard, C., Vormoor, J., Murdoch, B., Hoang, T., Caceres-Cortes, J., Minden, M., Paterson, B., Caligiuri, M.A., and Dick, J.E. (1994) A cell initiating human acute myeloid leukaemia after transplantation into SCID mice. *Nature.* **367,** 645-648

6. Bonnet, D., and Dick, J.E. (1997) Human acute myeloid leukemia is organized as a hierarchy that originates from a primitive hematopoietic cell. *Nat.Med.* **3,** 730-737

7. Reya, T., Morrison, S.J., Clarke, M.F., and Weissman, I.L. (2001) Stem cells, cancer, and cancer stem cells. *Nature.* **414,** 105-111

8. Johnson, B.E., Mazor, T., Hong, C., Barnes, M., Aihara, K., McLean, C.Y., Fouse, S.D., Yamamoto, S., Ueda, H., Tatsuno, K., Asthana, S., Jalbert, L.E., Nelson, S.J., Bollen, A.W., Gustafson, W.C., Charron, E., Weiss, W.A., Smirnov, I.V., Song, J.S., Olshen, A.B., Cha, S., Zhao, Y., Moore, R.A., Mungall, A.J., Jones, S.J., Hirst, M., Marra, M.A., Saito, N., Aburatani, H., Mukasa, A., Berger, M.S., Chang, S.M., Taylor, B.S., and Costello, J.F. (2014) Mutational analysis reveals the origin and therapy-driven evolution of recurrent glioma. *Science.* **343,** 189-193

9. Hartmann, C., Hentschel, B., Wick, W., Capper, D., Felsberg, J., Simon, M., Westphal, M., Schackert, G., Meyermann, R., Pietsch, T., Reifenberger, G., Weller, M., Loeffler, M., and von Deimling, A. (2010) Patients with IDH1 wild type anaplastic astrocytomas exhibit worse prognosis than IDH1-mutated glioblastomas, and IDH1 mutation status accounts for the unfavorable prognostic effect of higher age: implications for classification of gliomas. *Acta Neuropathol.* **120,** 707-718

10. Cancer Genome Atlas Research Network (2008) Comprehensive genomic characterization defines human glioblastoma genes and core pathways. *Nature.* **455,** 1061-1068

11. Guan, X., Vengoechea, J., Zheng, S., Sloan, A.E., Chen, Y., Brat, D.J., O'Neill, B.P., de Groot, J., Yust-Katz, S., Yung, W.K., Cohen, M.L., Aldape, K.D., Rosenfeld, S., Verhaak, R.G., and Barnholtz-Sloan, J.S. (2014) Molecular subtypes of glioblastoma are relevant to lower grade glioma. *PLoS One.* **9,** e91216

12. Verhaak, R.G., Hoadley, K.A., Purdom, E., Wang, V., Qi, Y., Wilkerson, M.D., Miller, C.R., Ding, L., Golub, T., Mesirov, J.P., Alexe, G., Lawrence, M., O'Kelly, M., Tamayo, P., Weir, B.A., Gabriel, S., Winckler, W., Gupta, S., Jakkula, L., Feiler, H.S., Hodgson, J.G., James, C.D., Sarkaria, J.N., Brennan, C., Kahn, A., Spellman, P.T., Wilson, R.K., Speed, T.P., Gray, J.W., Meyerson, M., Getz, G., Perou, C.M., Hayes, D.N., and Cancer Genome Atlas Research Network (2010) Integrated genomic analysis identifies clinically relevant subtypes of glioblastoma characterized by abnormalities in PDGFRA, IDH1, EGFR, and NF1. *Cancer.Cell.* **17,** 98-110

13. Sugawa, N., Ekstrand, A.J., James, C.D., and Collins, V.P. (1990) Identical splicing of aberrant epidermal growth factor receptor transcripts from amplified rearranged genes in human glioblastomas. *Proc.Natl.Acad.Sci.U.S.A.* **87,** 8602-8606

14. Ekstrand, A.J., James, C.D., Cavenee, W.K., Seliger, B., Pettersson, R.F., and Collins, V.P. (1991) Genes for epidermal growth factor receptor, transforming growth factor alpha, and epidermal growth factor and their expression in human gliomas in vivo. *Cancer Res.* **51,** 2164-2172

15. Wong, A.J., Ruppert, J.M., Bigner, S.H., Grzeschik, C.H., Humphrey, P.A., Bigner, D.S., and Vogelstein, B. (1992) Structural alterations of the epidermal growth factor receptor gene in human gliomas. *Proc.Natl.Acad.Sci.U.S.A.* **89,** 2965-2969

16. Aldape, K.D., Ballman, K., Furth, A., Buckner, J.C., Giannini, C., Burger, P.C., Scheithauer, B.W., Jenkins, R.B., and James, C.D. (2004) Immunohistochemical detection of EGFRvIII in high malignancy grade astrocytomas and evaluation of prognostic significance. *J.Neuropathol.Exp.Neurol.* **63,** 700-707

17. Zhang, H., Berezov, A., Wang, Q., Zhang, G., Drebin, J., Murali, R., and Greene, M.I. (2007) ErbB receptors: from oncogenes to targeted cancer therapies. *J.Clin.Invest.* **117,** 2051-2058

18. Verhaak, R.G., Hoadley, K.A., Purdom, E., Wang, V., Qi, Y., Wilkerson, M.D., Miller, C.R., Ding, L., Golub, T., Mesirov, J.P., Alexe, G., Lawrence, M., O'Kelly, M., Tamayo, P., Weir, B.A., Gabriel, S., Winckler, W., Gupta, S., Jakkula, L., Feiler, H.S., Hodgson, J.G., James, C.D., Sarkaria, J.N., Brennan, C., Kahn, A., Spellman, P.T., Wilson, R.K., Speed, T.P., Gray, J.W., Meyerson, M., Getz, G., Perou, C.M., Hayes, D.N., and Cancer Genome Atlas Research Network (2010) Integrated genomic analysis identifies clinically relevant subtypes of glioblastoma characterized by abnormalities in PDGFRA, IDH1, EGFR, and NF1. *Cancer.Cell.* **17,** 98-110

19. Libermann, T.A., Nusbaum, H.R., Razon, N., Kris, R., Lax, I., Soreq, H., Whittle, N., Waterfield, M.D., Ullrich, A., and Schlessinger, J. (1985) Amplification, enhanced expression and possible rearrangement of EGF receptor gene in primary human brain tumours of glial origin. *Nature.* **313,** 144-147

20. Wong, A.J., Bigner, S.H., Bigner, D.D., Kinzler, K.W., Hamilton, S.R., and Vogelstein, B. (1987) Increased expression of the epidermal growth factor receptor gene in malignant gliomas is invariably associated with gene amplification. *Proc.Natl.Acad.Sci.U.S.A.* **84,** 6899-6903

21. Frederick, L., Wang, X.Y., Eley, G., and James, C.D. (2000) Diversity and frequency of epidermal growth factor receptor mutations in human glioblastomas. *Cancer Res.* **60,** 1383-1387

22. Hanahan, D., and Weinberg, R.A. (2011) Hallmarks of cancer: the next generation. *Cell.* **144,** 646-674

23. Friedman, H.S., Prados, M.D., Wen, P.Y., Mikkelsen, T., Schiff, D., Abrey, L.E., Yung, W.K., Paleologos, N., Nicholas, M.K., Jensen, R., Vredenburgh, J., Huang, J., Zheng, M., and Cloughesy, T. (2009) Bevacizumab alone and in combination with irinotecan in recurrent glioblastoma. *J.Clin.Oncol.* **27,** 4733-4740

24. Gilbert, M.R., Dignam, J.J., Armstrong, T.S., Wefel, J.S., Blumenthal, D.T., Vogelbaum, M.A., Colman, H., Chakravarti, A., Pugh, S., Won, M., Jeraj, R., Brown, P.D., Jaeckle, K.A., Schiff, D., Stieber, V.W., Brachman, D.G., Werner-Wasik, M., Tremont-Lukats, I.W., Sulman, E.P., Aldape, K.D., Curran, W.J.,Jr, and Mehta, M.P. (2014) A randomized trial of bevacizumab for newly diagnosed glioblastoma. *N.Engl.J.Med.* **370,** 699-708

25. de Groot, J.F., Fuller, G., Kumar, A.J., Piao, Y., Eterovic, K., Ji, Y., and Conrad, C.A. (2010) Tumor invasion after treatment of glioblastoma with bevacizumab: radiographic and pathologic correlation in humans and mice. *Neuro Oncol.* **12,** 233-242

26. Keunen, O., Johansson, M., Oudin, A., Sanzey, M., Rahim, S.A., Fack, F., Thorsen, F., Taxt, T., Bartos, M., Jirik, R., Miletic, H., Wang, J., Stieber, D., Stuhr, L., Moen, I., Rygh, C.B., Bjerkvig, R., and Niclou, S.P. (2011) Anti-VEGF treatment reduces blood supply and increases tumor cell invasion in glioblastoma. *Proc.Natl.Acad.Sci.U.S.A.* **108,** 3749-3754

27. Rich, J.N., Reardon, D.A., Peery, T., Dowell, J.M., Quinn, J.A., Penne, K.L., Wikstrand, C.J., Van Duyn, L.B., Dancey, J.E., McLendon, R.E., Kao, J.C., Stenzel, T.T., Ahmed Rasheed, B.K., Tourt-Uhlig, S.E., Herndon, J.E.,2nd, Vredenburgh, J.J., Sampson, J.H., Friedman, A.H., Bigner, D.D., and Friedman, H.S. (2004) Phase II trial of gefitinib in recurrent glioblastoma. *J.Clin.Oncol.* **22,** 133-142

28. van den Bent, M.J., Brandes, A.A., Rampling, R., Kouwenhoven, M.C., Kros, J.M., Carpentier, A.F., Clement, P.M., Frenay, M., Campone, M., Baurain, J.F., Armand, J.P., Taphoorn, M.J., Tosoni, A., Kletzl, H., Klughammer, B., Lacombe, D., and Gorlia, T. (2009) Randomized phase II trial of erlotinib versus temozolomide or carmustine in recurrent glioblastoma: EORTC brain tumor group study 26034. *J.Clin.Oncol.* **27,** 1268-1274

29. Reardon, D.A., Desjardins, A., Vredenburgh, J.J., Gururangan, S., Friedman, A.H., Herndon, J.E.,2nd, Marcello, J., Norfleet, J.A., McLendon, R.E., Sampson, J.H., and Friedman, H.S. (2010) Phase 2 trial of erlotinib plus sirolimus in adults with recurrent glioblastoma. *J.Neurooncol.* **96,** 219-230

30. Wen, P.Y., Yung, W.K., Lamborn, K.R., Dahia, P.L., Wang, Y., Peng, B., Abrey, L.E., Raizer, J., Cloughesy, T.F., Fink, K., Gilbert, M., Chang, S., Junck, L., Schiff, D., Lieberman, F., Fine, H.A., Mehta, M., Robins, H.I., DeAngelis, L.M., Groves, M.D., Puduvalli, V.K., Levin, V., Conrad, C., Maher, E.A., Aldape, K., Hayes, M., Letvak, L., Egorin, M.J., Capdeville, R., Kaplan, R., Murgo, A.J., Stiles, C., and Prados, M.D. (2006) Phase I/II study of imatinib mesylate for recurrent malignant gliomas: North American Brain Tumor Consortium Study 99-08. *Clin.Cancer Res.* **12,** 4899-4907

31. Razis, E., Selviaridis, P., Labropoulos, S., Norris, J.L., Zhu, M.J., Song, D.D., Kalebic, T., Torrens, M., Kalogera-Fountzila, A., Karkavelas, G., Karanastasi, S., Fletcher, J.A., and Fountzilas, G. (2009) Phase II study of neoadjuvant imatinib in glioblastoma: evaluation of clinical and molecular effects of the treatment. *Clin.Cancer Res.* **15,** 6258-6266

32. Kreisl, T.N., Smith, P., Iwamoto, F., Sul, J., Butman, J.A., and Fine, H.A. (2010) A phase II trial of Sunitinib in the treatment of recurrent glioblastoma (GBM). *Neuro-oncology.* **12,** iv71

33. Ding, Y., Hubert, C.G., Herman, J., Corrin, P., Toledo, C.M., Skutt-Kakaria, K., Vazquez, J., Basom, R., Zhang, B., Risler, J.K., Pollard, S.M., Nam, D.H., Delrow, J.J., Zhu, J., Lee, J., DeLuca, J., Olson, J.M., and Paddison, P.J. (2013) Cancer-Specific requirement for BUB1B/BUBR1 in human brain tumor isolates and genetically transformed cells. *Cancer.Discov.* **3,** 198-211

34. Stupp, R., Wong, E.T., Kanner, A.A., Steinberg, D., Engelhard, H., Heidecke, V., Kirson, E.D., Taillibert, S., Liebermann, F., Dbaly, V., Ram, Z., Villano, J.L., Rainov, N., Weinberg, U., Schiff, D., Kunschner, L., Raizer, J., Honnorat, J., Sloan, A., Malkin, M., Landolfi, J.C., Payer, F., Mehdorn, M., Weil, R.J., Pannullo, S.C., Westphal, M., Smrcka, M., Chin, L., Kostron, H., Hofer, S., Bruce, J., Cosgrove, R., Paleologous, N., Palti, Y., and Gutin, P.H. (2012) NovoTTF-100A versus physician's choice chemotherapy in recurrent glioblastoma: a randomised phase III trial of a novel treatment modality. *Eur.J.Cancer.* **48,** 2192-2202

35. Kastan, M.B., and Bartek, J. (2004) Cell-cycle checkpoints and cancer. *Nature.* **432,** 316-323

36. Lee, A.J., Endesfelder, D., Rowan, A.J., Walther, A., Birkbak, N.J., Futreal, P.A., Downward, J., Szallasi, Z., Tomlinson, I.P., Howell, M., Kschischo, M., and Swanton, C. (2011) Chromosomal instability confers intrinsic multidrug resistance. *Cancer Res.* **71,** 1858-1870

37. Carter, S.L., Eklund, A.C., Kohane, I.S., Harris, L.N., and Szallasi, Z. (2006) A signature of chromosomal instability inferred from gene expression profiles predicts clinical outcome in multiple human cancers. *Nat.Genet.* **38,** 1043-1048

38. McGranahan, N., Burrell, R.A., Endesfelder, D., Novelli, M.R., and Swanton, C. (2012) Cancer chromosomal instability: therapeutic and diagnostic challenges. *EMBO Rep.* **13,** 528-538

39. Birkbak, N.J., Eklund, A.C., Li, Q., McClelland, S.E., Endesfelder, D., Tan, P., Tan, I.B., Richardson, A.L., Szallasi, Z., and Swanton, C. (2011) Paradoxical relationship between chromosomal instability and survival outcome in cancer. *Cancer Res.* **71,** 3447-3452

40. Tang, Y.C., Williams, B.R., Siegel, J.J., and Amon, A. (2011) Identification of aneuploidy-selective antiproliferation compounds. *Cell.* **144,** 499-512

41. Yuan, B., Xu, Y., Woo, J.H., Wang, Y., Bae, Y.K., Yoon, D.S., Wersto, R.P., Tully, E., Wilsbach, K., and Gabrielson, E. (2006) Increased expression of mitotic checkpoint genes in breast cancer cells with chromosomal instability. *Clin.Cancer Res.* **12,** 405-410

42. Baker, D.J., Dawlaty, M.M., Wijshake, T., Jeganathan, K.B., Malureanu, L., van Ree, J.H., Crespo-Diaz, R., Reyes, S., Seaburg, L., Shapiro, V., Behfar, A., Terzic, A., van de Sluis, B., and van Deursen, J.M. (2013) Increased expression of BubR1 protects against aneuploidy and cancer and extends healthy lifespan. *Nat.Cell Biol.* **15,** 96-102

43. Schmidt, M., and Medema, R.H. (2006) Exploiting the compromised spindle assembly checkpoint function of tumor cells: dawn on the horizon?. *Cell.Cycle.* **5,** 159-163

44. Herman, J.A., Toledo, C.M., Olson, J.M., DeLuca, J.G., and Paddison, P.J. (2015) Molecular pathways: regulation and targeting of kinetochore-microtubule attachment in cancer. *Clin.Cancer Res.* **21,** 233-239

45. Slee, R.B., Grimes, B.R., Bansal, R., Gore, J., Blackburn, C., Brown, L., Gasaway, R., Jeong, J., Victorino, J., March, K.L., Colombo, R., Herbert, B.S., and Korc, M. (2014) Selective inhibition of pancreatic ductal adenocarcinoma cell growth by the mitotic MPS1 kinase inhibitor NMS-P715. *Mol.Cancer.Ther.* **13,** 307-315

46. Danovi, D., Folarin, A., Gogolok, S., Ender, C., Elbatsh, A.M., Engstrom, P.G., Stricker, S.H., Gagrica, S., Georgian, A., Yu, D., U, K.P., Harvey, K.J., Ferretti, P., Paddison, P.J., Preston, J.E., Abbott, N.J., Bertone, P., Smith, A., and Pollard, S.M. (2013) A high-content small molecule screen identifies sensitivity of glioblastoma stem cells to inhibition of polo-like kinase 1. *PLoS One.* **8,** e77053

47. Pezuk, J.A., Brassesco, M.S., Morales, A.G., de Oliveira, J.C., de Paula Queiroz, R.G., Machado, H.R., Carlotti, C.G.,Jr, Neder, L., Scrideli, C.A., and Tone, L.G. (2013) Polo-like kinase 1 inhibition causes decreased proliferation by cell cycle arrest, leading to cell death in glioblastoma. *Cancer Gene Ther.* **20,** 499-506

48. Colombo, R., Caldarelli, M., Mennecozzi, M., Giorgini, M.L., Sola, F., Cappella, P., Perrera, C., Depaolini, S.R., Rusconi, L., Cucchi, U., Avanzi, N., Bertrand, J.A., Bossi, R.T., Pesenti, E., Galvani, A., Isacchi, A., Colotta, F., Donati, D., and Moll, J. (2010) Targeting the mitotic checkpoint for cancer therapy with NMS-P715, an inhibitor of MPS1 kinase. *Cancer Res.* **70,** 10255-10264

49. Jemaa, M., Galluzzi, L., Kepp, O., Senovilla, L., Brands, M., Boemer, U., Koppitz, M., Lienau, P., Prechtl, S., Schulze, V., Siemeister, G., Wengner, A.M., Mumberg, D., Ziegelbauer, K., Abrieu, A., Castedo, M., Vitale, I., and Kroemer, G. (2013) Characterization of novel MPS1 inhibitors with preclinical anticancer activity. *Cell Death Differ.* **20,** 1532-1545

50. Tannous, B.A., Kerami, M., Van der Stoop, P.M., Kwiatkowski, N., Wang, J., Zhou, W., Kessler, A.F., Lewandrowski, G., Hiddingh, L., Sol, N., Lagerweij, T., Wedekind, L., Niers, J.M., Barazas, M., Nilsson, R.J., Geerts, D., De Witt Hamer, P.C., Hagemann, C., Vandertop, W.P., Van Tellingen, O., Noske, D.P., Gray, N.S., and Wurdinger, T. (2013) Effects of the selective MPS1 inhibitor MPS1-IN-3 on glioblastoma sensitivity to antimitotic drugs. *J.Natl.Cancer Inst.* **105,** 1322-1331

51. Topham, C.H., and Taylor, S.S. (2013) Mitosis and apoptosis: how is the balance set?. *Curr.Opin.Cell Biol.* **25,** 780-785

52. Dumontet, C., and Jordan, M.A. (2010) Microtubule-binding agents: a dynamic field of cancer therapeutics. *Nat.Rev.Drug Discov.* **9,** 790-803

53. Levin, V.A., Silver, P., Hannigan, J., Wara, W.M., Gutin, P.H., Davis, R.L., and Wilson, C.B. (1990) Superiority of post-radiotherapy adjuvant chemotherapy with CCNU, procarbazine, and vincristine (PCV) over BCNU for anaplastic gliomas: NCOG 6G61 final report. *Int.J.Radiat.Oncol.Biol.Phys.* **18,** 321-324

54. Aydin, B., Patil, M., Bekele, N., and Wolff, J.E. (2010) Vincristine in high-grade glioma. *Anticancer Res.* **30,** 2303-2310

55. Boyle, F.M., Eller, S.L., and Grossman, S.A. (2004) Penetration of intra-arterially administered vincristine in experimental brain tumor. *Neuro Oncol.* **6,** 300-305

56. Hunt, J.T. (2009) Discovery of ixabepilone. *Mol.Cancer.Ther.* **8,** 275-281

57. Hoffmann, J., Fichtner, I., Lemm, M., Lienau, P., Hess-Stumpp, H., Rotgeri, A., Hofmann, B., and Klar, U. (2009) Sagopilone crosses the blood-brain barrier in vivo to inhibit brain tumor growth and metastases. *Neuro Oncol.* **11,** 158-166

58. Galmarini, C.M. (2009) Sagopilone, a microtubule stabilizer for the potential treatment of cancer. *Curr.Opin.Investig Drugs.* **10,** 1359-1371

59. Silvani, A., Gaviani, P., Fiumani, A., Scaioli, V., Lamperti, E., Eoli, M., Botturi, A., and Salmaggi, A. (2009) Systemic sagopilone (ZK-EPO) treatment of patients with recurrent malignant gliomas. *J.Neurooncol.* **95,** 61-64

60. Stupp, R., Tosoni, A., Bromberg, J.E., Hau, P., Campone, M., Gijtenbeek, J., Frenay, M., Breimer, L., Wiesinger, H., Allgeier, A., van den Bent, M.J., Bogdahn, U., van der Graaf, W., Yun, H.J., Gorlia, T., Lacombe, D., and Brandes, A.A. (2011) Sagopilone (ZK-EPO, ZK 219477) for recurrent glioblastoma. A phase II multicenter trial by the European Organisation for Research and Treatment of Cancer (EORTC) Brain Tumor Group. *Ann.Oncol.* **22,** 2144-2149

61. Kirson, E.D., Gurvich, Z., Schneiderman, R., Dekel, E., Itzhaki, A., Wasserman, Y., Schatzberger, R., and Palti, Y. (2004) Disruption of cancer cell replication by alternating electric fields. *Cancer Res.* **64,** 3288-3295

62. Pierce, K.L., Premont, R.T., and Lefkowitz, R.J. (2002) Seven-transmembrane receptors. *Nat.Rev.Mol.Cell Biol.* **3,** 639-650

63. Pierce, K.L., Premont, R.T., and Lefkowitz, R.J. (2002) Seven-transmembrane receptors. *Nat.Rev.Mol.Cell Biol.* **3,** 639-650

64. Aguado, T., Carracedo, A., Julien, B., Velasco, G., Milman, G., Mechoulam, R., Alvarez, L., Guzman, M., and Galve-Roperh, I. (2007) Cannabinoids induce glioma stem-like cell differentiation and inhibit gliomagenesis. *J.Biol.Chem.* **282,** 6854-6862

65. Bar, E.E., Chaudhry, A., Lin, A., Fan, X., Schreck, K., Matsui, W., Piccirillo, S., Vescovi, A.L., DiMeco, F., Olivi, A., and Eberhart, C.G. (2007) Cyclopamine-mediated hedgehog pathway inhibition depletes stem-like cancer cells in glioblastoma. *Stem Cells.* **25,** 2524-2533

66. Feve, M., Saliou, J.M., Zeniou, M., Lennon, S., Carapito, C., Dong, J., Van Dorsselaer, A., Junier, M.P., Chneiweiss, H., Cianferani, S., Haiech, J., and Kilhoffer, M.C. (2014) Comparative expression study of the endo-G protein coupled receptor (GPCR) repertoire in human glioblastoma cancer stem-like cells, U87-MG cells and non malignant cells of neural origin unveils new potential therapeutic targets. *PLoS One.* **9,** e91519

67. Woerner, B.M., Luo, J., Brown, K.R., Jackson, E., Dahiya, S.M., Mischel, P., Benovic, J.L., Piwnica-Worms, D., and Rubin, J.B. (2012) Suppression of G-protein-coupled receptor kinase 3 expression is a feature of classical GBM that is required for maximal growth. *Mol.Cancer.Res.* **10,** 156-166

68. Mandell, J.W., Glass, G., Gianchandani, E.P., Locke, C.N., Amos, S., Bourne, T.D., Schiff, D., and Papin, J.A. (2009) Dephosphorylation of beta-arrestin 1 in glioblastomas. *J.Neuropathol.Exp.Neurol.* **68,** 535-541

69. DeWire, S.M., Ahn, S., Lefkowitz, R.J., and Shenoy, S.K. (2007) Beta-arrestins and cell signaling. *Annu.Rev.Physiol.* **69,** 483-510

70. Kaur, G., Kim, J., Kaur, R., Tan, I., Bloch, O., Sun, M.Z., Safaee, M., Oh, M.C., Sughrue, M., Phillips, J., and Parsa, A.T. (2013) G-protein coupled receptor kinase (GRK)-5 regulates proliferation of glioblastoma-derived stem cells. *J.Clin.Neurosci.* **20,** 1014-1018

71. Filardo, E.J., Quinn, J.A., Bland, K.I., and Frackelton, A.R.,Jr (2000) Estrogen-induced activation of Erk-1 and Erk-2 requires the G protein-coupled receptor homolog, GPR30, and occurs via trans-activation of the epidermal growth factor receptor through release of HB-EGF. *Mol.Endocrinol.* **14,** 1649-1660

72. Hart, S., Fischer, O.M., Prenzel, N., Zwick-Wallasch, E., Schneider, M., Hennighausen, L., and Ullrich, A. (2005) GPCR-induced migration of breast carcinoma cells depends on both EGFR signal transactivation and EGFR-independent pathways. *Biol.Chem.* **386,** 845-855

73. Thomas, S.M., Bhola, N.E., Zhang, Q., Contrucci, S.C., Wentzel, A.L., Freilino, M.L., Gooding, W.E., Siegfried, J.M., Chan, D.C., and Grandis, J.R. (2006) Cross-talk between G protein-coupled receptor and epidermal growth factor receptor signaling pathways contributes to growth and invasion of head and neck squamous cell carcinoma. *Cancer Res.* **66,** 11831-11839

74. Daub, H., Wallasch, C., Lankenau, A., Herrlich, A., and Ullrich, A. (1997) Signal characteristics of G protein-transactivated EGF receptor. *EMBO J.* **16,** 7032-7044

75. Pierce, K.L., Luttrell, L.M., and Lefkowitz, R.J. (2001) New mechanisms in heptahelical receptor signaling to mitogen activated protein kinase cascades. *Oncogene.* **20,** 1532-1539

76. Bhola, N.E., and Grandis, J.R. (2008) Crosstalk between G-protein-coupled receptors and epidermal growth factor receptor in cancer. *Front.Biosci.* **13,** 1857-1865

77. Prenzel, N., Zwick, E., Daub, H., Leserer, M., Abraham, R., Wallasch, C., and Ullrich, A. (1999) EGF receptor transactivation by G-protein-coupled receptors requires metalloproteinase cleavage of proHB-EGF. *Nature.* **402,** 884-888

78. Gschwind, A., Hart, S., Fischer, O.M., and Ullrich, A. (2003) TACE cleavage of proamphiregulin regulates GPCR-induced proliferation and motility of cancer cells. *EMBO J.* **22,** 2411-2421

79. Schafer, B., Marg, B., Gschwind, A., and Ullrich, A. (2004) Distinct ADAM metalloproteinases regulate G protein-coupled receptor-induced cell proliferation and survival. *J.Biol.Chem.* **279,** 47929-47938

80. Ma, Y.C., Huang, J., Ali, S., Lowry, W., and Huang, X.Y. (2000) Src tyrosine kinase is a novel direct effector of G proteins. *Cell.* **102,** 635-646

81. Piiper, A., and Zeuzem, S. (2004) Receptor tyrosine kinases are signaling intermediates of G protein-coupled receptors. *Curr.Pharm.Des.* **10,** 3539-3545

82. Huang, J., Hu, J., Bian, X., Chen, K., Gong, W., Dunlop, N.M., Howard, O.M., and Wang, J.M. (2007) Transactivation of the epidermal growth factor receptor by formylpeptide receptor exacerbates the malignant behavior of human glioblastoma cells. *Cancer Res.* **67,** 5906-5913

83. Axelson, M., Liu, K., Jiang, X., He, K., Wang, J., Zhao, H., Kufrin, D., Palmby, T., Dong, Z., Russell, A.M., Miksinski, S., Keegan, P., and Pazdur, R. (2013) U.S. Food and Drug Administration approval: vismodegib for recurrent, locally advanced, or metastatic basal cell carcinoma. *Clin.Cancer Res.* **19,** 2289-2293

84. Spectrum Health Hospitals, and Phoenix Children's Hospital Erivedge (Vismodegib) in the Treatment of Pediatric Patients With Refractory Pontine Glioma**2014, Jul 09,**

85. Yan, G.N., Yang, L., Lv, Y.F., Shi, Y., Shen, L.L., Yao, X.H., Guo, Q.N., Zhang, P., Cui, Y.H., Zhang, X., Bian, X.W., and Guo, D.Y. (2014) Endothelial Cells Promote Stem-like Phenotype of Glioma Cells through Activating Hedgehog Pathway. *J.Pathol.*

86. Ehtesham, M., Sarangi, A., Valadez, J.G., Chanthaphaychith, S., Becher, M.W., Abel, T.W., Thompson, R.C., and Cooper, M.K. (2007) Ligand-dependent activation of the hedgehog pathway in glioma progenitor cells. *Oncogene.* **26,** 5752-5761

87. Sarangi, A., Valadez, J.G., Rush, S., Abel, T.W., Thompson, R.C., and Cooper, M.K. (2009) Targeted inhibition of the Hedgehog pathway in established malignant glioma xenografts enhances survival. *Oncogene.* **28,** 3468-3476

88. Dana-Farber Cancer Institute, Brigham and Women's Hospital, Massachusetts General Hospital, and Genzyme (2014) Plerixafor (AMD3100) and Bevacizumab for Recurrent High-Grade Glioma**2014 July 09,**

89. Rubin, J.B., Kung, A.L., Klein, R.S., Chan, J.A., Sun, Y., Schmidt, K., Kieran, M.W., Luster, A.D., and Segal, R.A. (2003) A small-molecule antagonist of CXCR4 inhibits intracranial growth of primary brain tumors. *Proc.Natl.Acad.Sci.U.S.A.* **100,** 13513-13518

90. Ali, M.M., Kumar, S., Shankar, A., Varma, N.R., Iskander, A.S., Janic, B., Chwang, W.B., Jain, R., Babajeni-Feremi, A., Borin, T.F., Bagher-Ebadian, H., Brown, S.L., Ewing, J.R., and Arbab, A.S. (2013) Effects of tyrosine kinase inhibitors and CXCR4 antagonist on tumor growth and angiogenesis in rat glioma model: MRI and protein analysis study. *Transl.Oncol.* **6,** 660-669

91. Kioi, M., Vogel, H., Schultz, G., Hoffman, R.M., Harsh, G.R., and Brown, J.M. (2010) Inhibition of vasculogenesis, but not angiogenesis, prevents the recurrence of glioblastoma after irradiation in mice. *J.Clin.Invest.* **120,** 694-705

92. Barbero, S., Bonavia, R., Bajetto, A., Porcile, C., Pirani, P., Ravetti, J.L., Zona, G.L., Spaziante, R., Florio, T., and Schettini, G. (2003) Stromal cell-derived factor 1alpha stimulates human glioblastoma cell growth through the activation of both extracellular signal-regulated kinases 1/2 and Akt. *Cancer Res.* **63,** 1969-1974

93. Calatozzolo, C., Canazza, A., Pollo, B., Di Pierro, E., Ciusani, E., Maderna, E., Salce, E., Sponza, V., Frigerio, S., Di Meco, F., Schinelli, S., and Salmaggi, A. (2011) Expression of the new CXCL12 receptor, CXCR7, in gliomas. *Cancer.Biol.Ther.* **11,** 242-253

94. Hattermann, K., Held-Feindt, J., Lucius, R., Muerkoster, S.S., Penfold, M.E., Schall, T.J., and Mentlein, R. (2010) The chemokine receptor CXCR7 is highly expressed in human glioma cells and mediates antiapoptotic effects. *Cancer Res.* **70,** 3299-3308

95. Liu, C., Pham, K., Luo, D., Reynolds, B.A., Hothi, P., Foltz, G., and Harrison, J.K. (2013) Expression and functional heterogeneity of chemokine receptors CXCR4 and CXCR7 in primary patient-derived glioblastoma cells. *PLoS One.* **8,** e59750

96. Ehtesham, M., Winston, J.A., Kabos, P., and Thompson, R.C. (2006) CXCR4 expression mediates glioma cell invasiveness. *Oncogene.* **25,** 2801-2806

97. Bajetto, A., Barbieri, F., Dorcaratto, A., Barbero, S., Daga, A., Porcile, C., Ravetti, J.L., Zona, G., Spaziante, R., Corte, G., Schettini, G., and Florio, T. (2006) Expression of CXC

chemokine receptors 1-5 and their ligands in human glioma tissues: role of CXCR4 and SDF1 in glioma cell proliferation and migration. *Neurochem.Int.* **49,** 423-432

98. Hendrix, C.W., Flexner, C., MacFarland, R.T., Giandomenico, C., Fuchs, E.J., Redpath, E., Bridger, G., and Henson, G.W. (2000) Pharmacokinetics and safety of AMD-3100, a novel antagonist of the CXCR-4 chemokine receptor, in human volunteers. *Antimicrob.Agents Chemother.* **44,** 1667-1673

99. Bifulco, M., and Di Marzo, V. (2002) Targeting the endocannabinoid system in cancer therapy: a call for further research. *Nat.Med.* **8,** 547-550

100. Pisanti, S., Picardi, P., D'Alessandro, A., Laezza, C., and Bifulco, M. (2013) The endocannabinoid signaling system in cancer. *Trends Pharmacol.Sci.* **34,** 273-282

101. Galve-Roperh, I., Sanchez, C., Cortes, M.L., Gomez del Pulgar, T., Izquierdo, M., and Guzman, M. (2000) Anti-tumoral action of cannabinoids: involvement of sustained ceramide accumulation and extracellular signal-regulated kinase activation. *Nat.Med.* **6,** 313-319

102. Devane, W.A., Hanus, L., Breuer, A., Pertwee, R.G., Stevenson, L.A., Griffin, G., Gibson, D., Mandelbaum, A., Etinger, A., and Mechoulam, R. (1992) Isolation and structure of a brain constituent that binds to the cannabinoid receptor. *Science.* **258,** 1946-1949

103. Mechoulam, R., Ben-Shabat, S., Hanus, L., Ligumsky, M., Kaminski, N.E., Schatz, A.R., Gopher, A., Almog, S., Martin, B.R., and Compton, D.R. (1995) Identification of an endogenous 2-monoglyceride, present in canine gut, that binds to cannabinoid receptors. *Biochem.Pharmacol.* **50,** 83-90

104. Sugiura, T., Kondo, S., Sukagawa, A., Nakane, S., Shinoda, A., Itoh, K., Yamashita, A., and Waku, K. (1995) 2-Arachidonoylglycerol: a possible endogenous cannabinoid receptor ligand in brain. *Biochem.Biophys.Res.Commun.* **215,** 89-97

105. Stella, N., Schweitzer, P., and Piomelli, D. (1997) A second endogenous cannabinoid that modulates long-term potentiation. *Nature.* **388,** 773-778

106. Matsuda, L.A., Lolait, S.J., Brownstein, M.J., Young, A.C., and Bonner, T.I. (1990) Structure of a cannabinoid receptor and functional expression of the cloned cDNA. *Nature.* **346,** 561-564

107. Munro, S., Thomas, K.L., and Abu-Shaar, M. (1993) Molecular characterization of a peripheral receptor for cannabinoids. *Nature.* **365,** 61-65

108. Lopez-Redondo, F., Lees, G.M., and Pertwee, R.G. (1997) Effects of cannabinoid receptor ligands on electrophysiological properties of myenteric neurones of the guinea-pig ileum. *Br.J.Pharmacol.* **122,** 330-334

109. Pertwee, R.G. (2001) Cannabinoid receptors and pain. *Prog.Neurobiol.* **63,** 569-611

110. Di Carlo, G., and Izzo, A.A. (2003) Cannabinoids for gastrointestinal diseases: potential therapeutic applications. *Expert Opin.Investig.Drugs.* **12,** 39-49

111. Munson, A.E., Harris, L.S., Friedman, M.A., Dewey, W.L., and Carchman, R.A. (1975) Antineoplastic activity of cannabinoids. *J.Natl.Cancer Inst.* **55,** 597-602

112. Velasco, G., Sanchez, C., and Guzman, M. (2012) Towards the use of cannabinoids as antitumour agents. *Nat.Rev.Cancer.* **12,** 436-444

113. Sanchez, C., de Ceballos, M.L., Gomez del Pulgar, T., Rueda, D., Corbacho, C., Velasco, G., Galve-Roperh, I., Huffman, J.W., Ramon y Cajal, S., and Guzman, M. (2001) Inhibition of glioma growth in vivo by selective activation of the CB(2) cannabinoid receptor. *Cancer Res.* **61,** 5784-5789

114. Guzman, M., Duarte, M.J., Blazquez, C., Ravina, J., Rosa, M.C., Galve-Roperh, I., Sanchez, C., Velasco, G., and Gonzalez-Feria, L. (2006) A pilot clinical study of Delta9-tetrahydrocannabinol in patients with recurrent glioblastoma multiforme. *Br.J.Cancer.* **95,** 197-203

115. Park, J.K., Hodges, T., Arko, L., Shen, M., Dello Iacono, D., McNabb, A., Olsen Bailey, N., Kreisl, T.N., Iwamoto, F.M., Sul, J., Auh, S., Park, G.E., Fine, H.A., and Black, P.M. (2010) Scale to predict survival after surgery for recurrent glioblastoma multiforme. *J.Clin.Oncol.* **28,** 3838-3843

116. Sanchez, C., Galve-Roperh, I., Canova, C., Brachet, P., and Guzman, M. (1998) Delta9-tetrahydrocannabinol induces apoptosis in C6 glioma cells. *FEBS Lett.* **436,** 6-10

117. Sanchez, C., Galve-Roperh, I., Rueda, D., and Guzman, M. (1998) Involvement of sphingomyelin hydrolysis and the mitogen-activated protein kinase cascade in the Delta9-tetrahydrocannabinol-induced stimulation of glucose metabolism in primary astrocytes. *Mol.Pharmacol.* **54,** 834-843

118. Blazquez, C., Galve-Roperh, I., and Guzman, M. (2000) De novo-synthesized ceramide signals apoptosis in astrocytes via extracellular signal-regulated kinase. *FASEB J.* **14,** 2315-2322

119. Cudaback, E., Marrs, W., Moeller, T., and Stella, N. (2010) The expression level of CB1 and CB2 receptors determines their efficacy at inducing apoptosis in astrocytomas. *PLoS One.* **5,** e8702

120. Stark, S., Pacheco, M.A., and Childers, S.R. (1997) Binding of aminoalkylindoles to noncannabinoid binding sites in NG108-15 cells. *Cell.Mol.Neurobiol.* **17,** 483-493

121. Breivogel, C.S., Griffin, G., Di Marzo, V., and Martin, B.R. (2001) Evidence for a new G protein-coupled cannabinoid receptor in mouse brain. *Mol.Pharmacol.* **60,** 155-163

122. Kreitzer, F.R., and Stella, N. (2009) The therapeutic potential of novel cannabinoid receptors. *Pharmacol.Ther.* **122,** 83-96

123. McAllister, S.D., Chan, C., Taft, R.J., Luu, T., Abood, M.E., Moore, D.H., Aldape, K., and Yount, G. (2005) Cannabinoids selectively inhibit proliferation and induce death of cultured human glioblastoma multiforme cells. *J.Neurooncol.* **74,** 31-40

124. Giuliano, M., Pellerito, O., Portanova, P., Calvaruso, G., Santulli, A., De Blasio, A., Vento, R., and Tesoriere, G. (2009) Apoptosis induced in HepG2 cells by the synthetic cannabinoid WIN: involvement of the transcription factor PPARgamma. *Biochimie.* **91,** 457-465

125. Widmer, M., Hanemann, C.O., and Zajicek, J. (2008) High concentrations of cannabinoids activate apoptosis in human U373MG glioma cells. *J.Neurosci.Res.* **86,** 3212-3220

126. Kline, T., and Stella, N. (2012) Composition and methods for treating glioblastoma

127. Kline, T., and Stella, N. (2013) Composition and methods for treating glioblastoma

128. Landen, J.W., Hau, V., Wang, M., Davis, T., Ciliax, B., Wainer, B.H., Van Meir, E.G., Glass, J.D., Joshi, H.C., and Archer, D.R. (2004) Noscapine crosses the blood-brain barrier and inhibits glioblastoma growth. *Clin.Cancer Res.* **10,** 5187-5201

129. Wakimoto, H., Mohapatra, G., Kanai, R., Curry, W.T.,Jr, Yip, S., Nitta, M., Patel, A.P., Barnard, Z.R., Stemmer-Rachamimov, A.O., Louis, D.N., Martuza, R.L., and Rabkin, S.D. (2012) Maintenance of primary tumor phenotype and genotype in glioblastoma stem cells. *Neuro Oncol.* **14,** 132-144

130. Lara-Gonzalez, P., Westhorpe, F.G., and Taylor, S.S. (2012) The spindle assembly checkpoint. *Curr.Biol.* **22,** R966-80

131. Kraft, J.C., Freeling, J.P., Wang, Z., and Ho, R.J. (2014) Emerging research and clinical development trends of liposome and lipid nanoparticle drug delivery systems. *J.Pharm.Sci.* **103,** 29-52

132. Meunier, S., and Vernos, I. (2012) Microtubule assembly during mitosis - from distinct origins to distinct functions?. *J.Cell.Sci.* **125,** 2805-2814

133. Beckers, T., Reissmann, T., Schmidt, M., Burger, A.M., Fiebig, H.H., Vanhoefer, U., Pongratz, H., Hufsky, H., Hockemeyer, J., Frieser, M., and Mahboobi, S. (2002) 2-Aroylindoles, a Novel Class of Potent, Orally Active Small Molecule Tubulin Inhibitors. *Cancer Res.* **62,** 3113-3119

134. Kuo, C.C., Hsieh, H.P., Pan, W.Y., Chen, C.P., Liou, J.P., Lee, S.J., Chang, Y.L., Chen, L.T., Chen, C.T., and Chang, J.Y. (2004) BPR0L075, a novel synthetic indole compound with antimitotic activity in human cancer cells, exerts effective antitumoral activity in vivo. *Cancer Res.* **64,** 4621-4628

135. Kaufmann, D., Pojarova, M., Vogel, S., Liebl, R., Gastpar, R., Gross, D., Nishino, T., Pfaller, T., and von Angerer, E. (2007) Antimitotic activities of 2-phenylindole-3-carbaldehydes in human breast cancer cells. *Bioorg.Med.Chem.* **15,** 5122-5136

136. Jordan, M.A., and Wilson, L. (2004) Microtubules as a target for anticancer drugs. *Nat.Rev.Cancer.* **4,** 253-265

137. Jordan, M.A., and Wilson, L. (1998) Microtubules and actin filaments: dynamic targets for cancer chemotherapy. *Curr.Opin.Cell Biol.* **10,** 123-130

138. Giannakakou, P., Sackett, D., and Fojo, T. (2000) Tubulin/microtubules: still a promising target for new chemotherapeutic agents. *J.Natl.Cancer Inst.* **92,** 182-183

139. Schinkel, A.H. (1999) P-Glycoprotein, a gatekeeper in the blood-brain barrier. *Adv.Drug Deliv.Rev.* **36,** 179-194

140. Goncalves, A., Braguer, D., Kamath, K., Martello, L., Briand, C., Horwitz, S., Wilson, L., and Jordan, M.A. (2001) Resistance to Taxol in lung cancer cells associated with increased microtubule dynamics. *Proc.Natl.Acad.Sci.U.S.A.* **98,** 11737-11742

141. Khan, S.M., Sleno, R., Gora, S., Zylbergold, P., Laverdure, J.P., Labbe, J.C., Miller, G.J., and Hebert, T.E. (2013) The expanding roles of Gbetagamma subunits in G protein-coupled receptor signaling and drug action. *Pharmacol.Rev.* **65,** 545-577

142. Dave, R.H., Saengsawang, W., Yu, J.Z., Donati, R., and Rasenick, M.M. (2009) Heterotrimeric G-proteins interact directly with cytoskeletal components to modify microtubule-dependent cellular processes. *Neurosignals.* **17,** 100-108

143. Cho, H., and Kehrl, J.H. (2008) Beyond the plasma membrane: new Functions for heterotrimeric G-protein signaling in asymmetric and symmetric cell division. *Cell.Cycle.* **7,** 573-577

144. Schaefer, M., Petronczki, M., Dorner, D., Forte, M., and Knoblich, J.A. (2001) Heterotrimeric G proteins direct two modes of asymmetric cell division in the Drosophila nervous system. *Cell.* **107,** 183-194

145. Roychowdhury, S., Martinez, L., Salgado, L., Das, S., and Rasenick, M.M. (2006) G protein activation is prerequisite for functional coupling between Galpha/Gbetagamma and tubulin/microtubules. *Biochem.Biophys.Res.Commun.* **340,** 441-448

146. Gillies, L., Lee, S.C., Long, J.S., Ktistakis, N., Pyne, N.J., and Pyne, S. (2009) The sphingosine 1-phosphate receptor 5 and sphingosine kinases 1 and 2 are localised in centrosomes: possible role in regulating cell division. *Cell.Signal.* **21,** 675-684

147. Ciruela, F., Robbins, M.J., Willis, A.C., and McIlhinney, R.A. (1999) Interactions of the C terminus of metabotropic glutamate receptor type 1alpha with rat brain proteins: evidence for a direct interaction with tubulin. *J.Neurochem.* **72,** 346-354

148. Saugstad, J.A., Yang, S., Pohl, J., Hall, R.A., and Conn, P.J. (2002) Interaction between metabotropic glutamate receptor 7 and alpha tubulin. *J.Neurochem.* **80,** 980-988

149. Ciruela, F., and McIlhinney, R.A. (2001) Metabotropic glutamate receptor type 1alpha and tubulin assemble into dynamic interacting complexes. *J.Neurochem.* **76,** 750-757

150. Jarzynka, M.J., Passey, D.K., Ignatius, P.F., Melan, M.A., Radio, N.M., Jockers, R., Rasenick, M.M., Brydon, L., and Witt-Enderby, P.A. (2006) Modulation of melatonin receptors and G-protein function by microtubules. *J.Pineal Res.* **41,** 324-336

151. Popova, J.S., and Rasenick, M.M. (2000) Muscarinic receptor activation promotes the membrane association of tubulin for the regulation of Gq-mediated phospholipase Cbeta(1) signaling. *J.Neurosci.* **20,** 2774-2782

152. St Croix, B., Rago, C., Velculescu, V., Traverso, G., Romans, K.E., Montgomery, E., Lal, A., Riggins, G.J., Lengauer, C., Vogelstein, B., and Kinzler, K.W. (2000) Genes expressed in human tumor endothelium. *Science.* **289,** 1197-1202

153. Carson-Walter, E.B., Watkins, D.N., Nanda, A., Vogelstein, B., Kinzler, K.W., and St Croix, B. (2001) Cell surface tumor endothelial markers are conserved in mice and humans. *Cancer Res.* **61,** 6649-6655

154. Vallon, M., and Essler, M. (2006) Proteolytically processed soluble tumor endothelial marker (TEM) 5 mediates endothelial cell survival during angiogenesis by linking integrin alpha(v)beta3 to glycosaminoglycans. *J.Biol.Chem.* **281,** 34179-34188

155. Vallon, M., Rohde, F., Janssen, K.P., and Essler, M. (2010) Tumor endothelial marker 5 expression in endothelial cells during capillary morphogenesis is induced by the small GTPase Rac and mediates contact inhibition of cell proliferation. *Exp.Cell Res.* **316,** 412-421

156. Wang, Y., Cho, S.G., Wu, X., Siwko, S., and Liu, M. (2014) G-protein coupled receptor 124 (GPR124) in endothelial cells regulates vascular endothelial growth factor (VEGF)-induced tumor angiogenesis. *Curr.Mol.Med.* **14,** 543-554

157. Ertych, N., Stolz, A., Stenzinger, A., Weichert, W., Kaulfuss, S., Burfeind, P., Aigner, A., Wordeman, L., and Bastians, H. (2014) Increased microtubule assembly rates influence chromosomal instability in colorectal cancer cells. *Nat.Cell Biol.* **16,** 779-791

158. Cullen, M., Elzarrad, M.K., Seaman, S., Zudaire, E., Stevens, J., Yang, M.Y., Li, X., Chaudhary, A., Xu, L., Hilton, M.B., Logsdon, D., Hsiao, E., Stein, E.V., Cuttitta, F., Haines, D.C., Nagashima, K., Tessarollo, L., and St Croix, B. (2011) GPR124, an orphan G protein-coupled receptor, is required for CNS-specific vascularization and establishment of the blood-brain barrier. *Proc.Natl.Acad.Sci.U.S.A.* **108,** 5759-5764

159. Zhou, Y., and Nathans, J. (2014) Gpr124 controls CNS angiogenesis and blood-brain barrier integrity by promoting ligand-specific canonical wnt signaling. *Dev.Cell.* **31,** 248-256

160. Posokhova, E., Shukla, A., Seaman, S., Volate, S., Hilton, M.B., Wu, B., Morris, H., Swing, D.A., Zhou, M., Zudaire, E., Rubin, J.S., and St Croix, B. (2015) GPR124 functions as a WNT7-specific coactivator of canonical beta-catenin signaling. *Cell.Rep.* **10,** 123-130

161. Kuhnert, F., Mancuso, M.R., Shamloo, A., Wang, H.T., Choksi, V., Florek, M., Su, H., Fruttiger, M., Young, W.L., Heilshorn, S.C., and Kuo, C.J. (2010) Essential regulation of CNS angiogenesis by the orphan G protein-coupled receptor GPR124. *Science.* **330,** 985-989

162. Ong, S.E., Blagoev, B., Kratchmarova, I., Kristensen, D.B., Steen, H., Pandey, A., and Mann, M. (2002) Stable isotope labeling by amino acids in cell culture, SILAC, as a simple and accurate approach to expression proteomics. *Mol.Cell.Proteomics.* **1,** 376-386

163. Lau, H.T., Suh, H.W., Golkowski, M., and Ong, S.E. (2014) Comparing SILAC- and stable isotope dimethyl-labeling approaches for quantitative proteomics. *J.Proteome Res.* **13,** 4164-4174

164. Charrasse, S., Schroeder, M., Gauthier-Rouviere, C., Ango, F., Cassimeris, L., Gard, D.L., and Larroque, C. (1998) The TOGp protein is a new human microtubule-associated protein homologous to the Xenopus XMAP215. *J.Cell.Sci.* **111 (Pt 10),** 1371-1383

165. Gard, D.L., and Kirschner, M.W. (1987) A microtubule-associated protein from Xenopus eggs that specifically promotes assembly at the plus-end. *J.Cell Biol.* **105,** 2203-2215

166. Brouhard, G.J., Stear, J.H., Noetzel, T.L., Al-Bassam, J., Kinoshita, K., Harrison, S.C., Howard, J., and Hyman, A.A. (2008) XMAP215 is a processive microtubule polymerase. *Cell.* **132,** 79-88

167. Gergely, F., Draviam, V.M., and Raff, J.W. (2003) The ch-TOG/XMAP215 protein is essential for spindle pole organization in human somatic cells. *Genes Dev.* **17,** 336-341

168. Cassimeris, L., and Morabito, J. (2004) TOGp, the human homolog of XMAP215/Dis1, is required for centrosome integrity, spindle pole organization, and bipolar spindle assembly. *Mol.Biol.Cell.* **15,** 1580-1590

169. Cassimeris, L., Becker, B., and Carney, B. (2009) TOGp regulates microtubule assembly and density during mitosis and contributes to chromosome directional instability. *Cell Motil.Cytoskeleton.* **66,** 535-545

170. Sironi, L., Solon, J., Conrad, C., Mayer, T.U., Brunner, D., and Ellenberg, J. (2011) Automatic quantification of microtubule dynamics enables RNAi-screening of new mitotic spindle regulators. *Cytoskeleton (Hoboken).* **68,** 266-278

171. Madoc-Jones, H., and Mauro, F. (1968) Interphase action of vinblastine and vincristine: differences in their lethal action through the mitotic cycle of cultured mammalian cells. *J.Cell.Physiol.* **72,** 185-196

172. Tsuchida, T., Yoshimura, K., Shirayama, Y., and Kawamoto, K. (1998) Colcemid-induced apoptosis of cultured human glioma: electron microscopic and confocal laser microscopic observation of cells sorted in different phases of cell cycle. *Cytometry.* **31,** 295-299

173. Sherwood, S.W., Sheridan, J.P., and Schimke, R.T. (1994) Induction of apoptosis by the anti-tubulin drug colcemid: relationship of mitotic checkpoint control to the induction of apoptosis in HeLa S3 cells. *Exp.Cell Res.* **215,** 373-379

174. Bakhoum, S.F., Silkworth, W.T., Nardi, I.K., Nicholson, J.M., Compton, D.A., and Cimini, D. (2014) The mitotic origin of chromosomal instability. *Curr.Biol.* **24,** R148-9

175. Bakhoum, S.F., and Compton, D.A. (2012) Chromosomal instability and cancer: a complex relationship with therapeutic potential. *J.Clin.Invest.* **122,** 1138-1143

176. Tonucci, F.M., Hidalgo, F., Ferretti, A., Almada, E., Favre, C., Goldenring, J.R., Kaverina, I., Kierbel, A., and Larocca, M.C. (2015) Centrosomal AKAP350 and CIP4 act in concert to define the polarized localization of the centrosome and Golgi in migratory cells. *J.Cell.Sci.* **128,** 3277-3289

177. Hurtado, L., Caballero, C., Gavilan, M.P., Cardenas, J., Bornens, M., and Rios, R.M. (2011) Disconnecting the Golgi ribbon from the centrosome prevents directional cell migration and ciliogenesis. *J.Cell Biol.* **193,** 917-933

178. Wakimoto, H., Kesari, S., Farrell, C.J., Curry, W.T.,Jr, Zaupa, C., Aghi, M., Kuroda, T., Stemmer-Rachamimov, A., Shah, K., Liu, T.C., Jeyaretna, D.S., Debasitis, J., Pruszak, J., Martuza, R.L., and Rabkin, S.D. (2009) Human glioblastoma-derived cancer stem cells: establishment of invasive glioma models and treatment with oncolytic herpes simplex virus vectors. *Cancer Res.* **69,** 3472-3481

179. Saura, J., Tusell, J.M., and Serratosa, J. (2003) High-yield isolation of murine microglia by mild trypsinization. *Glia.* **44,** 183-189

180. Marrs, W.R., Horne, E.A., Ortega-Gutierrez, S., Cisneros, J.A., Xu, C., Lin, Y.H., Muccioli, G.G., Lopez-Rodriguez, M.L., and Stella, N. (2011) Dual inhibition of alpha/beta-hydrolase domain 6 and fatty acid amide hydrolase increases endocannabinoid levels in neurons. *J.Biol.Chem.* **286,** 28723-28728

181. Hyman, A., Drechsel, D., Kellogg, D., Salser, S., Sawin, K., Steffen, P., Wordeman, L., and Mitchison, T. (1991) Preparation of modified tubulins. *Methods Enzymol.* **196,** 478-485

182. Canton, D.A., Keene, C.D., Swinney, K., Langeberg, L.K., Nguyen, V., Pelletier, L., Pawson, T., Wordeman, L., Stella, N., and Scott, J.D. (2012) Gravin is a transitory effector of polo-like kinase 1 during cell division. *Mol.Cell.* **48,** 547-559

183. Wordeman, L., Wagenbach, M., and von Dassow, G. (2007) MCAK facilitates chromosome movement by promoting kinetochore microtubule turnover. *J.Cell Biol.* **179,** 869-879

184. Jaqaman, K., Loerke, D., Mettlen, M., Kuwata, H., Grinstein, S., Schmid, S.L., and Danuser, G. (2008) Robust single-particle tracking in live-cell time-lapse sequences. *Nat.Methods.* **5,** 695-702

185. FOLCH, J., LEES, M., and SLOANE STANLEY, G.H. (1957) A simple method for the isolation and purification of total lipides from animal tissues. *J.Biol.Chem.* **226,** 497-509

186. Horne, E.A., Coy, J., Swinney, K., Fung, S., Cherry, A.E., Marrs, W.R., Naydenov, A.V., Lin, Y.H., Sun, X., Keene, C.D., Grouzmann, E., Muchowski, P., Bates, G.P., Mackie, K., and Stella, N. (2013) Downregulation of cannabinoid receptor 1 from neuropeptide Y interneurons in the basal ganglia of patients with Huntington's disease and mouse models. *Eur.J.Neurosci.* **37,** 429-440

187. Schmidt, K.F., Ziu, M., Schmidt, N.O., Vaghasia, P., Cargioli, T.G., Doshi, S., Albert, M.S., Black, P.M., Carroll, R.S., and Sun, Y. (2004) Volume reconstruction techniques improve the correlation between histological and in vivo tumor volume measurements in mouse models of human gliomas. *J.Neurooncol.* **68,** 207-215

188. da Fonseca, A.C., and Badie, B. (2013) Microglia and macrophages in malignant gliomas: recent discoveries and implications for promising therapies. *Clin.Dev.Immunol.* **2013,** 264124

189. Anderson, G.D., Farin, F.M., Bammler, T.K., Beyer, R.P., Swan, A.A., Wilkerson, H.W., Kantor, E.D., Hoane, M.R. (2011) The effect of progesterone dose on gene expression after traumatic brain injury. *J Neurotrauma.* **28**, 1827-1843.

190. Huber, W., Carey, V.J., Gentleman, R., Anders, S., Carlson, M., Carvalho, B.S., Bravo, H.C., Davis, S., Gatto, L., Girke, T., Gottardo, R., Hahne, F., Hansen, K.D., Irizarry, R.A., Lawrence, M., Love, M.I., MacDonald, J., Obenchain, V., Oleś, A.K., Pagès, H., Reyes, A., Shannon, P., Smyth, G.K., Tenenbaum, D., Waldron, L., Morgan, M. (2015) Orchestrating high-throughput genomic analysis with Bioconductor. *Nat Methods.* **12**, 115-121

191. Irizarry, R.A., Hobbs, B., Collin, F., Beazer-Barclay, Y.D., Antonellis, K.J., Scherf, U., Speed, T.P. (2003) Exploration, normalization, and summaries of high density oligonucleotide array probe level data. *Biostatistics.* **4**, 249-264

192. Ong, S.E., and Mann, M. (2006) A practical recipe for stable isotope labeling by amino acids in cell culture (SILAC). *Nat.Protoc.* **1,** 2650-2660

193. Ong, S.E. (2010) Unbiased identification of protein-bait interactions using biochemical enrichment and quantitative proteomics. *Cold Spring Harb Protoc.* **2010,** pdb.prot5400

194. Rappsilber, J., Mann, M., and Ishihama, Y. (2007) Protocol for micro-purification, enrichment, pre-fractionation and storage of peptides for proteomics using StageTips. *Nat.Protoc.* **2,** 1896-1906

195. Cox, J., and Mann, M. (2008) MaxQuant enables high peptide identification rates, individualized p.p.b.-range mass accuracies and proteome-wide protein quantification. *Nat.Biotechnol.* **26,** 1367-1372

196. Cox, J., Neuhauser, N., Michalski, A., Scheltema, R.A., Olsen, J.V., and Mann, M. (2011) Andromeda: a peptide search engine integrated into the MaxQuant environment. *J.Proteome Res.* **10,** 1794-1805